EESTI GEOLOOGIAKESKUS
GEOLOGICAL SURVEY OF ESTONIA

ESTONIAN GEOLOGICAL SECTIONS

BULLETIN 4

SOOVÄLJA (K–1) DRILL CORE

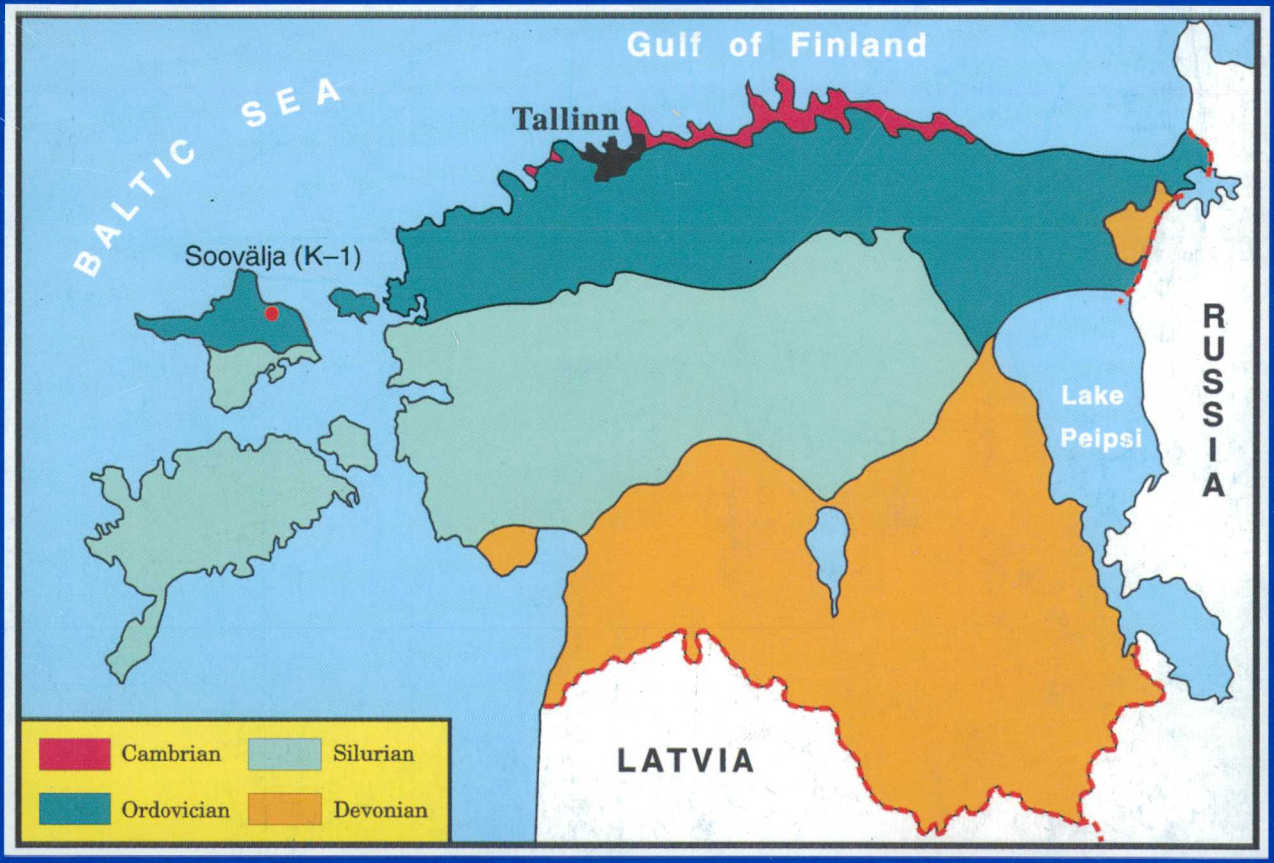

TALLINN 2002

Estonian Geological Sections
Ilmub 1998 aastast

Eesti Geoloogiakeskuse geoloogiline ajakiri.
Ilmub ebaregulaarselt.

Toimetus: Kadaka tee 82, 12618 Tallinn
Tel. (0) 672 0094
Faks (0) 672 0091
E-post egk@egk.ee

Koostaja: Anne Põldvere
Keeleline toimetaja: Anne Noor
Küljendaja: Mare Kukk
Kaanekujundus: Heikki Bauert

Estonian Geological Sections
Published since 1998

Geological journal of the Geological Survey of Estonia, published irregularly.

Editorial office: Kadaka tee 82, 12618 Tallinn
Tel. (372) 672 0094
Faks (372) 672 0091
E-mail egk@egk.ee

Editor: Anne Põldvere
English text revision: Anne Noor
Layout: Mare Kukk
Cover design: Heikki Bauert

ISSN 1406-3476
© Eesti Geoloogiakeskus, 2002

EESTI GEOLOOGIAKESKUS
GEOLOGICAL SURVEY OF ESTONIA

ESTONIAN GEOLOGICAL SECTIONS

BULLETIN 4

SOOVÄLJA (K–1) DRILL CORE

TALLINN 2002

CONTENTS

Preface. *Anne Põldvere* 3
Introduction. *Anne Põldvere* 3
Core description and terminology. *Anne Põldvere, Kalle Suuroja* 4
Geological setting of the Kärdla area. *Kalle Suuroja, Väino Puura, Juho Kirs, Mati Niin,* Anne Põldvere 6
Distribution of chitinozoans. *Jaak Nõlvak* 10
K-bentonite mineralogy and geochemistry. *Warren D. Huff, Stig M. Bergström, Dennis R. Kolata, Kalle Kirsimäe* 12
Characteristics of volcanism. *Tarmo Kiipli, Toivo Kallaste* 17
Physical properties. *Jüri Plado, Argo Jõeleht, Alla Shogenova* 21
References 25

Appendix 1. Description of the Soovälja (K–1) core 30
Appendix 2. Chemical composition of the Soovälja (K–1) core (wt %) 47
Appendix 3. XRF data of the Soovälja (K–1) core 49
Appendix 4. List of samples for semiquantitative emission spectral analyses of major and trace elements of the Soovälja (K–1) core 51
Appendix 5. Thin sections from Palaeoproterozoic rocks of the Soovälja (K–1) core 52
Appendix 6. Data of semiquantitative analyses of the mineral composition of the Soovälja (K–1) core 56
Appendix 7. Thin sections of the Soovälja (K–1) core with planar deformation features (PDFs) 56
Appendix 8. Grain-size distribution of insoluble residue in the Soovälja (K–1) core 57
Appendix 9. CaO, MgO, CO_2 and insoluble residue in the Ordovician rocks of the Soovälja (K–1) core 58
Appendix 10. List of chitinozoan samples from the Soovälja (K–1) core 58
Appendix 11. XRF data of the K-bentonite beds of the Soovälja (K–1) core 59
Appendix 12. Results of physical measurements from the Soovälja (K–1) core 60

Plates 1–4 Selected intervals of the Soovälja (K–1) core

PREFACE

The present issue of the journal *Estonian Geological Sections* deals with the Soovälja (K–1) drill core from the northern coast of Hiiumaa Island (Dagö), northwestern Estonia (Fig. 1). The Soovälja drill hole (815.2 m), the deepest drill hole in Estonia reaching the crystalline basement, was made in the Kärdla meteorite crater in the course of geological deep mapping of Hiiumaa Island in 1990 (Suuroja *et al.* 1991). The core is housed at Arbavere field station of the Geological Survey of Estonia. The source material for this research is available in reports of mapping (Suuroja *et al.* 1991, 1993, 1997) and applied geological studies (Suuroja *et al.* 1974), held in the Depository of Manuscript Reports, Kadaka tee 82, Tallinn. Results of detailed investigations and descriptions of the petrography, mineralogy and petrophysical properties of sediments, and impact lithology have been published in several papers (Lindström *et al.* 1992; Puura & Suuroja 1992a; Koppelmaa *et al.* 1996; Plado *et al.* 1996; Puura *et al.* 1996, 2000a, b, 2002; Suuroja 1994, 1996, 1997, 2002; Suuroja *et al.* 1999, 2002) and are used in the present work together with recently obtained data.

INTRODUCTION

The Soovälja (K–1 or F373) drill hole (58° 58,530' N, 22° 46,333' E) is located inside the circular Kärdla impact structure (Fig. 1). It penetrates 24 m thick Quaternary deposits, Ordovician post-impact sedimentary rocks (to a depth of 301.2 m) and the 221.6 m thick polymict clastic impact breccia complex (at 301.2–522.8 m). The following, 65.7 m interval is represented by the strongly brecciated crystalline basement (crater floor from monomictic breccia to a depth of 588.5 m; Fig. 2). The lowermost part of the Palaeoproterozoic subcrater basement is fractured (down to 815.2 m).

This report was completed through joint efforts of many specialists. Anne Põldvere (Geological Survey of Estonia) compiled the macrolithological characterization of the drill core using the description by Kalle Suuroja (Geological Survey of Estonia) based on the results of detailed mapping of the crater area (chemical, mineralogical and grain-size analyses, thin-section studies, etc.; Suuroja *et al.* 1991, 1997).

Petrographic descriptions of 59 thin sections from basement rocks together with their mineral compositions were provided by Mati Niin (Geological Survey of Estonia). The wet silicate chemical analyses of 17 rock samples (collected by Kalle Suuroja and Mati Niin) from impact-related basement rocks were performed at the laboratory of the Geological Survey of Estonia.

The content of trace elements in Palaeoproterozoic rocks was determined by Kiira Orlova (Laboratory of the Geological Survey of Estonia) on the basis of emission spectral analyses of 270 samples. Semiquantitative analysis of the mineral composition of the fractured and brecciated basement was performed at the University of Tartu (17 samples collected by Kalle Suuroja).

Twenty-seven core samples for the major and trace element study of the impact-influenced rocks were collected by Kalle Suuroja, Väino Puura (Institute of Geology, University of Tartu), Jaan Kivisilla, Heino Koppelmaa and Mati Niin. These samples were analysed by the instrumental neutron activation (INAA) method and X-ray fluorescence (XRF) spectrometry in the Institute of Geochemistry, University of Vienna (Austria). The iridium content of seven samples was determined by iridium coincidence spectrometry at Vienna laboratory (Puura *et al.* 2003).

Thin sections were made of 20 samples from the brecciated basement and impact breccias (collected by Väino Puura) to study mineralogical

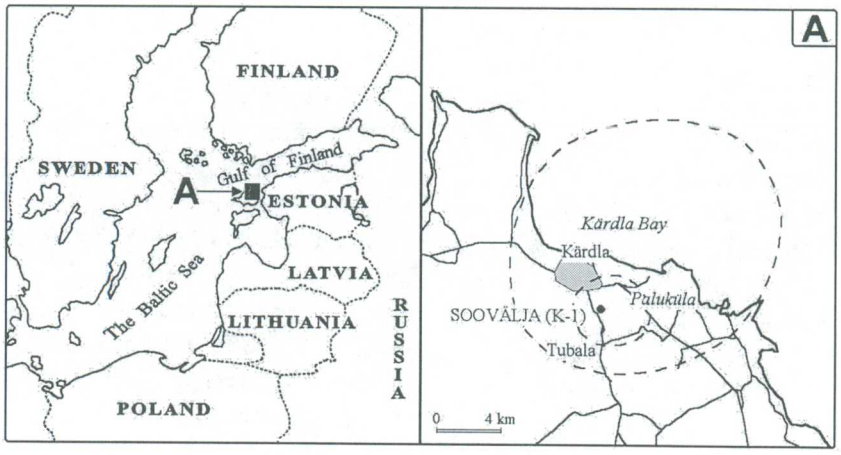

Fig. 1. Location of the Soovälja (K–1) drill hole. Dashed lines show the position of the buried rim wall (inner) and the ring fault (outer).

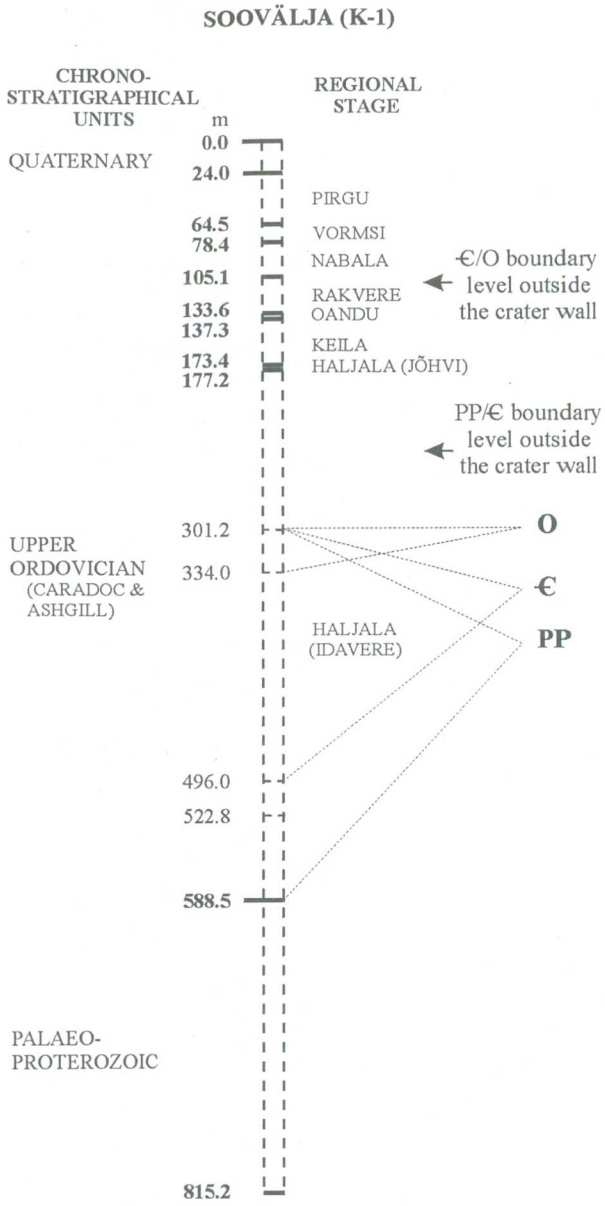

Fig. 2. Generalized stratigraphy and vertical distribution of impact-related mixed Palaeoproterozoic (PP), Cambrian (Є) or Ordovician breccia fragments in the Soovälja (K–1) core.

effects – K-enrichment and Na–Ca-depletion. These samples were examined using optical microscopy (by Väino Puura and Juho Kirs; both from the Institute of Geology, University of Tartu), electron microscopy and microanalyses (by Väino Puura and Aulis Kärki) in the Institute of Electron Optics, Oulu University, Finland. The same collection of thin sections was used for the quantitative study of the planar deformation features (PDFs) of quartz (Juho Kirs, Ulla Preeden, Väino Puura; all from the Institute of Geology, University of Tartu).

The contents of CaO, MgO, CO_2 and insoluble residue (8 samples, collected by Anne Põldvere) and grain size distribution of insoluble residue (17 samples, collected by Kalle Suuroja) in the crater filling and covering complexes were analysed at the Laboratory of the Geological Survey of Estonia.

To improve the stratigraphic subdivision of post-impact sedimentary rocks, the Ordovician part of the core was additionally sampled for microfossils (27 samples). Chitinozoans were identified by Jaak Nõlvak (Institute of Geology at Tallinn Technical University).

Data on electron microprobe analysis of biotite, X-ray diffractometry (XRD), XRF and INAA in 27 Ordovician volcanogenic interbeds were provided by Toivo Kallaste (Institute of Geology at Tallinn Technical University), Kiira Orlova (Geological Survey of Estonia), Kalle Kirsimäe (Institute of Geology, University of Tartu), Warren D. Huff (University of Cincinnati, USA), Stig M. Bergström (Ohio State University, USA) and Dennis R. Kolata (Illinois Geological Survey, USA).

Physical measurements of the core (92 samples) were performed by Jüri Plado, Argo Jõeleht (both from the Institute of Geology, University of Tartu) and Alla Shogenova (Institute of Geology at Tallinn Technical University). Photos of the core were taken by Tõnis Saadre (Pl. 1) and Heikki Bauert (Pls 2–4).

Useful comments by Jüri Plado, Juho Kirs and Jaan Kivisilla were of great help in finalizing the report.

The assistance of all contributors is gratefully acknowledged.

CORE DESCRIPTION AND TERMINOLOGY

The description of the Soovälja (K–1) core is presented as a table on 15 sheets including the main lithological features of the rock (Appendix 1). The first six sheets are given in the form previously used in Põldvere (1999, 2001); sheets 7–15 concentrate on impact-related features and, therefore, another is used.

Sixty-six samples were studied from the crater filling post-impact Ordovician complex (24.0–301.2 m): 26 for grain-size composition, 8 for the content of CaO, MgO, CO_2 and insoluble residue, 5 for physical properties and 27 for the distribution of chitinozoans. Twenty-seven volcanogenic and claystone interbeds (interval 170.9–256.0 m) were subjected to XRD or XRF analysis. From the Kinnekulle bed (173.0–173.4 m) microprobe analyses of biotite were performed.

Characterization of the impact-related deposits (301.2–588.5 m) comprises the results of 17 chemical analyses, 10 XRF analyses, 10 semiquantitative mineral composition analyses, 91 semiquantitative emission spectral analyses, 48 petrophysical measurements, 16 thin-section stu-

dies of the lithological–mineralogical composition and 19 thin-section studies for the description of PDFs. The description of the crystalline basement (588.5–815.2 m) rocks is based on 29 chemical analyses, 17 XRF, 7 semiquantitative mineral composition analyses, 179 semiquantitative emission spectral analyses, 39 petrophysical measurements and 43 + 1 (lithological–mineralogical composition + PDFs) thin sections.

To determine the degree of dolomitization of the carbonate rocks, 3% hydrochloric acid was used during field-work. The content of clay, the most common terrigenous component in carbonate rocks, was assessed visually, according to the scheme by Oraspõld (1975), as follows: slightly argillaceous (insoluble residue 10–15%), medium argillaceous (15–20%) and highly argillaceous (20–25%).

The descriptions of the textures of carbonate rocks are based on the traditional Estonian classifications by Vingisaar *et al.* (1965) and Loog & Oraspõld (1982), where the relative amounts of clastic and micritic components are crucial to identification of the textures. The content of carbonaceous clasts (including bioclasts) is given in most cases in per cent.

The particles with the diameter >0.05 mm are described as grains. For the major part of the core, the amount of grains was determined with the magnifying glass on the slabbed surfaces of the core. The micritic component consists of particles <0.05 mm in diameter. The terms used for textures are explained in Appendix 1. In case of mixed texture, the dominant component is given last, while less important components are given before as appositions. The same principles were followed in derivation of descriptive terms also for other characteristics of the rock. The comparison of the Estonian classification with Dunham's classification (Dunham 1962; Põldvere & Kleesment 1998) is given, if possible, at the end of the short description.

Several sedimentary structures are described in the way traditionally used in this bulletin (see Põldvere 1999, 2001). The relationships between different parts of rock are given in Appendix 1.

The classification of sandstones is based on the generally used 5-fractional classification of Pettijohn *et al.* (1987), where the diameter of the finest sand particles is 0.05 mm. Fractions and terms for silt and sand are described in Appendix 1. Gravel-sized fragments (diameter 2–10 mm) are larger than coarse sand and finer than pebbles. Large angular fragments of rocks (with diameter >256 mm) are referred to as blocks. The term "terrigenous" is essentially synonymous with "noncarbonate" (e.g. *terrigenous sand* vs. *carbonate sand*) and is applied to sediments originating from the land area and transported mechanically to the basin of deposition (Scholle 1978).

The names of igneous rocks were derived on the bases on their genesis, and chemical and mineralogical composition. Grain size limits are explained in Appendix 1.

Directional movement of rock particles along straight or arc-shaped lines inside impact-related sediments is observed on several levels. The surfaces of moved sediments are various, depending on the composition of the material, and size and character of flow directions.

The terminology concerning impact-related rocks and processes is based on Stöffler & Grieve (1994) and geological dictionaries. Below, a short glossary is given.

Allochthonous (allogenic) impact breccia – synonymous to polymict impact breccia; includes clastic matrix breccias (fragmental breccias, suevite breccias), impact melt breccias and dike breccias.

Autochthonous (authigenic) impact breccia – synonymous to monomict (cataclastic) impact breccia.

Breccio-conglomerate – a rudaceous rock containing both angular and rounded fragments.

Cataclasis – the process of mechanical fracture or break-up of rocks, usually associated with dynamic metamorphism or faulting. The term is used both for small-scale, i.e. microscopic, structures, and also for large-scale phenomena. Hence cataclastic (adjective), and cataclasite – any rock produced by cataclasis. Another form of cataclasis is impacting, which involves planetesimal bodies such as asteroids striking the planet with enough energy to pulverize, or even melt, rock.

Ejecta (impact ejecta) – material, such as glass and fragmented rock, thrown out of an impact crater during its formation.

Fragmental (impact) breccia – polymict impact breccia with clastic matrix containing shocked and unshocked mineral and lithic clasts but lacking cogenetic impact melt particles; forms the bulk of the continuous ejecta blanket (⇛ *Impact formation*) of impact craters.

Impact – collision of two (planetary) bodies at or near cosmic velocity, which causes the propagation of a shock wave in both the impactor and target body.

Impact breccia – monomict or polymict breccia, which occurs around, inside and below impact craters. ⇛ *Monomict impact breccia.* ⇛ *Polymict impact breccia.*

Impact crater – generally circular crater formed either by impact of an interplanetary body (projectile) on a planetary surface or by an experimental hypervelocity impact of a projectile into solid matter;

craters formed by very oblique impacts may be elliptical.

Impact formation – geological formation produced by impact; includes various lithological and structural units inside and beneath an impact crater (inner impact formations), the continuous ejecta blanket (outer impact formations) and distal ejecta such as tektites and impactoclastic air fall beds.

Impact melt – melt formed by shock melting of rocks in impact craters.

Impact melt breccia – impact melt rock containing lithic and mineral clasts displaying variable degrees of shock metamorphism in a crystalline, semihyaline or hyaline matrix (crystalline or glassy impact melt breccia).

Impact melt rock – crystalline, semihyaline or hyaline rock solidified from impact melt.

Impact metamorphism – metamorphism associated with the impact upon Earth of an extraterrestrial body.

Impact structure – geological structure caused by impact irrespective of its state of preservation.

Impactite – rock affected by impact metamorphism (includes shocked rocks, impact breccias and impact melt rocks).

Impactoclast – rock fragment resulting from impact-induced comminution (⇛ *Comminution*) of rocks; may display variable degrees of shock metamorphism (different shock stages).

Meteorite crater – impact crater with remaining fragments of the impacted meteoroid.

Monomict impact breccia – cataclasite (⇛ *cataclasis*, ⇛ *autochthonous (authigenic) impact breccia*) produced by impact and generally displaying weak or no shock metamorphism; occurs in the (par)authochthonous basement of an impact crater or as clast (up to the size of blocks and megablocks) within allochthonous impact breccias (*synonymous to polymict impact breccia*).

Planar deformation features (PDFs) – submicroscopic amorphous lamellae occuring in shocked minerals as multiple sets of planar lamellae (optical dicontinuities under the petrographic microscope) parallel to rational crystallographic planes; indicative of shock metamorphism; synonymous with the terms "planar elements" and "shock lamellae" which should be discarded.

Planar fractures (PFs) – fractures occuring in shocked minerals as multiple sets of planar fissures parallel to rational crystallographic planes, which are usually not observed as cleavage planes under normal geological (non-shock) conditions.

Planar microstructures – collective term comprising shock-induced planar fractures and planar deformation features.

Polymict impact breccia – breccia (⇛ *allochthonous (allogenic) impact breccia*) with clastic matrix or crystalline matrix (derived from the crystallization of impact melt) containing lithic and mineral clasts of different degree of shock metamorphism excavated by an impact from different regions of the target rock section, transported, mixed and deposited inside or around an impact crater or injected into the target rocks as dikes.

Resurge breccia – polymict impact breccia produced by force of resurge wave under sea conditions. The impact blows water away from the impact site and this water will return as a huge resurge wave with mixed target rocks.

Shatter cone – rock feature formed when an intense shock wave travels through target rocks; points to the centre of impact and is one of the best macroscopic confirmations for impact.

Simple impact crater – bowl-shaped impact crater with a relatively high depth/diameter ratio.

Slumped breccia – breccial and internally highly deformed downwards slided sediment bodies (blocks), often with directional movement character.

Suevite or **suevite breccia** – polymict impact breccia with clastic matrix containing lithic and mineral clasts in various stages of shock metamorphism including cogenetic impact melt particles which are in a glassy or crystallized state; synonymous with suevitic impact breccia and mixed breccia.

Target rock(s) – rock(s) exposed at the site of an impact before crater formation.

GEOLOGICAL SETTING OF THE KÄRDLA AREA

A crater structure (Fig. 3) buried under a thin layer of Upper Ordovician limestone in the northeastern part of Hiiumaa Island (near the southeastern border of the town of Kärdla) was discovered in 1974. Its impact (meteoritic) origin was established in 1981 (Masaitis *et al.* 1980). The morphology, age, possible formation mode, etc. of the Kärdla crater as a unique geological object have been discussed in numerous papers (Puura 1974; Kala *et al.* 1978; Bauert *et al.* 1987; Kleesment *et al.* 1987; Žukov *et al.* 1987; Puura & Suuroja 1984, 1992; Lindström *et al.* 1992; Grahn & Nõlvak 1993; Grahn *et al.* 1996; Koppelmaa *et al.* 1996; Plado *et al.* 1996; Puura *et al.* 1989, 1994, 1996, 1999, 2000a, b, 2001; Suuroja *et al.* 1999, 2002; Suuroja 1994, 1996, 1997, 2002; Ainsaar *et al.* 2002).

The age of the crater

The age of the Kärdla impact event is precisely established by micropalaeontological data (see Nõlvak in this volume) and biostratigraphical corre-

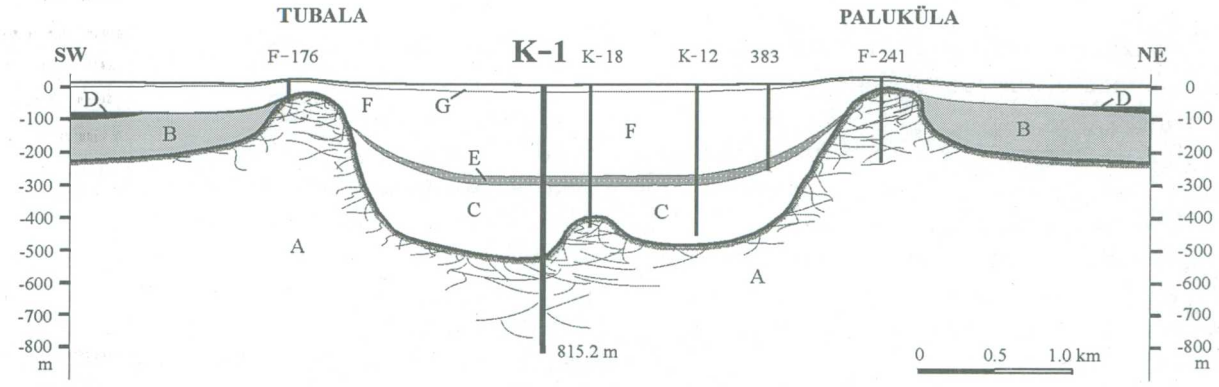

Fig. 3. Schematic geological section of the Kärdla crater and the location of main drill holes.

A – impact-influenced fractured, in the upper part (66 m) brecciated Palaeoproterozoic crystalline basement; B – impact-influenced rocks: Cambrian claystones, silt- and sandstones (thickness up to 120 m), Ordovician sandstones and argillites (up to 8 m) and Ordovician limestones (up to 14 m); C – impact breccias (up to 220 m); D – impact-related ejecta layer (up to 14 m); E – impact-related turbidites (up to 28 m); F – post-impact Ordovician filling (argillaceous limestones, organic build-ups on the rim wall at Paluküla) and covering (limestones) complex (up to 256 m); G – Quaternary deposits (till, varved clay and sand; up to 24 m).

lations. The crater was formed in a shallow epicontinental sea not far from the non-sedimentation area (Puura & Suuroja 1992; Ainsaar *et al.* 2002) 455 million years ago (Upper Ordovician, Idavere Regional Stage; Bauert *et al.* 1987; Puura & Suuroja 1992; Grahn *et al.* 1996). At that time the crystalline basement was covered by mainly soft, water-rich, poorly compacted siliciclastic and clayey Cambrian sediments and an about 20 m thick layer of Lower–Upper Ordovician carbonate rocks. During the post-impact geological history, the sedimentary cover has been compacted and thinned to 150 m (Puura & Suuroja 1992).

The morphology of the crater

The circular crater structure is 4 km wide and more than 500 m deep, with a central uplift (diameter about 800 m) rising about 130 m from the crater floor (Figs 1 and 3). The rim wall (the highest point 110 m above the target level) is cut by at least two resurge-excavated gullies (lowlands between the town of Kärdla and Paluküla village, and Ala and Tubala villages). The crater is surrounded by an elliptical ring fault (diameter 12–15 km), with deformed sedimentary rocks below the target level. Marine geophysical investigations in 1996 revealed a presumptive ring fault zone (Suuroja *et al.* 2002) at two sites in Kärdla Bay, marked by a 5–10 m high terrace in the bedrock and by a submarine beach ridge. The blocks of the Cambrian sedimentary cover between the rim wall and the ring fault are strongly disturbed, fractured and folded, but dislocations do not reach the crystalline basement. In physical properties the vertical influence of the impact is observable until the bottom of the Soovälja (K–1) core, but extends to the depth of about 950 m, that is about 430 m below the crater floor (Plado *et al.* 1996). The basement of the surroundings of the crater is overlain by sedimentary bedrock consisting of siliciclastic and carbonaceous rocks, which have formed partly during the Vendian, but mainly during Cambrian, Ordovician and Silurian times.

Crystalline basement of the crater area

The structure of the crater and its surroundings has been established by the study of 1950 m of core from 60 closely spaced drill holes (Suuroja *et al.* 1974, 1991, 1993; Puura & Suuroja 1992).

According to the deep drilling data, the well-smoothed surface of the basement lies at a depth of 175–330 m in Hiiumaa and is slightly sloping southwards (3–4 m per km). The basement of Hiiumaa Island consists of Palaeoproterozoic metamorphic rocks, geologically and structurally forming an extension of the Svecofennian folded belt in Southern Finland (Koistinen 1994). Metavolcanics and metasediments are mainly represented by amphibolites, biotite-amphibole, quartz-feldspar and mica gneisses, also by migmatite granites (Suuroja *et al.* 1991). The topmost 5–10 m of the basement was subjected to pre-Vendian weathering.

In the Kärdla crater area, the surface of the basement lies deeper than 500 m in the crater depression, while on the rim wall (at Paluküla) its altitude is some metres above sea level. The basement consists of Svecofennian late orogenic migmatite granites (Suuroja *et al.* 1991; Niin 1997), metabasites (amphibolites, biotite-amphibolite and biotite gneisses) and quartz-feldspar gneisses. At Paluküla (towards ENE), the rim wall is mainly built of migmatized metabasites, whereas at Tubala (towards the WSW) the rim wall and the crater depression together with the central uplift are composed of migmatite granites and quartz-feldspar gneisses. Simi-

lar rocks occur also outside the rim wall in the nearest surroundings of the crater (Suuroja *et al.* 1991; Koppelmaa *et al.* 1996).

Basement rocks are mainly fractured and in places penetrated by secondary carbonate veins. The secondary alteration processes (chemical weathering and hydrothermal processes) in the crater have been more intense than elsewhere in Hiiumaa. The thickness of the altered rocks ranges from some metres to 50 m and more.

The basement-derived granitoids and amphibolites in allochthonous breccias were subjected to high pressure (20–35 GPa) of impact metamorphism but in autochthonous position they were subjected to low shock pressure (less than 8 GPa). Rocks and minerals are variably fractured and brecciated. The impact initiated significant chemical (K-enrichment) and mineralogical alteration (see Appendixes 2, 3) of rocks. Of major components, the content of MgO is slightly higher in the brecciated samples due to the replacement of hornblende and biotite by chlorite. The trace element spectra show no (or not detectable) enrichment of crater rocks in an extraterrestrial component (Appendix 3; Puura *et al.* 2003).

Optical microscopy of rocks shows that plagioclase has been widely substituted by submicroscopical earthy material resembling sericite or saussurite. The X-ray diffractometry, scanning electron microscopy and electron probe microanalyser studies, however, have revealed the replacement of plagioclase by K-feldspar of orthoclase type (Puura *et al.* 2000). Hornblende-type amphibole is widely chloritized and biotite shows kink-banding. Cross-hatched microcline has disappeared in places and been replaced by orthoclase. Only quartz is chemically relatively stable, but has undergone crushing.

The occurrences of post-impact polymetallic ore (Pb, Zn-sulphides) formations are common in the crater region both in basement rocks and sedimentary bedrock (Suuroja *et al.* 1991, 1993; Koppelmaa *et al.* 1996; Suuroja 2002; see also Appendix 4).

The sub-crater basement section in the Soovälja (K–1) core is 226.7 m thick (interval 588.5–815.2 m; Appendix 1, sheets 11–15). Dominating rock types are mainly pinkish-red or reddish-brown granitoids – migmatite granites and vein-forming plagioclase-microcline granites (Appendixes 1, 5, 6). They are mostly of plagioclase-microcline composition, with microcline predominating over plagioclase (Appendix 5, thin section 16100). Often fractured and porous rocks have been subjected to cataclasis.

By chemical composition, coarse- to fine-grained, massive or gneissic migmatite granites correspond to K-rich syenogranites, seldom to normal granites. By mineralogical composition, the majority of the rocks should belong to granites (Koppelmaa *et al.* 1996). Plagioclase has been subjected to complete sericitization and pelitization, which has resulted in extensive outwashing of Na (together with Ca) and replacement by K. Quartz amounts to 30–35% (Appendix 5). Relatively small, rounded, prolongated or jagged quartz grains are often fractured and have undulatory extinction. K-feldspar is represented by cross-hatched microcline with quite fresh appearance, often replacing the earthy and corroded plagioclase. The amount of plagioclase in migmatite granites varies in wide limits. Plagioclase occurs as corroded and thoroughly altered with earthy masses crystals, often with very thin rims of pure albite. Frequently fresh microcline has grown into plagioclase, accompanied by the formation of myrmekites. Biotite (content below 5%) forms small, relatively weakly altered laminae. Migmatite granites contain only single grains of hornblende and garnet, but titanomagnetite, apatite and zircon are common.

The granites, occurring in up to 10 m thick veins are fine- to coarse-grained, rarely pegmatitic (Pl. 4, M), massive, in places gneissic. By mineral composition they are plagioclase-microcline, more rarely microcline granites (Appendix 5), by chemical composition mostly belong to syenogranites (Appendix 2).

The proportion of gneisses is insignificant. Quartz-feldspar gneisses are pinkish-red or greyish-brown, fine- to medium-grained, with weakly banded or gneissic structure and granoblastic or lepidogranoblastic texture. The quantity of quartz is 38–45% (Appendix 5).

Dark grey or greenish-black amphibolites occur in migmatite granites in the form of up to 40 cm thick veins, lenses or relicts (Appendix 1, sheets 11–15; Appendix 5). Migmatized amphibolites are medium- to fine-grained (grain size 1–3 mm), with layered or massive fabric (Appendixes 1, 5), the texture of amphibolites is nematogranoblastic, granonematoblastic, granoblastic or blastogabbroic.

Impact breccias

The polymict impact breccias of the Kärdla crater and its surroundings have been recovered by 160 drill holes, of which only K–1, K–12 and K–18 penetrate the entire complex inside the crater. The impact origin of the deposits was established by the discovery of quartz with planar deformation features (PDFs; Masaitis *et al.* 1980) showing mosaicism and up to 2–3 systems of PDFs (Appendix 7). In rare cases PDFs are seen also in cross-hatched microcline chips (Puura *et al.* 2000a, 2003). Dispersed and strongly altered impact melt (rarely exceeding 20%)

occurs in the Kärdla crater only in the suevite breccia (Suuroja *et al.* 2002).

Outside the crater, the impact event is marked by a 0.01–14.0 m thick ejecta layer of silt- to gravel-sized target rock debris. Shocked minerals (quartz, feldspar) often show multiple sets of planar fissures or deformational features (PDFs; Suuroja *et al.* 2002). Carbon-rich spherules are also found (Puura *et al.* 2000b). The continuous ejecta layer in the limestone sequence is distributed at least within a distance of about 30 km from the impact centre (Puura & Suuroja 1992). Coarse clasts (blocks, cobbles and pebbles) are found at a distance of up to 5 km from the impact site. The evenly decreasing grain size and thickness of the ejecta layer farther from the impact site bear evidence of the smooth sea floor at the time of the impact. The depth of water at the impact site might have been about 100 m. As numerical modelling of an impact has shown (Shuvalov 2002), a smaller water depth could not have caused a resurge wave powerful enough to smash up the rim wall.

The target rocks have been subject to brecciation and fracturing of variable degree. There occur breccia dikes, metre-sized blocks, fine-grained clasts in breccia matrix and microfracturing of mineral grains. Fragmental breccia dikes are found at different levels in the crater walls and in the crater basement.

Two formations, Kärdla (Appendix 1, sheets 7–11, 301.2–588.5 m; Pl. 1, figs 6, 7; Pls 2, 3; Pl. 4, I, J, K, L) and Paluküla (Appendix 1, sheets 4–6, 189.4–301.2 m; Suuroja *et al.* 1991), are represented in the impact-related section (stratotype of the Soovälja (K–1) core). The about 50 m thick suevite-like impact breccia layer (Appendix 1, sheets 9–10, interval 471.0–522.8 m; Pl. 2, D; Pl. 3, E, F, G) upon the strongly brecciated crater floor (Appendix 1, sheets 10–11; interval 522.8–588.5 m; Pl. 3, H; Pl. 4, I, J, K, L) consists of crystalline basement blocks and clasts. As a result of K-metasomatosis caused by the impact, the breccias have become depleted in Na_2O and CaO and enriched in K_2O (Appendix 2). This enrichment in K is petrographically associated with the replacement of plagioclase by submicroscopic orthoclase masses. The borderline between autochthonous (lower) and allochthonous (upper) breccias is at 522.8 m. The layer of slumped breccias (contains over 90% strongly deformed Cambrian blocks) is thinner over the central uplift and thicker above the ring depression (ca. 40 and 140 m, respectively; Appendix 1, sheets 7–9, interval 334.0–471.0 m). Impact suevite-like and slumped breccias are covered by resurge deposits (Appendix 1, sheet 7, interval 301.2–334.0 m; Pl. 1, fig. 6) consisting prevailingly (up to 40 vol%) of the clasts or blocks (up to 5 m in diameter) from the topmost part of the target and shock-influenced clasts of crystalline basement rocks.

Turbidites and post-impact sediments

Turbidites in the crater are deposited from the mudflow suspension and display a sorting effect: the coarsest material in beds is at the base and the finest material at the top. The lower complex (thickness 1–2 m; Appendix 1, sheet 6, 300.0–301.2 m; Pl. 1, fig. 5) contains particles in size ranges 2–10 mm and 20–100 mm. The immediately overlying layer (thickness 2–4 m; Appendix 1, sheet 6, 296.0–300.0 m; Pl. 1, fig. 5) consists of particles 0.1–2.0 mm in diameter and is covered by 22–26 m thick (Appendix 1, sheet 6, 279.8–296.0 m) sediments with 0.005–0.1 mm grain size. Fine-grained well-rounded sand- and siltstone consists mainly of quartz. Conglomeratic to coarse sand-sized particles are angular and contain abundant clasts of the crystalline basement rocks. Shock metamorphosed grains of quartz with PDFs are found in all described siliciclastic layers.

The thickness of post-impact carbonaceous limestones and marls in the crater deep is up to 300 m, in the surrounding area about 90 m and above the rim wall only 15–20 m. The crater depression on the sea bottom has behaved as a sediment trap (Suuroja *et al.* 1997).

In the crater deep, the turbidites are directly overlain by about 90 m (Appendix 1, sheets 4–6, 189.4–279.8 m) of calcareous sediments with 5–50 cm thick interbeds comprising angular siliciclastic material (Appendixes 8, 9) and features of directional movement. Three 2–8 cm thick volcanogenic (metabentonite) interbeds have been registered, not found outside the crater. Simultaneously (during about 100 000 years) about 0.5 m of lime sediments accumulated in the crater surroundings (Suuroja *et al.* 1997).

The crater filling ends with an about 50 m thick carbonate sediment complex (see Appendix 1, sheets 3, 4, 133.6–189.4 m; Pl. 1, figs 3, 4) where up to 17 volcanogenic interbeds have been recognized (core sections K–1 and K–18). Pyritized two-ply discontinuity surfaces in the upper part of the complex are mainly strongly impregnated, with up to 20 cm burrows and excavations. In the lower part of the complex, the surfaces are slightly impregnated, in places phosphatized and often covered with rock containing silt and sand. Sedimentary conditions were markedly different in a 100–300 m wide area near the inner and outer slopes of the rim wall in the surroundings of Paluküla village where 15–20 m thick organic build-ups of echinoderm columnal plates have formed. Abundant fragments of echinoderm

crowns are found from marls in the western part of the crater. Outside the crater, synchronous sediments are only 27–33 m thick.

By the beginning of Rakvere time the highest part of the rim wall was buried under calcareous mud. The conditions of sediment accumulation had equalized in different parts of the crater but the rate of accumulation was somewhat different. A 100–200 m wide arc-like ridge near Paluküla, and probably in the SW part of the rim wall, caused some difference in thicknesses of formations on the crater deep, on the rim wall and in the surroundings (respectively 70, 40 and 55 m; Appendix 1, sheets 2, 3, 64.5–133.6 m; Pl. 1, fig. 2). In the up to 4 m thick basal part (missing in K–1), formed at the beginning of Rakvere time only near Paluküla, the crypto- to microcrystalline limestone is rich in fossils, bioclasts (up to 50%) and cobble- to sand-sized crystalline rock fragments. The upper part of the Rakvere Stage contains 2–5 cm kukersite-bearing interbeds and 6–12 pyritized discontinuity surfaces. The latter are mainly slightly impregnated, smooth or uneven. Under these surfaces the limestone is often burrowed and penetrated by 2–10 cm deep excavations. The amount of clasts is variable in different sections.

The Nabala and Vormsi stages are represented by very finely crystalline or crypto- to microcrystalline limestones with marl and slightly argillaceous limestone interbeds. Of fossils, fragments of brachiopods, trilobites, rugosae and calcareous algae are present. In the basal part near Paluküla village quartz and feldspar sand occurs. The upper part of the Vormsi Stage revealed 2–4 phosphatized or pyritized two-ply discontinuity surfaces, which are strongly impregnated, uneven or wavy with excavations. Pyritized bioclasts are often found under these surfaces.

The thickness of the Pirgu Stage in the crater area is 38–42 m, decreasing in the crater surroundings to 34 m. Micro- and very finely crystalline limestone with marl interbeds (Pl. 1, fig. 1) is rich in pyritized discontinuity surfaces (up to 42). They are mostly slightly impregnated, uneven (wavy) or disjointed. Burrows and excavations reach up to 10 cm below the surface. Inside the crater, the widely distributed Pirgu sediments are overlain by some relicts of the rocks of the latest Ordovician Porkuni Stage and the Silurian Juuru Stage, buried under the Quaternary cover.

The Quaternary cover inside the crater is 18–24 m (see also Appendix 1, sheet 1), but on the rim wall mostly 0.2–2 m thick. In the crater proper, the Upper Pleistocene till and varved clay (Baltic Ice Lake) layers are covered by Holocene Limnea Sea sand. The Pleistocene glaciation essentially contributed to the formation of the bedrock topography of the Kärdla impact structure area. The pressure of 2–3 km thick glaciers has compacted the underlying sediments. For example, the lower boundary of the Saunja Formation is tilted by up to 30° on the slopes of the rim wall, sunk down by about 60 m inside the crater and uplifted by up to 60 m above the rim wall. Thus the maximum divergence of the post-deposition vertical movements in the crater area was up to 120 m.

The Pleistocene glaciation removed about 60 m of the sedimentary cover from the rim wall. In the uplifted crater area, however, the erosion rate was higher (Možaev 1973). We cannot exclude also the influence of the post-burial deposits – the probably up to 300 m thick cover of the Silurian and Devonian rocks (at present missing in northern Hiiumaa), but lithostatic pressure from continental glacier was still of greater importance.

DISTRIBUTION OF CHITINOZOANS

A total of 27 samples (Appendix 10) from the lowermost part of more or less normal sediments of the Soovälja (K–1) core (fine-grained sandstones and calcareous mudstones, Appendix 1, sheets 5, 6), formed after the impact event, were studied for acid-resistant microfossils. The main purpose of this study was to answer the question: which groups were the first to invade the crater? In contrast to the sequences surrounding the crater, which give the precise age of the event, those within the crater are virtually complete and therefore good models for ecological studies of restricted environments.

In the early 1970s the distribution of acid-resistant microfossils was studied using drill cores from the northeast margin of the Kärdla impact crater – Paluküla 412 and Paluküla 383. The data obtained from the latter were published in Grahn *et al.* (1996, fig. 8). The age of the Kärdla impact event in the light of chitinozoans was determined in the Männamaa F367 core (Grahn *et al.* 1996, fig. 9), about 20 km to the southwest of the crater. In this core the impact-related layer lies in the transition between the *Angochitina curvata* and *Lagenochitina dalbyensis* zones in terms of the chitinozoan zonation (Nõlvak & Grahn 1993; Nõlvak 1999), in the early Idavere Age (Grahn & Nõlvak 1993, fig. 2).

Almost all samples from the Soovälja (K–1) core contained at least some remains of organic-walled fossils (chitinozoans, acritarchs, graptoloids and also scolecodonts), except for the lowermost one (sample M-14080, Fig. 4). The sample size varied from 0.2 to 0.5 kg (0.3 kg on average). Altogether 31 chitinozoan taxa were identified, the distribution

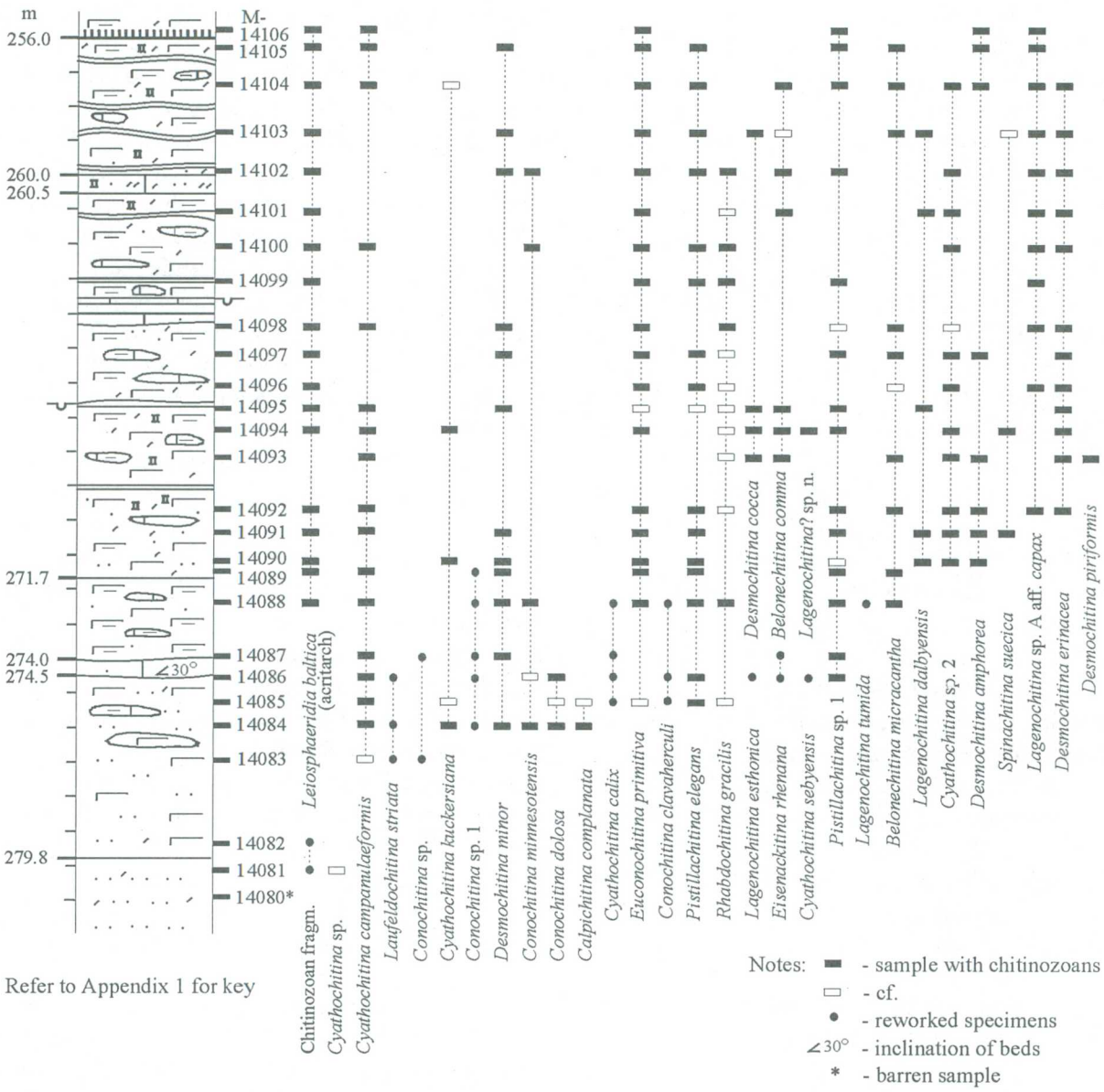

Fig. 4. Distribution of chitinozoans and the acritarch *Leiosphaeridia baltica* in the Haljala Stage (Idavere Substage; Caradoc) of the Soovälja (K–1) core.

of which is shown in Fig. 4. The number of specimens per sample increases upwards step by step and is relatively very high (more than 2–3 specimens per gram of rock) above the 271.4 m level (M-14089–M-14106). However, the preservation of chitinozoans varies largely. Below the 270 m level, they are totally flattened and bigger forms are often broken. Higher in section (in more argillaceous beds), they are poorly preserved in some layers, but generally specimens are not as compressed as in the ten lower samples.

At the same level (M-14089) the first graptoloids (*Climacograptus* sp., *Pseudoclimacograptus* sp., *Dicellograptus* sp.) come in, but the first fragments of scolecodonts appear together with chitinozoans. Rare colonies of the (blue-green?) alga *Cloeocapsamorpha prisca* were found in M-14085 and M-14086.

It can be concluded that in general the chitinozoan assemblage in beds higher the 271.4 m level is very similar to that in both Paluküla (383 and 412) sections. A similar assemblage is widely distributed in the lower Idavere Substage in many studied sections in the whole North Estonian Confacies Belt (Nõlvak 2002b), where these beds have a much more restricted thickness (up to 5 m). The species content of the Soovälja (K–1) core is rather stable and no marked changes are registered in the species level, except for the fossiliferous lowermost part where interesting variations are observed.

The chitinozoan assemblage of the lower part of the Soovälja (K–1) core (below a depth of 271.4 m) has a specific characteristic, not registered in the other sections inside the crater, e.g. Paluküla 412 (interval 240.0–274.0 m, 14 samples)

and Paluküla 383 (Grahn *et al.* 1996, fig. 8, interval 144.3–225.0 m, 88 samples), where beds of the Idavere Substage were studied very carefully. That specific element of the chitinozoan assemblage consists in one to three (in one case five) specimens, which until now (according to the data available) are known from much older layers. For example, *Laufeldochitina striata* is known not higher than the upper Uhaku Stage; *Conochitina clavaherculi* from the Lasnamägi and lower Uhaku stages; *Conochitina* sp. 1 from the lower and *Eisenckitina rhenana* from the whole Kukruse Stage, etc. Most of these are stratigraphically important zonal forms among chitinozoans (Nõlvak & Grahn 1993; see also Taga-Roostoja (25A) section in Nõlvak 1999 and Valga (10) section in Nõlvak 2001).

Such an unusual content of chitinozoans (marked with a black circle in Fig. 4) may be due to reworking. The acid-resistant residues in the lower half of the investigated beds are very rich in fine-grained mica, the amount of which decreases upwards. Mica has in general the same size as the most flattened chitinozoan specimens, which are interpreted here as reworked material from much older deposits. These chitinozoans were washed out of more argillaceous older layers and deposited into younger sediments (below 271.4 m) in the same way as small flakes of mica. This statement is supported by the fact that in the Soovälja (K–1) core all specimens not common in beds of this age are at the same time flattened and very rare.

K-BENTONITE MINERALOGY AND GEOCHEMISTRY

The Soovälja (K–1) core that penetrates the crater-filling sequence in the Kärdla impact structure includes approximately 140 m of carbonate rocks from the Upper Ordovician Haljala and Keila stages (Appendix 1, sheets 3–6). Twenty-seven K-bentonite beds ranging from 2–40 cm in thickness are found within this section (Appendix 1, sheets 4, 5). The thickest bed (173.0–173.4 m) occurs on the base of the Keila Stage and can be correlated with the widespread Kinnekulle K-bentonite (Pl. 1, fig. 4) of Baltoscandia (Bergström *et al.* 1995). Here, additional information on clay mineralogy, whole-rock major and trace element geochemistry and biotite geochemistry is reported. These data are applied to stratigraphic and tectonomagmatic models in order to further constrain the nature and setting of ash beds.

Clay mineralogy

With few exceptions, all Lower Palaeozoic K-bentonites are characterized by a clay matrix that consists chiefly of mixed-layer illite-smectite (I-S) with lesser amounts of kaolinite and mixed-layer chlorite-smectite (Kolata *et al.* 1996; Huff *et al.* 1997). These clays are seldom found in abundance in other Lower Palaeozoic sedimentary deposits, hence, clay mineral identification has become a useful means of establishing the volcanogenic identity of K-bentonite beds. Other methods of establishing their origin include petrographic identification of primary volcanic minerals such as euhedral zircon, apatite, biotite, sanidine, plagioclase, beta-form quartz, and various amphiboles and pyroxenes (Haynes 1994; Bergström *et al.* 1997; Huff *et al.* 1998).

Powder X-ray diffraction (XRD) scans of the clay minerals in several Soovälja (K–1) beds were made in order to evaluate their suspected volcanogenic origin. Clay samples were prepared for XRD analysis by separation of the <2 μm and <0.2 μm size fractions in an aqueous suspension. The clay suspensions were applied to glass substrates by the pipette method and allowed to dry at room temperature to achieve oriented clay aggregates. Air-dried and ethylene glycol solvated slides were scanned from 2° to 32°2Θ on a Siemens D-500 diffractometer with Cu *K*α radiation at a scan rate of 0.2°2Θ/min at the Department of Geology, University of Cincinnati, and from 2° to 40°2Θ on a Dron 3M diffractometer with Cu *K*α radiation in Estonia, with a step size of 0.02°2Θ and a count time of 3 s. Quantitative estimation of illite and smectite in mixed-layer I-S was made using the computer program NEWMOD (Reynolds 1985) and the interpretive diagrams of Środoń (1984) and Moore & Reynolds (1997).

Powder X-ray diffraction scans (Figs 5, 6) indicated that all K-bentonites are characterized by interstratified I-S with R1 to R2 ordered interstratification. The appearance of 14.2, 7.1 and 3.53 Å peaks in the <2 μm fraction of some K-bentonite samples (Figs 5, 6) suggests that there has been some mixing of detrital muds with the ash. Computer modelling of ethylene glycol solvated patterns measured at the University of Cincinnati indicates that the illite component constitutes as much as 87% of the in R2 ordered mixed-layer I-S. However, experimental evidence from the University of Tartu suggests the illite content in I-S varies from 70 to 75% when computed following the methods of Moore & Reynolds (1997) whereas the ordering of interstratification is intermediate between R1 and R2 (Fig. 7). XRD pattern modelling using NEWMOD calculations of the same patterns (Fig. 8) obtained the best fit between calculated and measured pro-

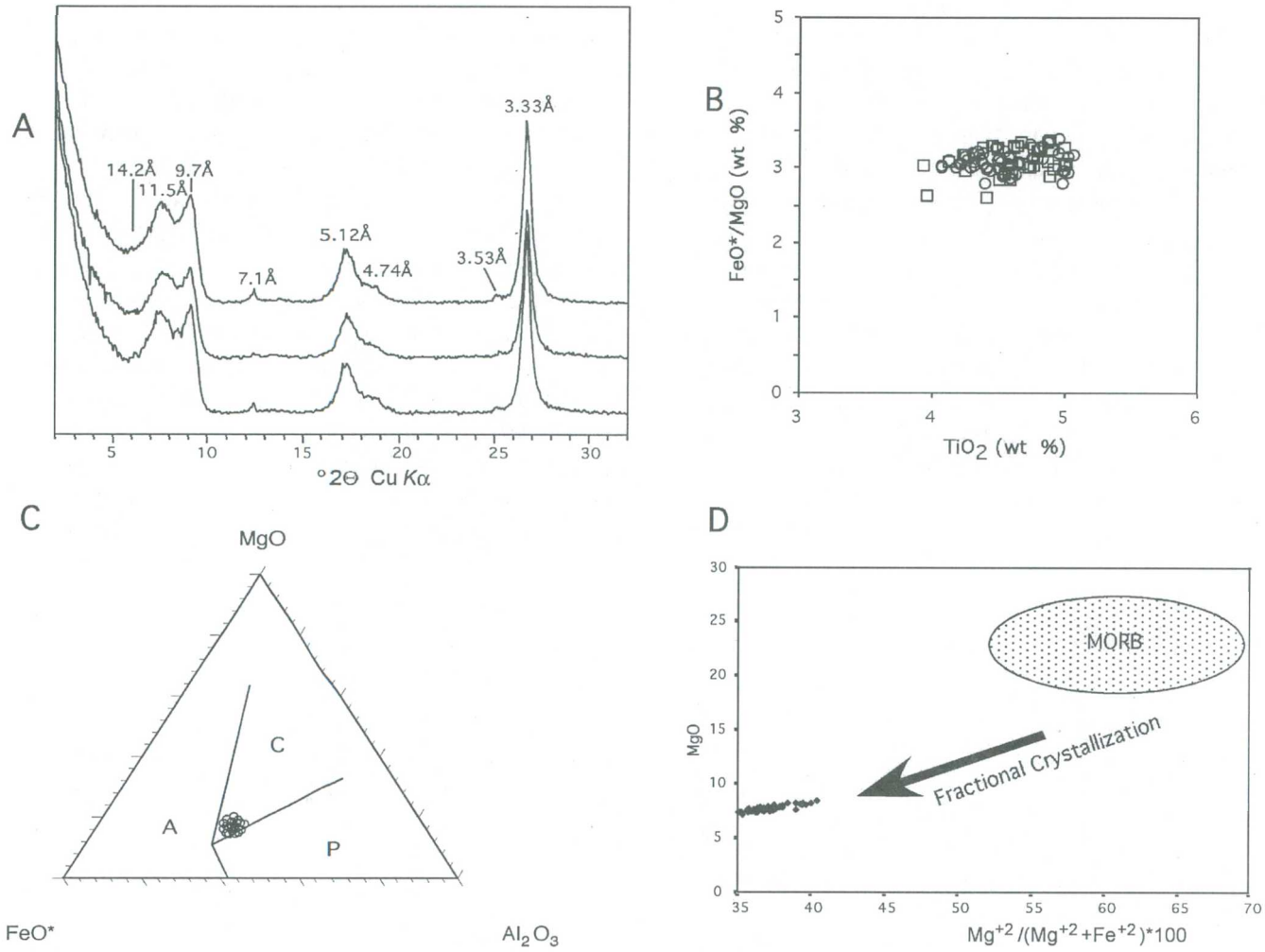

Fig. 5. (A) Powder XRD patterns of ethylene glycol saturated samples. (B) Bivariate plot of Ti vs Fe/Mg oxides. Circles represent Soovälja (K–1) and Viki biotites and squares represent Kinnekulle samples from Mossen, Sweden. (C) Ternary plot of biotites after the method of Abdel-Rahman (1994). A = anorogenic alkaline suites, P = Peraluminous S-type suites and C = calc-alkaline orogenic suites. FeO* = total Fe as FeO. (D) Plot of $Mg^{+2}/(Mg^{+2}+Fe^{+2})*100$ vs. MgO showing the highly evolved nature of the source magma for the Soovälja (K–1) and Viki biotites.

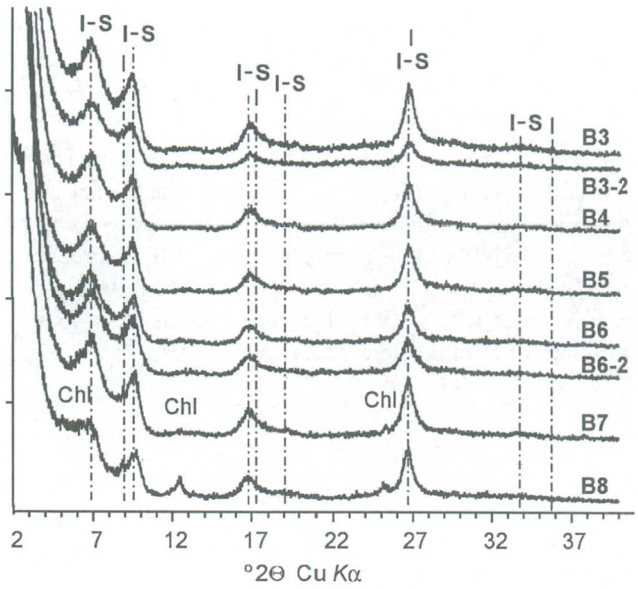

Fig. 6. Representative XRD patterns of the glycolated oriented aggregates of K-bentonite clay from the Soovälja (K–1) core analysed at the University of Tartu. Samples: B3 – depth 173.2 m, < 2 μm; B3-2 – 173.2 m, < 0.2 μm; B4 – 174.6 m, < 2 μm; B5 – 177.4 m, < 2 μm; B6 – 179.1 m, < 2 μm; B6-2 – 179.1 m, < 0.2 μm; B7 – 181.4 m, < 2 μm; B8 – 185.3 m, < 2 μm. Legend: I-S – illite-smectite, I – illite, Chl – chlorite. Samples B3 and B3-2 represent the Kinnekulle bed at the Haljala–Keila Stage boundary, B4 is a sample of the Sinsen K-bentonite complex (Jõhvi Substage of the Haljala Stage) and samples B5–B8 represent individual beds of the Grefsen complex (Idavere Substage of the Haljala Stage). See Bergström *et al.* (1995) for details.

files for I-S with 72% illite in R1.5 ordered interstratification ($N = 3...12$). The reasons for these differences in expandability estimates are not known yet. Illite-smectite ordering and the related percentage of the illite component in both cases do not appear to follow any systematic pattern of distribution with respect to the stratigraphic position or facies within the sediments investigated in the Kärdla crater.

While some studies have shown a general relationship between the degree of burial metamorphism and illite percentage in I-S, there is no evidence of low-grade metamorphism or a deep burial history in these beds. By comparison, anchizonal metamorphism converted Silurian K-bentonites to I-S with about 95% illite in the Southern Uplands (Merriman & Roberts 1990) and in north Yorkshire (Romano & Spears 1991), and maximum temperatures in these areas are estimated to have been on the order of 300 °C. Illitization reactions in I-S have been closely linked to periods of tectonism and basin deformation during which gravity-driven fluids mobilize available cations and increase their activity with respect to clay mineral structural exchange sites (Elliott & Aronson 1987). The K–Ar ages of the K-bentonite clay <0.2 μm fractions of the Kinnekulle bed in the northern Baltic basin vary between 357 and 384 Ma (K. Kirsimäe, unpublished data).

This period coincides roughly with the closure of the Iapetus Ocean and the Caledonian orogeny, when these sediments experienced the maximum burial under the Middle to Late Devonian sediments deposited in a Caledonian foreland basin. However, the thermally very immature state of the organic material of Palaeozoic sediments in the northern part of the Baltic basin suggest that these beds were not deeply buried (< 1.5 km) and/or heated above

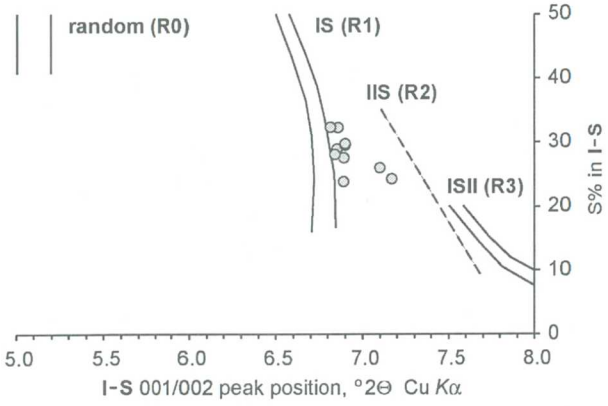

Fig. 7. Ordering type of the illite-smectite (I-S) interstratifications in the studied samples. Modified after Środoń (1984).

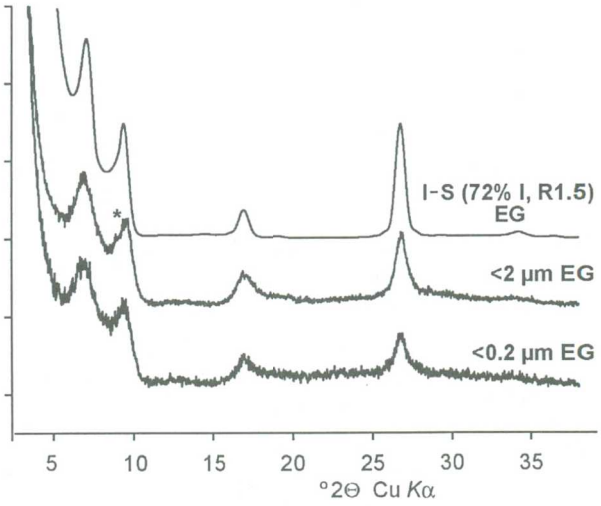

Fig. 8. XRD pattern of glycolated < 2 and < 0.2 μm fractions of the sample (depth 173.2 m) from the Kinnekulle bentonite bed of the Soovälja (K–1) core in the Kärdla crater, and a NEWMOD modelled pattern of R1.5 ordered I-S with 72% illite layers. Asterisk marks the illite and/or highly illitic I-S (> 95% illite) impurity in the < 2 μm fraction. EG – ethylene glycol solvated.

Table 1. Chemical composition of biotites of the Kinnekulle K-bentonite bed (173.0–173.4 m) of the Soovälja (K–1) and Viki cores by electron microprobe analyses

	*N**	SiO_2	Al_2O_3	FeO*	MgO	Al_2O_3	K_2O	Na_2O	MnO	TiO_2	CaO	SUM
Average	89	34.73	16.55	23.34	7.66	16.55	8.61	0.43	0.29	4.56	0.01	96.17
Maximum	89	35.53	16.97	25.05	8.43	16.97	8.96	0.52	0.44	5.29	0.05	98.30
Minimum	89	33.44	16.01	21.25	7.16	16.01	8.23	0.37	0.14	4.07	0.00	93.50
Median	89	34.80	16.55	23.37	7.62	16.55	8.60	0.42	0.29	4.51	0.01	96.17

*N** number of measurements; FeO* = total Fe as FeO.

50–80 °C (Talyzina *et al.* 2000; Viira *et al.* 2001). Illitization reactions are extremely sluggish (Lanson & Meunier 1995), however, and under very low-grade metamorphic or diagenetic conditions other geochemical and sedimentological factors are more likely to play a decisive role in controlling smectite-to-illite transformation in these K-bentonites.

Biotite geochemistry

Biotite was analysed by electron microprobe for the major oxides (Table 1). The data were used to calculate a widely applied fractionation index known as the magnesium number (Tatsumi & Eggins 1995). The magnesium number, expressed as $Mg^{+2}/(Mg^{+2} + Fe^{+2})*100$, is a useful indicator of the degree of crystal fractionation, assuming a mantle-derived primary magma. Initial magma generated from the mantle has a magnesium number of about 90. In early stages of crystallization, magnesium-rich minerals such as olivine and pyroxene crystallize out, so that differentiated magmas have a lower magnesium number. Magnesium and iron values in biotite and amphibole are only slightly higher than the coexisting melt (Hess 1989), so, the biotite composition is a reflection of the melt composition. Typical subduction zone magmas have a magnesium number around 60–70 (Hess 1989). Samples from the Soovälja (K–1) core have magnesium numbers between 35 and 42, indicating a highly fractionated magma (Fig. 5D).

Oxide weight percentages are between 93 and 99% of the total for biotite samples. Most of the variation accounting for the differences in weight percentages between samples was in the SiO_2 content. A small portion of the biotite crystal consists of volatiles such as water and fluorine, which accounts for some of the missing weight in the microprobe totals. In unaltered biotites, the K_2O concentration is approximately 9%. K_2O values for the biotite samples were between 8.3–8.9 wt%. Even in grains with low K_2O values, concentrations of other elements, particularly TiO_2, Al_2O_3, FeO* and MgO remained consistent within a sample, between altered and unaltered biotites. A bivariate plot of TiO_2 vs. FeO*/MgO (Fig. 5B) compares the Soovälja (K–1) and Viki core (from Saaremaa Island) biotite compositions with the Kinnekulle K-bentonite from Mossen, Sweden (Bergström *et al.* 1995). The beds are virtually indistinguishable and confirm the chemostratigraphic identification of the Kinnekulle bed in the Estonian cores. Figure 5C shows a ternary plot of Al_2O_3, FeO*and MgO. This plot is based on the data of known volcanic compositions from 26 separate volcanoes and 329 biotite samples representing alkaline, calc-alkaline and peraluminous magma sources (Abdel-Rahman 1994). Al_2O_3, FeO and MgO were used because they are interchangeable in the octahedral cation site of biotite. Alkaline magmas are iron-rich, due to crystal fractionation and the fact that iron oxides and iron-titanium oxides form late in the fractionation sequence (Abdel-Rahman 1994). Calc-alkaline magmas are relatively magnesium-rich as a result of the increased water content that allows iron oxides and iron-rich amphiboles to crystallize early, removing iron from the system. Peraluminous magmas are enriched in aluminium due to partial melting of the continental crust, with abundant aluminium-rich minerals. Most biotite samples of the Soovälja (K–1) core K-bentonites plot within the calc-alkaline magma source based on this plot.

Trace element geochemistry

The use of immobile trace elements in altered and unaltered volcanic rocks to discriminate compositions erupted in different tectonic settings is well known (Pearce & Cann 1973; Winchester & Floyd 1977; Wood 1980; Pearce *et al.* 1984; Harris *et al.* 1986). Discrimination diagrams, which are derived empirically from many analyses of lavas, must be cautiously applied to the interpretation of altered pyroclastics, however, and with due consideration for the possible effects of phenocryst fallout and other lateral changes on the whole-rock composition. These problems are minimized in the case of rapidly formed vitric ash beds since pyroclastic glass tends to maintain a constant composition with distance from its source (Sarna-Wojcicki *et al.* 1987).

Preliminary studies of high field strength elements in K-bentonites (Merriman & Roberts 1990; Roberts & Merriman 1990; Huff *et al.* 1991) indicate that they largely behave as immobile elements and do, within the range of sensitivity offered by empirical discrimination diagrams, preserve characteristics of the original magma. They can thus be useful in reconstructing the setting of subduction-related island arc and plate margin volcanism. While not providing conclusive proof of origin, immobile element compositions of K-bentonites can reveal important information concerning both the compositional characteristics of the parent magmas and the probable tectonic environment in which the eruptions occurred. Roberts & Merriman (1990) studied the mineralogy and trace element geochemistry of one Ordovician (Caradoc) and three Cambrian K-bentonites from the Welsh Basin, and concluded that they all were derived from felsic magmas in a within-plate tectonic setting. In a companion study (Merriman & Roberts 1990) of Upper Ordovician–Lower Silurian K-bentonites from the Southern Uplands they found evidence that the tectonic setting of the source volcanoes changed from an ensialic arc transitional to a back-arc setting and involved attenuated sialic lithosphere and depleted mantle in the generation of the parent magma. We report here on the extension of these studies to include Ordovician K-bentonites in the U.K. ranging in age from Llanvirn to Ashgill and representing marine shelf and basin depositional environments on both the northwest and southeast margins of the Lower Palaeozoic Iapetus prior to its closure. For comparative purposes we have included in our data the Caradoc K-bentonite sample BRM–620 studied previously by Roberts & Merriman (1990).

On the magmatic discrimination diagram of Winchester & Floyd (1977) the Soovälja (K–1) K-bentonite sample plots as a calc-alkaline trachyandesite (Fig. 9; Table 2). The sample has an Nb/Y ratio less than 1.0, which is characteristic of subalkaline magmas, whereas peralkaline magmas tend to have Nb/Y ratios greater than 2.0 (Winchester & Floyd 1977). Huff *et al.* (1993) showed that Llanvirn–Llandeilo samples in Ordovician K-bentonites of Great Britain have a slightly less fractionated character than the Caradoc–Ashgill samples. The latter show a higher Nb/Y ratio generally considered to be characteristic of alkaline suites (Pearce & Cann 1973).

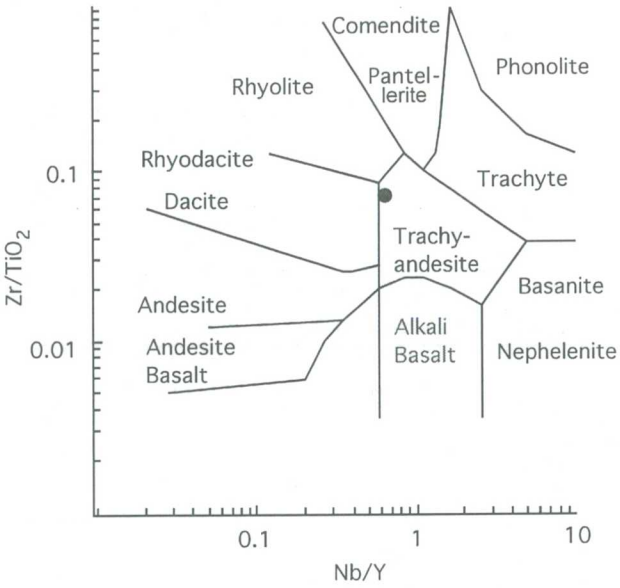

Fig. 9. Magmatic discrimination diagram after Winchester & Floyd (1977) based on whole-rock trace element data from the Kinnekulle bed (173.0–173.4 m) in the Soovälja (K–1) core.

Table 2. Major and trace element composition of the Kinnekulle K-bentonite bed (interval 173.0–173.4 m) in the Soovälja (K–1) core

Oxide (wt%)		Element (ppm)											
SiO_2	55.30	Ag	0.5	Cr	10.0	P	550.0	Tl	0.2	Pr	4.10	Tm	0.30
Al_2O_3	20.20	As	0.6	Cs	9.0	Pb	2.0	U	5.3	Nd	18.80	Yb	1.60
CaO	0.60	Au	1.0	Cu	2.9	Rb	143.0	V	17.0	Sm	4.10	Lu	0.19
MgO	4.34	B	490.0	Ga	21.0	S	320.0	W	9.0	Eu	0.42	Pt	10.00
Na_2O	0.44	Ba	200.0	Hf	5.5	Sb	0.2	Y	25.0	Gd	4.20	Pd	1.00
K_2O	6.49	Be	2.0	Li	190.0	Sn	2.0	Zn	11.0	Tb	0.70	Hg	8.00
Fe_2O_3	2.74	Bi	0.6	Mo	2.0	Sr	100.0	Zr	170.0	Dy	4.70	Sc	6.00
TiO_2	0.22	Cd	0.2	Nb	22.0	Ta	1.0	La	11.1	Ho	0.88	Mn	38.00
SUM	90.33	Co	5.0	Ni	1.0	Th	12.0	Ce	28.2	Er	2.00		

Analysed by the instrumental neutron activation method; Fe_2O_3 – total Fe calculated as Fe_2O_3.

Conclusions

The Soovälja (K–1) core from the Kärdla impact structure preserves a remarkable record of Middle Ordovician explosive volcanism in the form of 27 distinct ash beds. These beds appear to be the product of a highly evolved magmatic source, most likely involving crustal contamination of partial melting of the collision margin. The magnesium number derived from biotite analyses serves as a useful proxy for whole-rock data and provides further evidence of the felsic nature of the source magma. Trace element discrimination diagrams support this conclusion. Clay minerals present are dominantly R2 ordered illite-smectite and suggest that these rocks have not been subjected to extensive burial diagenesis or low-grade metamorphism, as is seen elsewhere throughout the East European Platform.

CHARACTERISTICS OF VOLCANISM

Interbeds of K-bentonites and terrigenous claystone (interval 173.10–255.98 m) were investigated in the Soovälja (K–1) drill core (Table 3; Appendix 1, sheets 4, 5), whereas a large number of K-bentonites, 1–40 cm thick, were established between the depths of 177.0 and 187.0 m. These K-bentonites correlate with the Grefsen K-bentonite complex (Bergström *et al.* 1995). The Kinnekulle K-bentonite (Pl. 1, fig. 4) in the Soovälja core lies at 173.0–173.4 m, above the Sinsen K-bentonites (174.5 and 174.8 m).

Argillaceous interbeds are lithologically variable, containing usually light grey, in places yellowish-grey 3–12 cm thick K-bentonite in the lower part and dark greenish-grey argillaceous marl, claystone or K-bentonite in the 2–10 cm thick upper part (see Table 3). Some beds consist of only K-bentonite or grey claystone covered by limestone.

Main minerals

Main minerals in the bulk sample were identified by X-ray diffractometry (XRD). On the basis of the main mineral association and previous experience, the samples were further divided into volcanogenic K-bentonites and terrigenous claystones. K-bentonites (14 samples) were considered to consist of illite-smectite, often with authigenic K-feldspar. In two K-bentonite samples (at depths of 198.25 and 203.03 m) traces of chlorite were found.

The six samples containing illite and quartz, less potassium feldspar, chlorite and calcite, were treated as terrigenous claystone. Five samples were identified as mixture of terrigenous and volcanic material.

Sanidine composition

After washing out fine clay material, the 0.04–0.1 mm fraction was separated from rest of the sample by sieving. The sanidine composition in it was studied by XRD following the method of Orville (1967) and adjusted for bentonites (Kiipli & Kallaste 2002). Previous experience has shown that this fraction contains abundantly pyroclastic grains.

The coarsest K-bentonite fractions contain sanidine with a wide $\bar{1}$ reflection, possibly giving evidence about variable sanidine composition. Such sanidine cannot be used for reliable correlations. Sanidine containing 25.1 mol% $NaAlSi_3O_8$ was detected in the sample at 173.1 m (K-bentonite at 173.0–173.4 m; Table 3 and Appendix 1, sheet 4), which proves correlation of this level with the Kinnekulle bed at the lower boundary of the Keila Stage (Kiipli & Kallaste 2001). Sanidine with a well measurable sharp reflection (containing 22.5 mol% $NaAlSi_3O_8$) was identified also in another bed, at a depth of 177.35 m (Table 3). On the basis of the sanidine composition this bed can potentially be determined in other sections as well.

Comparison of the chemical composition of bentonite and terrigenous claystone

Some trace and major elements were analysed by X-ray fluorescence (XRF) spectrometry (Fig. 10; Appendix 11). Potassium is a most important diagnostic major element in bentonites (Kiipli *et al.* 1997). The K_2O content is below 5% in bentonites consisting mainly of smectite or kaolinite, 5–8% in K-bentonites containing mostly illite-smectite and above 8% in K-bentonites rich in authigenic K-feldspar. In altered volcanic ashes, dominated by authigenic K-feldspar, the K_2O content ranges from 12 to more than 15%, in argillites and acidic magmatic rocks commonly from 3 to 6%. In the Soovälja (K–1) core altered volcanic ash beds contain 5–10.5% K_2O, being therefore typical K-bentonites. Higher K_2O contents are registered in beds with maximum TiO_2 contents indicating less evolved source magma (Fig. 10). This K–Ti correlation suggests that the sedimentary-diagenetic environment in less acidic volcanic ash favours fixation of K_2O into the K-bentonite. The K_2O content of marl- and claystone is close to that of K-bentonites but considerably higher than in typical argillites. This supports the suggestion that terrigenous material in the Soovälja (K–1) core is largely reworked from volcanic ash.

Comparison of the distribution of elements in K-bentonites and claystones revealed higher concentrations of several elements in terrigenous (also mixed with K-bentonite) samples: CaO, Mn and Sr probably bound into carbonate minerals, and Fe_2O_3, Zn,

Table 3. K-bentonite and claystone or marl interbeds in the Soovälja (K–1) core (after field-description by Kalle Suuroja)

Sample	Sample depth (m)	Complexes by Bergström *et al.* 1995	Bed characteristics					
			No. on core box	Interval (m)	Thickness (m)	Thickness (in metres) and description of the upper (U), middle (M) and lower (L) parts		Upper / lower contact
K–1–1	173.10	KK*		173.00–173.40	0.4	U: 0.05 L: 0.35	Dark grey marl and claystone Light grey microbedded bentonite	Wavy, distinct / sharp, smooth
K–1–2	177.22	Grefsen K-bentonite complex	1	177.20–177.24	0.03–0.04		Greenish-grey marl and claystone	Both wavy, distinct
K–1–3 K–1–4	177.35 177.45		2	177.30–177.45	0.15	U: 0.08 L: 0.07	Dark grey, argillaceous bentonite Light grey microbedded bentonite	Wavy, indistinct / indistinct
K–1–5	177.62		3	177.60–177.64	0.04		Light greenish-grey, thin-bedded bentonite	Both sharp, smooth
K–1–6 K–1–7	177.90 178.00		4	177.85–178.00	0.15	U: 0.07 L: 0.08	Greenish-grey, argillaceous bentonite Light grey bentonite	Distinct / sharp, smooth
K–1–8	178.83		5	178.80–178.83	0.02–0.03		Light to dark grey argillaceous marl	Both wavy, distinct
K–1–9	178.90		6	178.90–178.95	0.05	U: 0.02 L: 0.03	Light grey bentonite Dark greenish-grey argillaceous marl	Sharp / sharp, smooth
K–1–10 K–1–11	179.05 179.10		7	179.00–179.15	0.15	U: 0.06 M: 0.05 L: 0.04	Greenish-grey argillaceous bentonite Light grey bentonite Greenish-grey argillaceous marl	Indistinct, wavy / distinct
K–1–12	180.32		8	180.20–180.35	0.15	U: 0.1 L: 0.05	Dark greenish-grey argillaceous marl, upper 0.02 m hard Light grey bentonite	Distinct / sharp, wavy
K–1–13	180.90		9	180.85–180.90	0.05		Light to dark greenish-grey argillaceous marl with clasts	Both distinct
K–1–14	181.02		10	181.00–181.08	0.05–0.08		Dark greenish-grey argillaceous marl and claystone	Both indistinct, wavy
K–1–15	181.40		11	181.35–181.45	0.1	U: 0.04 L: 0.06	Dark greenish-grey argillaceous marl Light grey bentonite	Indistinct, wavy / sharp
K–1–16	181.70		12	181.67–181.70	0.03		Greenish-grey sandy bentonite with clasts	Both indistinct
K–1–17	181.90		13	181.85–181.90	0.05		Marl and claystone, clasts on boundaries	Both indistinct
K–1–18	182.60		14	182.50–182.70	0.2	U: 0.07–0.1 L: 0.1	Light grey silty argillaceous marl Dark grey wavy thin-bedded argillaceous bentonite	Sharp, smooth / indistinct, wavy
K–1–19	185.32		15	185.30–185.33	0.03		Light grey bentonite, in the lower part clasts	Wavy / sharp
K–1–20	186.40		16	186.40–186.41	0.01		Light grey bentonite	Both distinct
K–1–21	197.21		17	197.20–197.22	0.02		Dark grey argillaceous claystone and bentonite	Indistinct / sharp
K–1–22 K–1–23	198.15 198.25		18	198.10–198.30	0.2	U: 0.08 L: 0.12	Dark grey argillaceous marl and claystone Light grey bentonite	Sharp / sharp, smooth
K–1–24	203.03		19	203.00–203.05	0.05		Dark grey bentonite	Both distinct, wavy
K–1–25	255.98		20	255.95–256.00	0.05	U: 0.02 L: 0.03	Greenish-grey argillaceous marl Mottled yellow bentonite	Indistinct / sharp, smooth

KK* Kinnekulle K-bentonite.

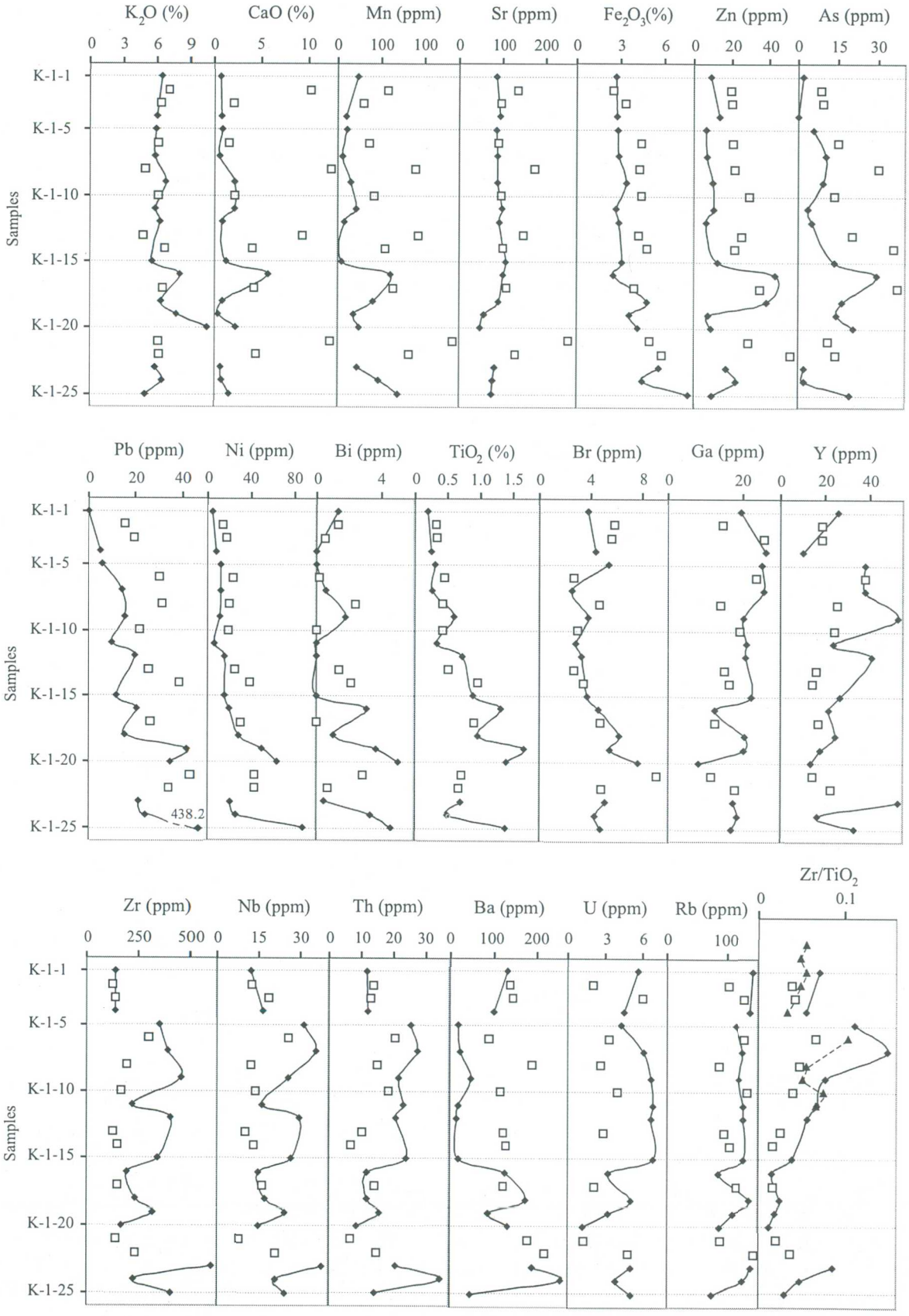

Fig. 10. Distribution of some trace elements and major components of K-bentonite beds in the Soovälja (K–1) core. Filled rhombs represent pure volcanogenic K-bentonites, empty quadrangles reworked terrigenous claystone or marl and mixed volcanogenic-terrigenous samples. Curves join the samples belonging to the same magmatic cycle. Triangles denote samples from the Röstånga section (Bergström *et al.* 1997). The samples succession see in Table 3.

As, Pb and Ni common in pyrite and other sulphide minerals. Possibly some initial organic matter existed in terrigenous sediments, generating anoxic conditions favouring sulphide formation. Also, higher concentrations were registered in lower layers both in bentonites, and marl- and claystone showing generally parallel trends. Remarkable is a high Pb content (438.2 ppm) in the lowermost K-bentonite at 255.95–256.0 m (Fig. 10; Appendix 11). Probably, the source of sulphide elements was the volcanic ash itself, but better preservation conditions in terrigenous interbeds caused differences in concentrations of elements.

Immobile trace elements Ti, Ga, Zr, Nb, Th and Y, too, have undergone changes during sedimentary reworking of volcanic material. The Ti content is slightly higher in terrigenous marl- or claystone than in close-lying bentonites in the upper part of the section. The opposite relation can be traced in the lower part of the section. This behaviour evidences about the intermediate Ti concentration in terrigenous admixture, causing an increase in lower volcanogenic concentrations and decrease in higher volcanogenic concentrations in the mixing process. Bromine distribution closely resembles that of Ti. Being a halogen, Br could be expected to be highly mobile in the sedimentary environment, but here it has retained the average level of magmatic rocks correlating well with immobile Ti. Incompatible trace elements Ga, Zr, Nb, Th and Y have generally lower concentrations in marl- or claystone samples. Concentrations of mobile (Rb, U) and immobile elements correlate well in the Soovälja (K–1) core. The content of immobile elements is lower in terrigenous sediments.

Barium is relatively stable (between 100 and 200 ppm) in marl or claystone samples but shows a peculiar distribution in bentonites. In the three lower samples (Fig. 10; Appendix 11), Ba has positive correlation with immobile Th, higher in section negative correlation with Th. Correlation of Ba with other incompatible elements is similar but less clear.

Source volcanoes

The composition of source magma in K-bentonites, which has altered fundamentally in sedimentary processes, cannot be determined from the content of main components. An alternative way is to use ratios of immobile trace elements. Following the approach of Pearce & Cann (1973), Batchelor & Weir (1988) used Ti, Zr and Nb ratios on their ternary diagram: Ti is higher in basic, Zr in acidic and Nb in felsic rocks. Based on this diagram, most of Soovälja (K–1) K-bentonites fall to the rhyolite and dacite field, but four K-bentonites (depths 181.67–181.7, 182.5–182.7, 185.30–185.33 and 186.40–186.41 m) can be identified as andesites. Plot of the Zr/TiO_2 ratio (Fig. 10) against the bed succession in the Soovälja (K–1) core revealed three magmatic cycles: (1) at 256.00–198.10 m, (2) at 186.41–177.60 m and (3) at 177.45–173.00 m. These cycles began with source magma of intermediate composition, which changed gradually towards acidic magma. It is possible that the earliest record of the first magmatic cycle in Estonia is an authigenic K-feldspar-rich bed in the uppermost part of the Kukruse Stage (recognized by J. Nõlvak in 1967; see Nõlvak 2002a), characterized by andesitic source magma. However, this bed is not present in the Soovälja (K–1) core. Changes within cycles probably refer to fractional crystallization and concentration of acidic material in the upper part of the magma chamber. Compositional shifts at cycle boundaries can be explained by the appearance of new volcanic sources, rise of fractionated magma from the lower parts of the magma chamber, or melting and intrusion of new portions of surrounding rocks. It is difficult to decide which of these versions is true. Differences between the cycles (opposite behaviour of Ba in the first magmatic cycle compared to the second and third cycles; notably higher maximum values of Zr and Nb and a considerable stratigraphic interval without bentonites between the first and the second cycle) suggest the probable formation of a new volcanic source at the beginning of the second cycle. The beginning of the third magmatic cycle is characterized by a big drop in the contents of Zr, Nb, Th, and rise in Ba. No great changes are observed in the Ti content. Two studied K-bentonites from this interval contained sanidine with a well measurable composition contrary to the lower beds where sanidine composition was variable. All these features favour again the hypothesis of a new volcanic source also at the beginning of the third cycle.

The Kinnekulle bed in Estonia and K-bentonite beds from the upper part of the Idavere Substage of the Haljala Stage contain among volcanic phenocrysts much of garnet (almandine; Vingisaar & Murnikova 1973). Similar in this respect volcanic rocks are well known from the Caradoc of the Lake District area in England (Fitton *et al.* 1982). Garnet is a rare phenocryst in volcanic rocks; for example, it is not mentioned in two review studies on recent volcanic rocks (Ewart 1979, 1982). Therefore, the presence of almandine in volcanic rocks of both mentioned areas strongly speaks in favour of the same source. Volcanoes were most probably located under the North Sea in the area where elongation of the Lake District–Southeast Ireland Ordovician island arc (Fitton *et al.* 1982) crosses the Kinnekulle ash distribution axis (Huff *et al.* 1996). Unusually great thickness of the Grefsen K-bentonites

at Röstånga in southernmost Sweden (Bergström *et al.* 1997) points to the more southerly location of the source for the second volcanic cycle (uppermost part of the Idavere Substage).

Comparison with the Röstånga section

Bergström *et al.* (1997) described Ordovician K-bentonites in the Röstånga section in southernmost Sweden and correlated them with some probability with the K-bentonites formerly studied from the Baltoscandian region (Bergström *et al.* 1995). The lower part of the Röstånga section was correlated with the upper part of the Grefsen K-bentonite complex. The Zr/TiO_2 ratio obtained from the table by Bergström *et al.* (1997) reveals a change from the second to the third magmatic cycle similar to that in the Soovälja (K–1) core (see Fig. 10). This confirms the correlation of sections in Bergström *et al.* (1997), although exact bed-by-bed correlations are not possible.

PHYSICAL PROPERTIES

A total of 92 samples from the Soovälja (K–1) core were measured for their physical properties in the 1990s (Appendix 12). Densities, porosity, magnetic, electrical and thermal properties were investigated mostly in the laboratories of the Geological Survey of Finland and Research Institute of Earth's Crust of St. Petersburg University. For detailed description of the methods and techniques, see Järvimäki & Puranen (1979), Prijatkin & Poljakov (1983) and Puranen & Sulkanen (1985). The results and interpretations are published in Jõeleht (1995), Plado *et al.* (1996), Puura *et al.* (2000a) and outlined below.

Most of the samples were taken from the lower part of the core (Fig. 11, Appendix 12): 55 from the fractured (588.5–815.2 m) and strongly brecciated basement (522.8–588.5 m), 32 from the crystalline- and sedimentary-rock-derived allochthonous breccias (301.2–522.8 m) and 5 from the post-impact sediments (24.0–301.2 m; see also Appendix 1, sheets 2–15). The lower quarter of the crystalline-rock-derived allochthonous breccias (471.0–522.8 m; 23 samples), i.e. granitoid-rich polymict breccias consisting of small-size fragments, has been sampled more densely than the uppermost part. The upper, sedimentary-rock-rich allochthonous breccias consist of large clasts that are believed to reflect mainly the impact target properties.

The grain density of the rocks of the Soovälja (K–1) core is fairly variable between lithological units (Fig. 11). Generally, density is inversely proportional to the porosity, and proportional to the compressional (P-wave) velocity and electric resistivity. The post-impact limestones have mean grain (δ_g) and water-saturated (δ_w) densities of 2690 and 2510 kgm^{-3} (Table 4), respectively, which are comparable to densities of limestones and marls from other areas of Estonia (Shogenova & Puura 1998; Jõeleht & Kukkonen 2002). However, in the Soovälja (K–1) core, densities tend to decrease towards the lowermost Ordovician part of the sequence due to an increase in the clay content. All the impacted rocks show low densities compared to the unshocked basement of Hiiumaa Island (Plado *et al.* 1996). It is notable that δ_g is relatively similar in all three varieties of breccias (Fig. 11 and Table 4), but δ_w shows much larger variations, which are mainly due to varying porosities. Crystalline- and sedimentary-rock-derived allochthonous breccias and strongly brecciated basement have the lowest δ_w values that are more variable in the allochthonous sequence (Table 4). The fractured basement (588.5–815.2 m) shows an increase in δ_w with depth from the values of about 2400 up to about 2550 kg m^{-3}. Part of the density increase is probably due to compaction, but another part could be related to gradual decrease in shock-induced stress and fracturing with depth. A slight downward increase in δ_g is observed as well, possibly having two simultaneous reasons: (1) the existence of numerous impact-produced microfractures that are non-penetrable to fluids at laboratory measurements and, therefore, give lower densities at depths closer to the impact centre; and (2) lower values may be due to post-impact metasomatic processes, which occasioned precipitation of low-density K-feldspar in impact-produced fractures.

The porosities of the post-impact limestones vary from 5.9 to 15.6% (Table 4), revealing the original sedimentary and diagenetic porosities. Relatively high porosity and wide fluctuation are characteristic of crystalline- and sedimentary-rock-derived allochthonous breccias and strongly brecciated basement. A very sharp boundary (588.5 m) exists in porosity, as well as in most of the other physical properties, between strongly brecciated and fractured basements. It shows that these two basement types have different impact-related origin. Because of the porosity increase with depth within the strongly brecciated basement (see Fig. 11) and presence of the sharp boundary, we suppose that the strongly brecciated basement has been mobile in respect to the fractured basement during the modification stage of cratering. There are also lithological differences above and below 588.5 m (see Fig. 11) that influence porosity and may have affected the cratering process as well. Compared to brecciated basement,

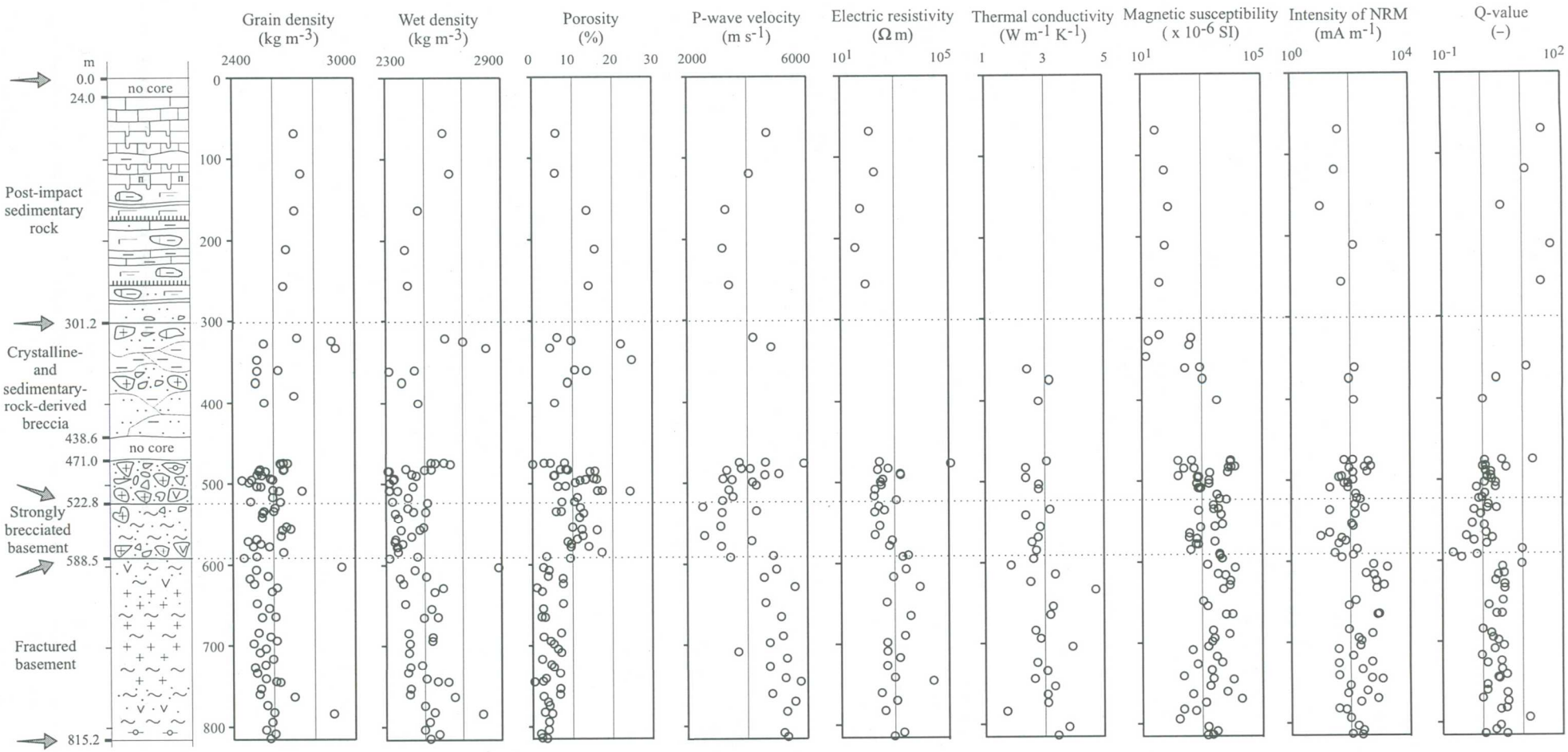

Fig. 11. Physical properties of the Soovälja (K–1) core. Refer to Appendix 1 for lithology.

Table 4. Statistical parameters of petrophysical properties of the Soovälja (K–1) core

Rock type	Interval (m)		δ_g (kg m^{-3})	δ_w (kg m^{-3})	ϕ (%)	v_P (m s^{-1})	ρ (Ω m)	λ (W m^{-1} K^{-1})	χ (× 10^{-6} SI)	NRM (mA m^{-1})	Q (-)
Post-impact sedimentary rock	0.0–301.2	*N*	5	5	5	5	5	0	5	5	5
		Avg.	2 690	2 510	11.1	3 740	99		50	50	25.3
		Med.	2 700	2 470	13.8	3 420	86		60	40	29.4
		Min.	2 648	2 405	5.9	3 210	36		30	10	2.9
		Max.	2 737	2 636	15.6	4 670	190		80	130	50.9
Crystalline- and sedimentary-rock-derived allochthonous breccia	301.2–522.8	*N*	32	32	32	17	12	8	32	20	20
		Avg.	2 600	2 420	10.9	4 080	10 470	2.7	2 440	150	2.9
		Med.	2 570	2 400	10.0	4 100	331	2.8	810	120	1.5
		Min.	2 444	2 145	0.1	3 190	171	2.4	14	20	0.7
		Max.	2 907	2 822	24.6	5 880	118 950	3.2	12 010	460	17.6
Strongly brecciated basement	522.8–588.5	*N*	16	16	16	7	7	6	16	14	14
		Avg.	2 590	2 410	11.1	3 280	390	2.7	2 080	110	1.7
		Med.	2 590	2 380	11.5	3 140	280	2.7	1 630	120	1.2
		Min.	2 474	2 345	5.9	2 520	179	2.4	370	10	0.4
		Max.	2 684	2 516	13.4	4 300	797	3.2	6 700	300	9.8
Fractured basement	588.5–815.2	*N*	36	36	38	19	19	19	39	39	39
		Avg.	2 580	2 510	4.3	4 950	3 080	3.0	3 990	370	2.8
		Med.	2 560	2 510	3.9	5 120	1 150	3.1	2 310	220	2.4
		Min.	2 454	2 318	0.4	3 440	314	1.7	170	30	0.2
		Max.	2 939	2 886	9.4	5 760	26 118	4.7	19 550	1 640	14.8

Physical properties: δ_g – grain density; δ_w – wet density; ϕ – porosity; v_p – P-wave velocity; ρ – electric resistivity; λ – thermal conductivity; χ – magnetic susceptibility; NRM – intensity of the natural remanent magnetization; Q – Koenigsberger ratio.

Statistical properties: *N* – number of measurements; Avg. – average; Med. – median; Min. – Minimum, Max. – maximum. Refer to Appendix 12 for individual values.

the mean porosity of the fractured basement is smaller (4.3%; Table 4) and varies in a much narrower scale. A trend towards decrease in porosity with depth is observed here. The primary reason for that is the decreasing shock pressure away from the impact centre. Secondary processes, such as hydrothermal activity and compaction, have also influenced the slope of the trend.

The average P-wave velocity in the post-impact sediments is generally low (3740 m s^{-1}; Table 4), decreasing downwards where limestones are richer in clay. P-wave velocities in the crystalline- and sedimentary-rock-derived allochthonous breccias vary largely from 3190 to 5880 m s^{-1}. High individual values are from the samples that contain bigger clasts of relatively unfractured rocks. Because of high porosities, the strongly brecciated basement shows low velocities (as low as 2520 m s^{-1}). Similarly to density and porosity, a depth-sensitive trend in P-wave velocity appears in the fractured basement (Fig. 11).

Electric resistivity of post-impact limestones is low (around 100 Ω m), whereas all the other rock types show higher values (Table 4). Only 12 measurements come from the lower part of allochthonous breccias. Therefore, one high value (118 950 Ω m; unfractured granitic clast at a depth of 476.5 m) has great influence on the mean resistivity of the interval, the median being as low as 346 Ω m. The strongly brecciated basement reveals distinctly lower values (Fig. 11) because of the smaller clasts sampled. Unlike other physical properties of the fractured basement, no distinct trend is observed in electric resistivity; the slightly higher values at dephts from 625 to 700 m may have lithological reasons. Compared to unshocked granitic rocks in the crater surroundings (about 60% of measurements revealed resistivities above the detection limit, 100 000 Ω m; see Plado *et al.* 1996), all the impacted rocks are good conductors. It is definitely due to a shock-induced increase in the porosity and, thus, in the fluid content of shocked rocks.

The thermal conductivities of crystalline- and sedimentary-rock-derived allochthonous breccias and strongly brecciated basement are all in the same range (Fig. 11), and are low in general. This can be explained with the porosity effect and K-feldspar-rich lithologies. The thermal conductivity of the fractured basement is getting close to typical values of granitic rocks elsewhere in Estonia (Jõeleht 1995). Only two measurements of thermal conductivity of

amphibolite samples are available. They both show unexpectedly low values (1.72 and 1.86 W m^{-1} K^{-1}) considering that the hornblende in amphibolites is replaced by thermally more conductive chlorite. The porosity of these samples is less than 5%. The reduced conductivity may be explained by the occurrence of Fe-rich chlorite, which has a lower value than usual in chlorite, and the small grain size of plagioclase. The sedimentary sequence has been studied in the neighbouring lithologically and petrophysically similar K–18 drill core (Jõeleht 1995). There, the decrease in thermal conductivity with depth (from about 3 W m^{-1} K^{-1} to 2.3 W m^{-1} K^{-1}) is due to high clay content in carbonate rocks, whereas the high values of resurge conglomerates (up to 4.2 W m^{-1} K^{-1}) can be attributed to the increased quartz content.

The magnetic susceptibility and intensity of the natural remanent magnetization (NRM) of post-impact sediments are typically low in limestones (Shogenova & Puura 1997, 1998). The Q-values (Koenigsberger ratio) of the sediments are fairly high, but as the low magnetic susceptibilities and NRMs are close to the detection limit, some of the high values may be artefacts and cannot be regarded as reliable. All the impacted rocks have low susceptibilities and NRM intensities, especially in comparison with unfractured varieties (see Plado *et al.* 1996). Depending on the samples (rich in clasts/matrix), the magnetic properties of allochthonous breccias are highly variable but generally similar to those of the strongly brecciated basement (Table 4). The low susceptibility values at 320–350 m are from the sedimentary clasts (Appendix 1, sheet 7). Mixing of crystalline rocks with dia- and paramagnetic sediments, higher porosity and post-impact processes (oxidation, formation of new magnetic phases) are the possible reasons for lower susceptibilities of allochthonous breccias and strongly brecciated basement compared to the fractured basement counterparts. The strongly brecciated basement reveals significantly lower NRM intensities and, therefore, lower Q-values than the fractured basement. Additionally to the above reasons, we note the possible impact-caused rotation of magnetization vectors that, on the sample level, gives low NRM values due to the randomizing. Magnetic susceptibility and NRM intensity of the fractured basement do not show significant depth-related trends. However, systematic changes in the palaeomagnetic behaviour as a function of depth are reported in Plado *et al.* (1996).

REFERENCES

Abdel-Rahman, A.-F. M. 1994. Nature of biotites from alkaline, calc-alkaline, and peraluminous magmas. *Journal of Petrology*, **35**, 525–541.

Ainsaar, L., Suuroja, K. & Semidor, M. 2002. Long-term effect of the Kärdla crater (Hiiumaa, Estonia) on Late Ordovician carbonate sedimentation. *Deep-Sea Research II: Topical Studies in Oceanography*, **49**, 1145–1155.

Batchelor R. A. & Weir J. A. 1988. Metabentonite geochemistry: magmatic cycles and graptolite extinctions at Dob's Linn, southern Scotland. *Transactions of the Royal Society of Edinburgh Earth Sciences*, **79**, 19–41.

Bauert, H. A., Männil, R. M. & Suuroja, K. A. 1987. O vremeni obrazovanija Kärdlaskogo kratera [On the age of the formation of the Kärdla crater]. In *Tezisy dokladov Vsesojuznoj meteoritnoj konferencii* [Abstracts of the All-Union meteorite conference]. Moskva, p. 48. [In Russian].

Bergström, S. M., Huff, W. D., Kolata, D. R. & Bauert, H. 1995. Nomenclature, stratigraphy, chemical fingerprinting, and areal distribution of some Middle Ordovician K-bentonites in Baltoscandia. *Geologiska Föreningens i Stockholm Förhandlingar (GFF)*, **117**, 1–13.

Bergström, S. M., Huff, W. D., Kolata, D. R., Yost, D. A. & Hart, C. 1997. A unique Middle Ordovician K-bentonite bed succession at Röstånga, S. Sweden. *Geologiska Föreningens i Stockholm Förhandlingar (GFF)*, **119**, 231–244.

Dunham, R. J. 1962. Classification of carbonate rocks according to depositional texture. In: *Classification of carbonate rocks* (Ham, W. E., ed.), *AAPG Memoirs*, **1**, 108–121.

Elliott, C. W. & Aronson, J. L. 1987. Alleghanian episode of K-bentonite illitization in the southern Appalachian Basin. *Geology*, **15**, 735–739.

Ewart, A. 1979. A review of the mineralogy and chemistry of Tertiary–Recent dacitic, rhyolitic and related salic volcanic rocks. In: *Trondhjemites, dacites and related rocks* (Barker, F., ed.). Elsevier, Amsterdam, 13–121.

Ewart, A. 1982. The mineralogy and petrology of Tertiary–Recent orogenic volcanic rocks: with special reference to the andesitic–basaltic compositional range. In: *Andesites* (Thorpe, R. S., ed.). Wiley, Chichester, 25–94.

Fitton, J. G., Thirwall, M. F. & Hughes, D. J. 1982. Volcanism in the Caledonian orogenic belt of Britain. In: *Andesites* (Thorpe R. S., ed.). Wiley, Chichester, 611–636.

Grahn, Y. & Nõlvak, J. 1993. Chitinozoan dating of Ordovician impact events in Sweden and Estonia. A preliminary note. *Geologiska Föreningens i Stockholm Förhandlingar (GFF)*, 115, **3**, 263–264.

Grahn, Y., Nõlvak, J. & Paris, F. 1996. Precise chitinozoan dating of Ordovician impact events in Baltoscandia. *Journal of Micropaleontology*, **15**, 21–35.

Harris, N. B. W., Pearce, J. A. & Tindle, A. G. 1986. Geochemical characteristics of collision-zone magmatism. In: *Collision Tectonics* (Coward, M. P. & Ries, A. C., eds), *Geological Society of America Special Publication*, **19**, 67–81.

Haynes, J. T. 1994. The Ordovician Deicke and Millbrig K-bentonite beds of the Cincinnati Arch and the southern Valley and Ridge Province. *Geological Society of America Special Paper*, **290**, 1–80.

Hess, P. C. 1989. *Origins of igneous rocks*. Harvard University Press, Cambridge, 336 p.

Huff, W. D., Anderson, T. B., Rundle, C. C. & Odin, G. S. 1991. Chemostratigraphy, K–Ar ages and illitization of Silurian K-bentonites from the Central Belt of the Southern Uplands–Down–Longford Terrane, British Isles. *Journal of the Geological Society of London*, **148**, Part 5, 861–868.

Huff, W. D., Merriman, R. J., Morgan, D. J. & Roberts, B. 1993. Distribution and tectonic setting of Ordovician K-bentonites in the United Kingdom. *Geological Magazine*, **130**, 93–100.

Huff, W. D., Kolata, D. R., Bergström, S. M. & Zhang, Y.-S. 1996. Large magnitude middle Ordovician volcanic ash falls in North America and Europe: dimensions, emplacement and post-emplacement characteristics. *Journal of Volcanology and Geothermal Research*, **73**, 285–301.

Huff, W. D., Kolata, D. R. & Bergström, S. M. 1997. Middle Ordovician K-bentonites of eastern North America. *Regional geologic implications*. Geological Society of America. Abstracts with Programs, **29**, p. 54.

Huff, W. D., Bergström, S. M., Kolata, D. R. & Sun, H. 1998. The Lower Silurian Osmundsberg K-bentonite. Part II. Mineralogy, geochemistry, chemostratigraphy, and tectonomagmatic significance. *Geological Magazine*, **135**, 15–26.

Järvimäki, P. & Puranen, M. 1979. Heat flow measurements in Finland. In: *Terrestrial heat flow in Europe* (Čermak, V. & Rybach, L., eds). Springer, Berlin, 172–178.

Jõeleht, A. 1995. Petrophysical properties of Estonian bedrock. Unpublished report of Geologi-

cal Survey of Estonia, Tallinn, 32 pp. [In Estonian].

Jõeleht, A. & Kukkonen, I. T. 2002. Physical properties of Vendian to Devonian sedimentary rocks in Estonia. *GFF*, **124**, 65–72.

Kala, E. A., Puura, V. A. & Suuroja, K. A., 1978. O Kärdlaskoj krateroobraznoj strukture na o. Hiiumaa [About the Kärdla crater-like structure on Hiiumaa Island]. In: *Lokal'nye struktury Belorussii i Pribaltiki* [Local structures of Belorus and East Baltic] (Laškov, E. M., ed.), Vilnius, 88–91. [In Russian].

Kiipli, T. & Kallaste, T. 2001. Volcanogenic interbed. In: *Valga (10) drill core* (Põldvere, A., ed.), *Estonian Geological Sections,* **3**, 16–17.

Kiipli, T. & Kallaste, T. 2002. Correlation of Telychian sections from shallow to deep sea facies in Estonia and Latvia based on the sanidine composition of bentonites. *Proceedings of the Estonian Academy of Sciences, Geology*, **51**, 143–156.

Kiipli, T., Kiipli, E. & Kallaste, T. 1997. Metabentonite composition related to sedimentary facies in the Lower Silurian of Estonia. *Proceedings of the Estonian Academy of Sciences, Geology*, **46**, 93–104.

Kleesment, A., Pirrus, E., Suuroja, K. & Tiirmaa, R. 1987. Geology of the North-Eastern outer slope of the mound of the Kärdla buried crater. *Proceedings of the Estonian Academy of Sciences, Geology*, **36**, 131–139. [In Russian with English summary].

Koistinen, T., Laitakari, I., Virransalo, P., Korsman, K., Puura, V., Vaher, R., Klein, V., Niin, M., Koppelmaa, H., Tikhomirov, S., Amantov, A., Savitskiy, A., Saltykova, T. & Janovskiy, A. 1994. Precambrian basement of the Gulf of Finland and surrounding area, 1:1 000 000. In: *Explanation to the map of Precambrian basement of the Gulf of Finland and surrounding area 1 : 1 mill.* (Koistinen, T., ed., 1996), *Geological Survey of Finland Special Paper,* **21**, 141 pp.

Kolata, D. R., Huff, W. D. & Bergström, S. M. 1996. Ordovician K-bentonites of eastern North America. *Geological Society of America Special Paper*, **313**, 1–84.

Koppelmaa, H., Niin, M. & Kivisilla, J. 1996. About the petrography and mineralogy of the crystalline basement rocks in the Kärdla impact crater area, Hiiumaa Island, Estonia. *Bulletin of the Geological Survey of Estonia*, **6/1**, 4–24.

Lanson, B. & Meunier, A. 1995. The transformation of ordered (S>1) mixed layers illite-smectite to illite in a diagenetic series. State of the art and prospects. *Bulletin Centres Recherche Exploration–Production Elf Aquitaine*, **19**, 149–165.

Lindström, M., Floden, T., Puura, V. & Suuroja, K. 1992. The Kärdla, Tvären and Lockne craters–possible evidences of an Ordovician asteroid swarm. *Proceedings of the Estonian Academy of Sciences, Geology*, **41**, 45–53.

Loog, A. & Oraspõld, A. 1982. *Settekivimite ja setete (setendite) uurimismeetodid* [Methods of the study of sediments and sedimentary rocks]. TRÜ geoloogia kateeder, Tartu, 83 pp. [In Estonian].

Masaitis, V. P., Danilin, A. N., Maščak, M. S., Rajhlin, A. I., Selivanovskaja, T. V. & Šadenkov, T. N. 1980. *Geologija astroblem* [Astrobleme geology]. Nedra, Leningrad, 231 pp. [In Estonian].

Merriman, R. J. & Roberts, B. 1990. Metabentonites in the Moffat Shale Group, Southern Uplands of Scotland. Geochemical evidence of ensialic marginal basin volcanism. *Geological Magazine*, **127**, 259–271.

Moore, D. M. & Reynolds, R. C. (Jr.) 1997. *X-ray diffraction and the identification and analysis of clay minerals*. Oxford University Press, 378 pp.

Možaev, B. N. 1973. *Novejšaja tektonika Severo-Zapada Russkoj ravniny* [Recent tectonics of the nortwestern part of the Russian plain]. Nedra, Leningrad, 232 pp. [In Russian with English summary].

Niin, M. 1997. Svecofennian granitoids of the crystalline basement of Estonia: classification on the basis of geological structure, mineral and chemical composition. *Bulletin of the Geological Survey of Estonia*, **7/1**, 4–39.

Nõlvak, J. 1999. Distribution of chitinozoans. In: *Taga-Roostoja (25A) drill core* (Põldvere, A., ed.), *Estonian Geological Sections*, **2**, 10–12.

Nõlvak, J. 2001. Distribution of chitinozoans. In: *Valga (10) drill core* (Põldvere, A., ed.), *Estonian Geological Sections*, **3**, 8–10.

Nõlvak, J. 2002a. Bentonite in the uppermost Kukruse Stage in North Estonia. In: *The Fifth Baltic Stratigraphical Conference, Basin Stratigraphy–Modern Methods and Problems: Extended abstracts* (Satkūnas, J. & Lazauskienė, J., eds), Vilnius, Lithuania, 149–151.

Nõlvak, J. 2002b. *Chitinozoan biostratigraphy in the Ordovician of Baltoscandia*. Ph.D. thesis, Institute of Geology at Tallinn Technical University, 200 pp.

Nõlvak, J. & Grahn, Y. 1993. Ordovician chitinozoan zones from Baltoscandia. *Review of Palaeobotany and Palynology*, **79**, 245–269.

Oraspõld, A. 1975. Lithology of the Pirgu Stage in South Estonia. *Acta et Commentationes Universitatis Tartuensis*, **359**, 14–32. [In Russian with English summary].

Orville, P. M. 1967. Unit cell parameters of the microcline–low-albite and the sanidine high albite solid solution series. *American Mineralogist,* **52**, 55–86.

Pearce, J. A. & Cann, J. R. 1973. Tectonic setting of basic volcanic rocks determined using trace element analyses. *Earth and Planetary Science Letters*, **19**, 290–300.

Pearce, J. A., Harris, N. B. W. & Tindle, A. G. 1984. Trace element discrimination diagrams for the tectonic interpretation of granitic rocks. *Journal of Petrology*, **25**, 956–983.

Pettijohn, F. J., Potter, P. E. & Siever, R. 1987. *Sand and sandstone*. Springer-Verlag, New York, 553 pp.

Plado, J., Pesonen, L. J., Elo, S., Puura, V. & Suuroja, K. 1996. Geophysical research on the Kärdla impact structure, Hiiumaa Island, Estonia. *Meteoritics & Planetary Science*, **31**, 289–298.

Põldvere, A. 1999. Core description and terminology. In: *Taga-Roostoja (25A) drill core* (Põldvere, A., ed.), *Estonian Geological Sections*, **2**, 4–5.

Põldvere, A. 2001. Core description and terminology. In: *Valga (10) drill core* (Põldvere, A., ed.), *Estonian Geological Sections*, **3**, 4–5.

Põldvere, A. & Kleesment, A. 1998. Basic concepts and methodology. Description and terminology. In: *Tartu (453) drillcore* (Männik, P., ed.), *Estonian Geological Sections*, **1**, 7–10.

Prijatkin, A. A. & Poljakov, E. E. 1983. *Petrophysical methods of rock investigations*. Leningrad, 113 pp. [In Russian].

Puranen, R. & Sulkanen, K. 1985. *Technical description of microcomputer-controlled petrophysical laboratory*. Open file report Q15/27/85/1, Department of Geophysics, Geological Survey of Finland, Espoo, 252 pp.

Puura, V. A. 1974. *Struktura južnogo sklona Baltijskogo ščita* [The structure of the southern slope of the Baltic Shield]. Synopsis of the Candidate of Geol.-Mineral. Sci. thesis. Institute of Geology, Academy of Sciences of the ESSR, Tallinn, 28 pp. [In Russian].

Puura, V. & Suuroja, K. 1984. Kärdla kraater, maapõue varjatud uunikum [The Kärdla crater – a unique feature hidden in the bowels of the earth]. *Eesti Loodus*, **9**, 559–565. [In Estonian with English summary].

Puura, V. & Suuroja, K. 1992. Ordovician impact crater at Kärdla, Hiiumaa Island, Estonia. In: *Terrestrial impact craters and craterform structures with a special focus on Fennoscandia* (Pesonen, L. J. & Henkel, H., eds), *Tectonophysics*, **216**, **1/2**, 143–156.

Puura, V., Kala, E. & Suuroja, K. 1989. Stroenie astroblemy Kärdla [The structure of the Kärdla astrobleme]. *Meteoritika*, **48**, 150–161. [In Russian].

Puura, V., Kirs, J., Plado, J., Suuroja, K. & Suuroja, S. 1994. Shocked rocks of the Kärdla crater: divergency in chemistry, mineralogy, fluid inclusions and petrophysical properties. In: *Shock wave behaviour of solids in nature and experiments. Third ESF International Workshop: Abstract volume* (Schärer, U., Doukhan, J.- C. & Agrinier, P., eds). Limoges/Rochechouart, France, p. 54.

Puura, V., Kirsimäe, K., Kivisilla, J., Plado, J., Puura, I. & Suuroja, K. 1996. Geochemical anomalies of terrestrial compounds in nonmelted impactites at Kärdla, Estonia. *Meteoritics & Planetary Science*, **31**, 112–113.

Puura, V., Kärki, A., Kirs, J., Kirsimäe, K., Suuroja, K. & Suuroja, S. 1999. Orthoclase-enriched granitoids beneath the Kärdla Crater, Estonia. *Meteoritics & Planetary Science Supplement*, **34** (4), p. 95.

Puura, V., Kärki, A., Kirs, J., Kirsimäe, K., Kleesment, A., Konsa, M., Niin, M., Plado, J., Suuroja, K. & Suuroja, S. 2000a. Impact-induced replacement of plagioclase by K-feldspar in granitoids and amphibolites at Kärdla crater, Estonia. In: *Impacts and the Early Earth* (Gilmour, I. & Koeberl, C., eds). Springer, Berlin, 417–445.

Puura, V., Konsa, M., Kleesment, A., Kirs, J., Kirsimäe, K. & Suuroja, K. 2000b. Carbon-rich and magnetic spherules and particles from Kärdla ejecta, Estonia. In: *Meteorite impacts in Precambrian shields, Fourth ESF Workshop: Impact programme* (Plado, J. & Pesonen, J., eds). Geological Survey of Finland, Department of Geophysics, University of Helsinki, Espoo, p. 87.

Puura, V., Kärki, A., Konsa, M., Floden, T., Pihlaja, P. & Suuroja, K. 2001. Estolites–magnetic metalliferous particles from suevites from craters of Estonia, Fennoscandia, and Africa. *Meteoritics & Planetary Science Supplement*, **36** (9), A, 169–170.

Puura, V., Huber, H., Kirs, J., Kärki, A., Suuroja, K., Kirsimäe, K., Kivisilla, J., Kleesment, A., Konsa, M., Preeden, U., Suuroja, S. & Koeberl, C. 2003. Geology, petrography, shock petrography, and geochemistry of impactites and tar-

get rocks from the Kärdla crater, Estonia. *Meteoritics & Planetary Science* (in press).

Reynolds, R. C. J. 1985. NEWMOD©. A computer program for the calculation of one-dimensional diffraction patterns of mixed-layer clays. R. C. Reynolds Jr., 8 Brook Rd., Hanover, NH., 24 pp.

Roberts, B. & Merriman, R. J. 1990. Cambrian and Ordovician metabentonites and their relevance to the origins of associated mudrocks in the northern sector of the Lower Palaeozoic Welsh marginal basin. *Geological Magazine*, **127**, 31–43.

Romano, M. & Spears, D. A. 1991. Bentonites from the Horton Formation (Upper Silurian) of Ribblesdale, Yorkshire. *Proceedings of the Yorkshire Geological Society*, **48**, 277–285.

Sarna-Wojcicki, A. M., Morrison, S. D., Meyer, C. E. & Hillhouse, J. W. 1987. Correlation of upper Cenozoic tephra layers between sediments of the western United States and Eastern Pacific Ocean and comparison with biostratigraphic and magnetostratigraphic age data. *Geological Society of America Bulletin*, **98**, 207–223.

Scholle, P. A. 1978. *A color illustrated guide to carbonate rock constituents, textures, cements, and porosities*. American Association of Petroleum Geologists, Tulsa, Oklahoma, U.S.A., 241 pp.

Shogenova, A. & Puura, V. 1997. Petrophysical changes caused by dolomitization and leaching in fracture zones in lower Paleozoic carbonate rocks, North Estonia. In: *Second Nordic Symposium on Petrophysics: Fractured Reservoirs* (Middleton, M. F., ed.), *Nordic Petroleum Series*, **1**, 155–185.

Shogenova, A. & Puura, V. 1998. Composition and petrophysical properties of Estonian Early Palaeozoic carbonate rocks. In: *Research in petroleum technology* (Middleton, M. F., ed.), *Nordic Petroleum Series*, **4**, 183–202.

Środoń, J. 1984. X-ray powder diffraction identification of illitic materials. *Clays and Clay Minerals*, **32**, 337–349.

Stöffler, D. & Grieve, R. A. F. 1994. Classification and nomenclature of impact metamorphic rocks: a proposal to the IUGS subcommission on the systematic of metamorphic rocks. *Lunar and Planetary Science*, **25**, 1347–1348.

Suuroja, K. 1994. Post-impact history of the Kärdla crater. In: *Second ESF International Workshop: Impact Cratering and Evolution of Planet Earth. The identification and characterization of impacts, Abstracts*, Lockne, Sweden, p. 68.

Suuroja, K. 1996. *Formation and development of the Kärdla impact structure*. MSc thesis, Institute of Geology, University of Tartu, 57 pp. [In Estonian with English summary].

Suuroja, K. 2002. Natural resources of the Kärdla impact structure, Hiiumaa Island, Estonia. In: *Impacts in Precambrian shields* (Plado, J. & Pesonen, L. J., eds). Springer. Berlin, 295–306.

Suuroja, K., Gromov, O., Kala, E., Gromova, G., Petersell, V. & Puura, V. 1974. Otčet o poiskah podnjatij kristalličeskogo fundamenta v severovostočnoj časti o. Hiiumaa i ocenka ih na granitnyj ščeben' [Report on the study of the crystalline bedrock elevations in the SE part of Hiiumaa Island and the use of these rocks for the production of road material]. Unpublished report of the Geological Survey of Estonia, Tallinn, 150 pp. [In Russian].

Suuroja, K., Koppelmaa, H., Niin, M., Pukkonen, E., Gromov, O., Kivisilla, J. & Klein, V. 1991. Otčet o glubinnom geologičeskom kartirovanii o. Hiiumaa masštaba 1:200 000 za 1986-1991 gody [Report on deep geological mapping on Hiiumaa Island at a scale of 1:200 000 in 1986–1991]. Unpublished report of the Geological Survey of Estonia, Keila, 210 pp. [In Russian].

Suuroja, K., Mardim, T., Kadastik, E. & Eltermann, G. 1993. Hiiumaa kompleksse geoloogilise kaardistamise mõõtkavas 1:50 000 aruanne [Report on complex geological mapping on Hiiumaa Island at a scale of 1:50 000]. Unpublished report of Geological Survey of Estonia, Keila, 206 pp. [In Estonian].

Suuroja, K., Kadastik, E., Mardim, T. & Suuroja, S. 1997. Kärdla kraatriala detailne (mõõtkavas 1:10 000/1:25 000) geoloogiline kaardistamine. Hiiumaa [Detailed (scale 1:10 000/1:25 000) geological mapping of the Kärdla crater area, Hiiumaa]. Unpublished report of the Geological Survey of Estonia, Tallinn, 171 pp. [In Estonian].

Suuroja, K., Puura, V. & Suuroja, S. 1999. Kärdla crater (Hiiumaa Island, Estonia). The result of an impact in shallow epicontinental sea. In: *ESF Workshop, Oceanic impacts mechanisms and environmental perturbations, Abstracts and program*, Bremerhaven, p. 85.

Suuroja, K., Suuroja, S., All, T. & Floden, T. 2002. Kärdla (Hiiumaa Island, Estonia), the buried and well-preserved Ordovician marine impact structure. *Deep-Sea Research II: Topical Studies in Oceanography*, **49**, 1121–1144.

Suuroja, S., 1997. Shock effects in impact breccias of the Kärdla crater. In: *Impact and Extraterrestrial Spherules: New Tools for Global Correlation. International Symposium. IGCP Pro-*

ject 384. Impact and extraterrestrial spherules. Excursion guide and abstracts (Raukas, A., ed.), Institute of Geology, Tallinn, p. 55.

Shuvalov, V. 2002. Numerical modelling of impacts into shallow sea. In: *Impacts in Precambrian shields* (Plado, J. & Pesonen, L. J., eds), *Impact Studies*, 1, 323–336.

Talyzina, N. M., Moldowan, J. M., Johannisson, A. & Fago, F. J. 2000. Affinities of Earth Cambrian acritarchs studied by using microscopy, fluorescence flow cytometry and biomarkers. *Reviews of Paleobotany and Palynology*, **108**, 37–53.

Tatsumi, Y. & Eggins, S. 1995. *Subduction zone magmatism.* Blackwell Science, Cambridge, 211 pp.

Viira, V., Löfgren, A., Mägi, S. & Wickström, J. 2001. An Early to Middle Ordovician succession of conodont faunas at Mäekalda, northern Estonia. *Geological Magazine*, **138**, 699–718.

Vingisaar, P. & Murnikova, T. 1973. New data on the mineralogy of some Estonian Lower Caradocian metabentonites. *Proceedings of the Estonian Academy of Sciences. Chemistry. Geology*, **22**, 149–158.

Vingisaar, P., Oraspõld, A., Einasto, R. & Jürgenson, E. 1965. *Karbonaatkivimite ühtne klassifikatsioon ja legend.* Tallinn, 49 pp. [In Estonian and in Russian].

Winchester, J. A. & Floyd, P. A. 1977. Geochemical discrimination of different magma series and their differentiation products using immobile elements. *Chemical Geology*, **20**, 325–343.

Wood, D. A. 1980. The application of a Th–Hf–Ta diagram to problems of tectonomagmatic classification and to establishing the nature of crustal contamination of basaltic lavas of the British Tertiary Volcanic Province. *Earth and Planetary Science Letters*, **50**, 11–30.

Žukov, F., Petersell, V. & Fomin, Ju., 1987. The signs of Palaeozoic volcanicity in Estonia. *Proceedings of the Estonian Academy of Sciences. Geology*, **36**, 6–13. [In Russian with English summary].

APPENDIX 1

DESCRIPTION OF THE SOOVÄLJA (K–1) CORE

The description is given in a standardized form. The tables are divided into vertical columns based on the type of information. The format of the table is changed on sheets 7–15 concentrating on impact-related features. The values occurring rarely are given in parentheses.

STANDARD UNITS — Chronostratigraphic and geological time units.

LOCAL STRATIGRAPHIC UNITS — Stages, substages, formations, members and complexes.

CORE BOX NO./FIGURES — Numbers of boxes, location of the intervals of core illustrated in Plates 1–4.

DEPTH/SAMPLES — Depths of the boundaries and sample levels: B – electron microprobe analyses of biotite; Ch – chitinozoans; E – CaO, MgO, CO_2 and insoluble residue; F – X-ray fluorescence analyses; G – granulometric analysis of insoluble residue; K – chemical analyses; N – instrumental neutron activation analyses; Ph – physical properties; S – spectral analyses; T – thin sections, PDFs; X – X-ray diffractometry.

LITHOLOGY — For legend see next page. The core section is given at a scale of 1:400.

SEDIMENTARY STRUCTURES —According to thickness of beds: micro- (<0.2 cm), thin- (0.2–2.0 cm), medium- (2–10 cm) and thick-bedded (10–50 cm); massive – visible bedding is missing. According to size of nodules: thick-nodular (vertical diameter of nodules >5 cm), medium-nodular (2-5 cm) and thin-nodular (<2 cm).

MARL BEDS — The most frequent thicknesses of the marl beds; in parentheses – infrequent thicknesses. Colours were identified on damp core. Contacts between marl and other types of rock may be distinct (D) or indistinct (IND).

MARL PERCENTAGE — The content of marl beds in the described interval was estimated visually.

SHORT DESCRIPTION — Main types of rocks are in bold. The colour of rocks was identified on damp core; the dominant size of limestone crystals (in italics) was estimated visually: cryptocrystalline (or aphanitic) <0.005 mm, microcrystalline 0.005–0.01 mm, very finely crystalline 0.01–0.05 mm and finely crystalline 0.05–0.1 mm. The percentage of allochems, e.g. bioclasts and clastic material, is also indicated. In descriptions the rock types according to Dunham (1962) are given, if possible, in parentheses. Clastic fractions (size of particles; in italics) are described as follows: clay <0.005 mm, fine silt 0.005–0.01 mm, coarse silt 0.01–0.05 mm, very fine sand 0.05–0.1 mm, fine sand 0.1–0.25 mm, medium sand 0.25–0.5 mm, coarse sand 0.5–1.0 mm, very coarse sand >1 mm and gravel 2–10 mm. Grain size limits for igneous rocks (in italics) are as follows: fine-grained 1–2 mm, medium-grained 1–5 mm, coarse-grained 5–30 mm and very coarse-grained >30 mm.

ROCK FABRIC — Mainly mechanical and secondary changes in rock structures are described. Impact-related features are given in italics.

AGE & ABUNDANCE (%) OF MIXED CLASTS — Ages of rock fragments or sediments from lithologically distinct time divisions are estimated visually. Numbers denote the amount of clasts in the described interval. PP – Palaeoproterozoic; $Є_1$ – Lower Cambrian; O_2 – Middle Ordovician; O_3 – Upper Ordovician.

IMPACT-RELATED DEPOSITS — Distribution of the basement rocks and crater filling.

Appendix 1 continued

LEGEND

cultivated soil

limestone

argillaceous limestone

a sandy (a) and
b silty (b) limestone

marl (in general)

calcitic marl

argillaceous marl

claystone

silty claystone

siltstone

argillaceous siltstone

sandstone

a
b K-bentonite bed, on (a) or under (b) the boundary

breccia

conglomerate

granite

pegmatite

amphibolite

migmatite granite

granite and biotite gneiss

skeletal limestones:

grains 10 – 25%

grains 25 – 50%

crypto- and microcrystalline (aphanitic) limestone

fine bioclasts, pyritized

coarse bioclasts, pyritized

a
b
c horizontal bedding: thin- (a), medium- (b) and thick-bedded (c)

wavy bedding

nodular

thin intercalation

a
b nodules with distinct (a) or indistinct (b) contacts

discontinuity surface

4 number of discontinuity surfaces between the upper and the lower surface

slickenside

veins

directional movement of sediments

caverns

porous

weathered rock

macroscopic deformed rock

burrows

pyritic mottles

silicification

clastic material

anthraconite

glauconite grains

pyrite

sulphides

calcite

gypsum

micas (in general)

bitumen

kerogen

Q quartz grains

A amphibole grains

F feldspar grains

mottled, red-coloured and yellow streaks

tabulate corals

brachiopods

echinoderms

graptolites

bryozoans

calcareous algae

siliceous sponges

cephalopods

APPENDIX 1, SHEET 1

DESCRIPTION OF THE SOOVÄLJA (K–1) CORE

Location: 58° 58.530' N, 22° 46.333' E. Length of core 815.2 m. Elevation of the top 6.0 m above sea level.

STANDARD UNITS	LOCAL STRATIGRAPHIC UNITS	CORE BOX NO.	FIGURES	DEPTH (m)	SAMPLES	LITHOLOGY	SEDIMENTARY STRUCTURES	MARL BEDS	MARL PERCENTAGE	SHORT DESCRIPTION	
Quaternary, Holocene				0.0		core is missing				Cultivated soil cover, underlain by silty **sand** revealed by gamma logging. Sand is soiled light grey. Core yield 40%	Sediments typical of this region
Quaternary, Upper Pleistocene		1		4.6		core is missing				Varved clay revealed by gamma logging. Silt is grey or brownish-grey. Core yield 10%	
				20.0		core is missing				**Till**, represented only by cobbles and pebbles. Core yield 10%	
Ashgill	Pirgu Stage, Adila Formation	2, 3, 4		24.0		1, 4, 1	Irregularly thin- to medium-nodular, in places wavy medium-bedded	< 0.2 cm, up to 1 (2) cm, 1-5 cm D grey	20-30	Light grey, *microcrystalline* and *very finely crystalline* **limestone** (grains 10-25%, wackestone). Discontinuity surfaces (22) are pyritized, slightly impregnated, wavy, below with burrows and excavations (depth up to 10 cm)	
Ashgill	Pirgu Stage, Moe Formation	5, 6, 7	1	40.5	KX	1	Irregularly medium- to thick-nodular, in places medium- to thick-bedded	< 0.2 cm, up to 1 cm, 2-5 cm D grey or brownish-grey	5-10	Light grey, in places brownish-grey, *microcrystalline* **limestone** (grains < 10%, in places 10-25%, mud- or wackestone). In places occur *Palaeoporella* (=*Dasyporella*) fragments. Discontinuity surfaces (14) are pyritized, mainly slightly impregnated, wavy, below with burrows and excavations	

Selected intervals of the Soovälja (K–1) core

(depth increases towards the bottom of the page)

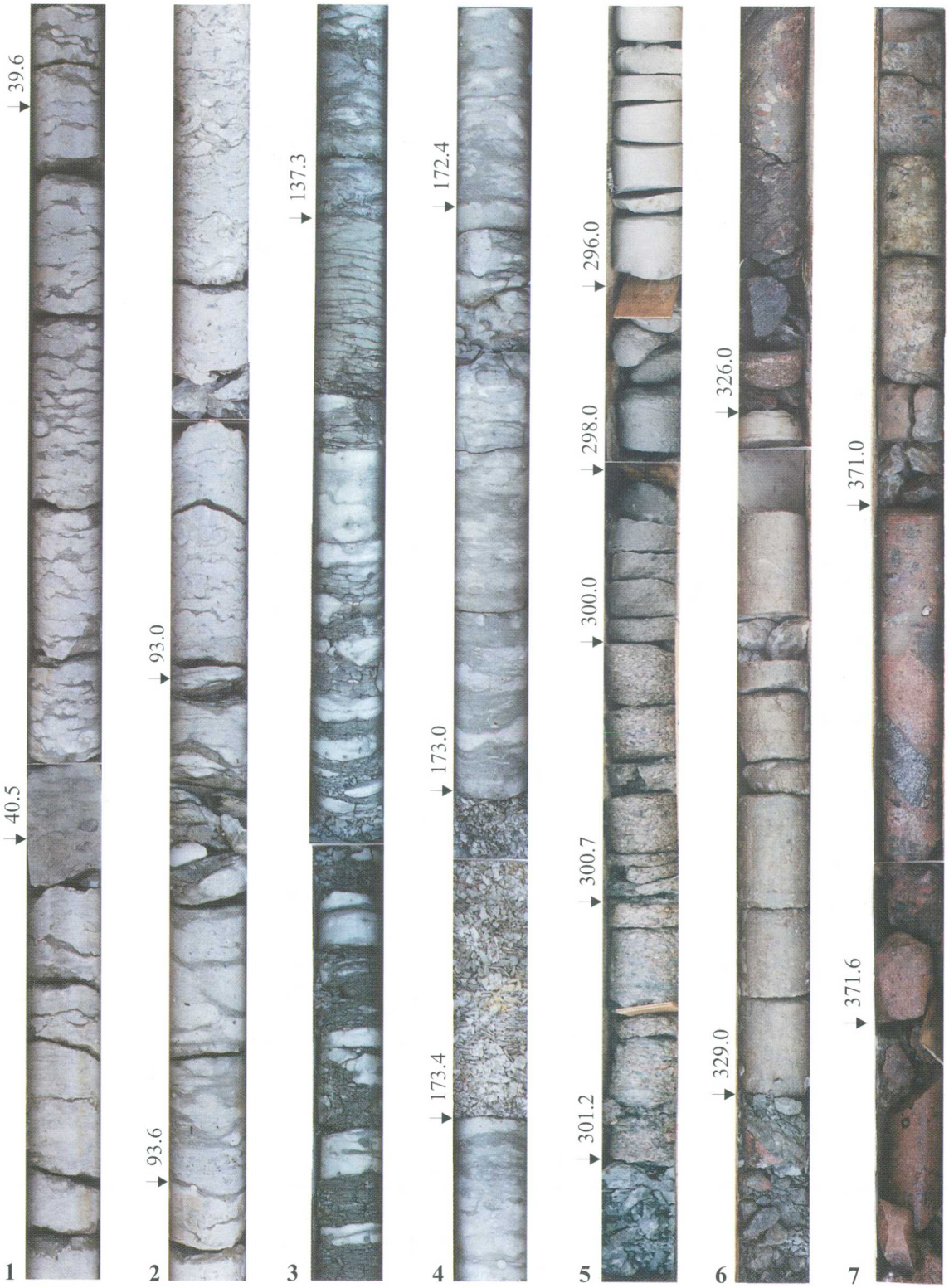

Fig. 1. **Moe to Adila formations**; 39.5–41.4 m. Fig. 2. **Paekna to Saunja formations**; 92.2–93.7 m. Fig. 3. **Kahula to Hirmuse formations**; 137.0–139.0 m. Fig. 4. **Haljala to Keila stages**; 172.2–173.6 m. Fig. 5. **Kärdla to Paluküla formations**; 295.5–301.4 m. Fig. 6. **Kärdla Formation**; 325.4–329.5 m. Fig. 7. **Kärdla Formation**; 366.4–371.8 m.

Selected intervals of the Soovälja (K–1) core

(depth increases towards the bottom of the page)

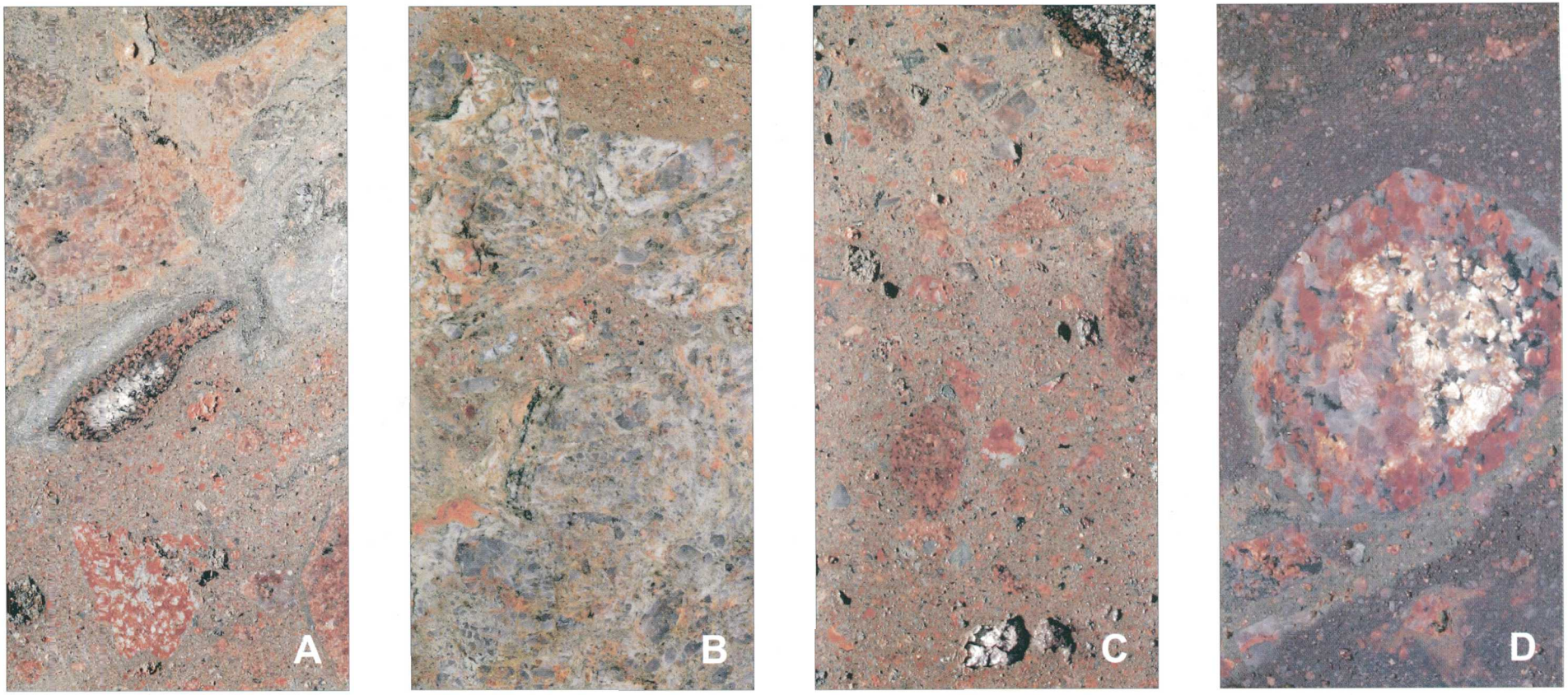

(A) Suevite-like breccia containing granitic clasts. Interval 365.95–366.08 m. (B) Suevite-like breccia containing disintegrated clasts of granite, quartz grains and cement crushed to submicroscopic scale. Interval 366.4–366.53 m. (C) Suevite-like breccia containing rounded or angular quartz grains, granite, gneiss, and microcline clasts in cement crushed to submicroscopic scale. Interval 374.90–375.04 m. (D) Impact breccia containing more or less rounded, zoned and disintegrated clasts of granitoids, migmatized amphibolites, biotite-amphibole gneisses in breccia cement with directional movement character. Interval 475.27–475.36 m.

Selected intervals of the Soovälja (K–1) core

(depth increases towards the bottom of the page)

(E) Variously disintegrated clasts of granite and quartz grains in cement crushed to submicroscopic scale. Particles of impact breccia are variously rounded. Interval 490.9–491.07 m. (F) Suevitic breccio-conglomerate with angular and rounded clasts of granite, quartz and microcline. Interval 495.1–495.24 m (G) Variously rounded clasts of granite, quartz and amphibolite in suevitic breccia cement (crushed to submicroscopic scale). Interval 508.9–509.08 m. (H) Biotite gneiss and migmatite granite of strongly fractured basement (crater floor) with suevitic breccia cement injection and white post-impact quartz veins. Interval 524.4–524.57 m.

Selected intervals of the Soovälja (K-1) core

(depth increases towards the bottom of the page)

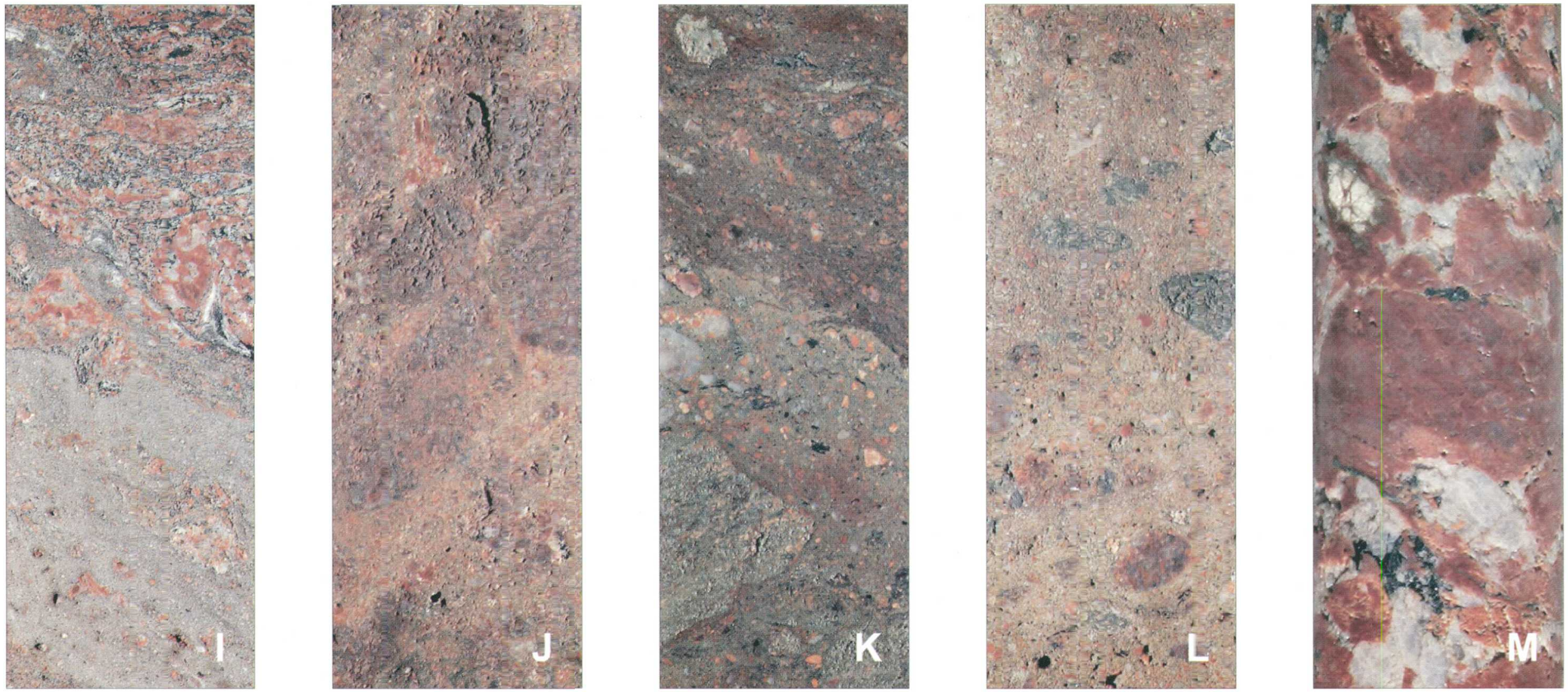

(I) Biotite gneiss and migmatite granite of strongly fractured basement (crater floor) and suevitic breccia cement crushed to submicroscopic scale. Interval 536.9–537.02 m. (J) Breccia with granitoid and gneiss fragments in strongly fractured basement (crater floor). Interval 572.30–572.44 m. (K) Breccia in strongly fractured basement (crater floor), containing variously rounded clasts of biotite gneiss, amphibolite and quartz grains. Veining breccia cement crushed to submicroscopic scale. Interval 580.9–0581.04 m. (L) Suevite-like breccia with variously rounded quartzite, granitoids and amphibolite clasts in strongly fractured basement (crater floor). Interval 584.46–584.59 m. (M) Brecciated granite-pegmatite in fractured basement. Interval 644.5–644.62 m.

STANDARD UNITS	LOCAL STRATIGRAPHIC UNITS	CORE BOX NO.	FIGURES	DEPTH (m)	SAMPLES	LITHOLOGY	SEDIMENTARY STRUCTURES	MARL BEDS	MARL PERCENTAGE	SHORT DESCRIPTION	
Ashgill	Pirgu Stage, Moe Formation	7, 8, 9, 10		64.5	K X, K X, 1					☞ follow up	Sediments typical of this region
	Vormsi Stage, Kõrgessaare Formation	11, 12, 13		78.4	1, G, Ph		Irregularly thin- to medium-nodular, wavy micro- to medium-bedded	D IND D IND IND D < 0.2 cm, 0.5-5 cm grey or dark grey	< 5 < 10 50 10 20	Light grey, in places greenish-grey, slightly to highly argillaceous, *microcrystalline to very finely crystalline* **limestone** (grains 10-25%, wackestone). Discontinuity surfaces are pyritized and phosphatized, two-ply, strongly impregnated, below with burrows and excavations	
Caradoc	Nabala Stage, Saunja Formation	14, 15, 16, 17		93.0			Wavy thick- to medium-bedded, in lower part thin- to medium-bedded	< 0.2 cm, up to 0.5 cm, 0.5-4 cm D brownish-grey or dark brownish-grey	< 10	Light beigish-grey, *aphanitic*, in the lower part *micro- to cryptocrystalline* **limestone** (grains < 10%, mudstone). Characteristic are calcite-filled primary and secondary veins. In the lower part some *Palaeoporella* (=*Dasyporella*) and *Vermiporella* fragments occur	
	Nabala Stage, Paekna Formation	18, 19, 20, 21	2	105.1	G, G, 1		Irregularly thin-, thick- to medium-nodular, in places wavy thin- to medium-bedded	< 0.2 cm, 0.2-1 cm, 2-7 cm IND dark greenish-grey	30-40	Light greenish-grey, in places slightly argillaceous, *very finely crystalline*, in the lower part *microcrystalline* **limestone** (grains 10-25%, wackestone). At 93.6-94.4 m and 101.3-101.8 m occurs beigish-grey aphanitic **limestone**. Discontinuity surfaces are pyritized, strongly (102.8 m) or slightly impregnated, wavy or with excavations and burrows	

STANDARD UNITS	LOCAL STRATIGRAPHIC UNITS	CORE BOX NO.	FIGURES	DEPTH (m)	SAMPLES	LITHOLOGY	SEDIMENTARY STRUCTURES	MARL BEDS	MARL PERCENTAGE	SHORT DESCRIPTION	
Caradoc	Rakvere Stage, Rägavere Formation, Tudu Mb.	22		105.1		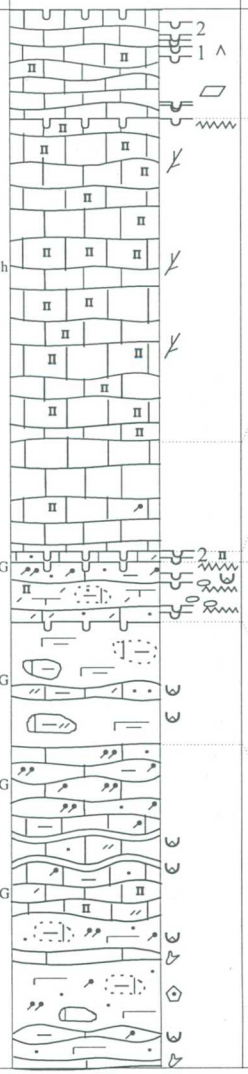	Wavy medium- to thin-bedded, (irregularly nodular)	< 0.2 cm, up to 1 cm, D greenish- to brownish-grey	< 5	Light grey to greyish-beige, *microcrystalline to aphanitic* **limestone** (grains < 10%, mudstone). Discontinuity surfaces are pyritized, mainly slightly impregnated, smooth, wavy or excavated	Sediments typical of this region
		23		110.8							
	Rakvere Stage, Rägavere Formation, Piilse Member	24					Irregularly medium- to thick-bedded, in places irregularly microbedded	< 0.2 cm, up to 2 cm IND or D grey	< 10	Light grey to beigish-grey, *aphanitic* **limestone** (grains < 10%, mudstone). Discontinuity surface is pyritized. At 116.0 m occur fragments of calcareous algae (*Dasycladaceae*?)	
		25			Ph						
		26									
		27					Wavy medium- to thick-bedded, in places irregularly microbedded	< 0.2 cm, 0.2-3 cm D grey to brownish-grey	< 5	Light grey to beigish-grey, *aphanitic* **limestone** (grains < 10%, mudstone). At 133.1-133.6 m occurs microcrystalline limestone	
				127.8							
	T* Kiideva*	28					Irregularly nodular	< 0.2 cm, up to 0.5 cm IND dark grey	< 5	Light grey, *microcrystalline* **limestone** (grains 10-25%, wackestone). In places occur sand grains. Discontinuity surfaces are pyritized, mainly strongly impregnated, wavy, smooth or excavated	
		29		133.6 134.1	G						
	Oandu* Hirm*	30	3	137.3			Irregularly nodular, thin- to medium-bedded	< 0.2 cm, up to 2 cm, in lower part 7 cm IND dark greenish-grey	20-70	Bluish-grey, in places greenish-grey, slightly to medium-argillaceous, *finely? crystalline* **limestone** (grains 25-50%; wackestone) and **marl** with bioclasts (up to 50%). Sand grains occur. Discontinuity surfaces are pyritized, mainly strongly impregnated, wavy or excavated	
	Keila Stage, Kahula Formation, Kurtna to Saue members, Lehtmetsa*	31			GG						
				143.8			Irregularly nodular and wavy bedded	< 0.2 cm, 1-25 cm, IND or D dark greenish-grey	60-80	Argillaceous **marl** with light greenish-grey, slightly to highly argillaceous, silt-containing *microcrystalline* **limestone** (grains 25-50%; wackestone) nodules	
		32			G						
		33					Irregularly thin- to thick-nodular, in places medium-bedded	< 0.2 cm, up to 1 (2-3) cm, up to 10 cm IND or D dark greenish-grey	10-30 40 20 40-70	Light grey or light greenish-grey, *very finely crystalline* and *microcrystalline* **limestone** (grains 10-50 %, wackestone), with slightly argillaceous interbeds. The lower part contains calcitic **marl** (bioclasts up to 25%) with **limestone** nodules. In places occur sand-gravel (quartz, feldspar, granite) grains. On the lower boundary lies light grey (upper 5 cm dark grey) K-bentonite bed (thickness 40 cm)	
		34			G						
		35									
		36									

Lehtmetsa*– Lehtmetsa Member; Oandu*– Oandu Stage; Hirm*– Hirmuse Formation; T*– Tõrremäe Member; Kiideva*– Kiideva Member

STANDARD UNITS	LOCAL STRATIGRAPHIC UNITS	CORE BOX NO.	FIGURES	DEPTH (m)	SAMPLES	LITHOLOGY	SEDIMENTARY STRUCTURES	MARL BEDS	MARL PERCENTAGE	SHORT DESCRIPTION	
Caradoc	Keila Stage, Kahula Formation, Kurtna to Saue members	36, 36A, 37, 38			Ph					☞ follow up	Sediments typical of this region
	Jõhvi*, Vasavere Mb.	38, 39	4	173.4	G, FBXN, X, G		Irregularly medium-nodular, in the lower part in places medium-bedded	0.2-2 (7) cm, IND greenish- to brownish-grey	20-40, 10	Light greenish-grey, slightly, in the lower part slightly to medium argillaceous, *very finely? crystalline* **limestone** (grains 10-25%, in the lower part 25-50%, wackestone), containing sand and silt grains, in the lower part granite pebbles. Discontinuity surfaces are pyritized or phosphatized, with burrows and excavations	
	Haljala Stage, Idavere Substage, Paluküla Formation, Upper member, Tatru*	39, 40, 41, 42, 43, 44, 45, 46, 47, 48, 49		177.2, 185.3, 189.4, 209.3	FFXF, FFF, XFFFF, F, FFXFF, GF, F, FX, F, G, G, F, FF, F, Ph		Wavy thin- to medium-bedded, in places irregularly nodular or lenticular	2-7 cm IND greenish-grey and dark greenish-grey	70, 10, 40-50, 60-70	Intercalation of calcitic **marl**, **limestone** and **volcanogenic interbeds**. Calcitic **marl** (bioclasts 10-50%) beds contain limestone nodules, sand and silt. Light grey or greenish-grey, in places slightly to highly argillaceous, *finely crystalline to microcrystalline* **limestone** (grains 10-50%, wackestone) contains sand and silt (in places quartz, feldspar and granite gravel) of different grain size. Rare argillaceous calcareous **sandstone** interbeds (thickness 2-3 cm) occur. At 182.7-182.9, 192.5-194.0 and 205.4-206.2 m are spherical limestone nodules 3-5 cm in diameter. **Volcanogenic K-bentonite interbeds** consist often of two parts. The lower part (thickness 2-12 cm) is light grey and the upper part (thickness 4-10 cm) is dark greenish-grey. Marl and clay content of beds changes vertically. Wavy or smooth contacts of beds are clear. Bed surfaces bear seldom sand-gravel grains and bioclasts. Discontinuity surfaces are pyritized and mainly slightly impregnated	Sediments non-typical of this region
		48, 49		209.3	Ph		Wavy medium- to thick-bedded, thin- (medium-) nodular	5-40 cm, mostly 25 cm D, IND greenish-grey	50-60	Intercalation of argillaceous or calcitic **marl** and **limestone**. **Marl** beds contain thin (medium) nodules of **limestone**. Light greenish-grey, slightly argillaceous, *microcrystalline and very finely crystalline* **limestone** (grains 10-25%, wackestone) beds alternate rhythmically (particularly at 209.3-227.0 m). Sand-silt grains (< 10%, unevenly concentrated) and bioclasts occur. At 232.4 m is 5 cm thick calcareous **sandstone** interbed with bioclasts. Indistinct discontinuity surfaces? are pyritized	

Tatru*– Tatruse Formation; Jõhvi*– Jõhvi Substage

STANDARD UNITS	LOCAL STRATIGRAPHIC UNITS	CORE BOX NO. / FIGURES	DEPTH (m)	SAMPLES	LITHOLOGY	SEDIMENTARY STRUCTURES	MARL BEDS	MARL PERCENTAGE	SHORT DESCRIPTION	
Caradoc	Haljala Stage Idavere Substage Paluküla Formation Upper Member	49 50 51 52 53 54 55		GG	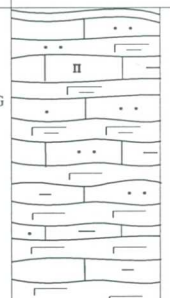				☞ follow up	Sediments non-typical of this region
		56 57 58 59	240.5	G E E G	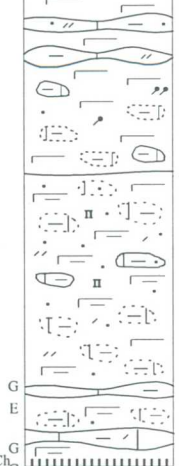	Medium- to thin-nodular or wavy thin-bedded	< 0.2 cm 0.2-2 (5) cm IND greenish-grey and dark greenish-grey	60-70	Argillaceous and calcitic **marl** with **limestone** nodules and interbeds. Sand and silt grains occur. Pyritized burrows (thickness 1-3 mm) in marl contain bioclasts. **Limestone** is light grey, slightly to highly argillaceous, *very finely*? *crystalline* (grains < 10-25%, mudstone)	
		60	256.0 260.0 260.5	F Ch G Ph Ch Ch Ch Ch G E E G Ch		Irregularly thin- and medium-nodular or lenticular Massive	0.2-2 cm, IND greenish-grey	60	Argillaceous and calcitic **marl** with **limestone** nodules and interbeds, containing sand- to silt-sized grains and bioclasts. At 259.8-259.9 m occurs a sandy limestone interbed Light grey sandy **limestone**	
		61 62 63	271.7	E Ch Ch Ch Ch G E Ch G Ch Ch Ch G		Wavy thin- to micro-bedded (medium- and thick-bedded), thin- (medium-) nodular or lenticular	< 0.2 cm 0.2-2 (5) cm, D, IND brownish-grey to dark grey	60	Argillaceous, mostly calcitic **marl** with **limestone** interbeds and nodules are characteristic. Light grey, in places with brownish tinge, sandy and silty **limestone** or calcitic **sandstone** interbeds with bioclasts, burrows, pyritized spots and clear contacts. Single **claystone** interbeds are present	

STANDARD UNITS	LOCAL STRATIGRAPHIC UNITS	CORE BOX NO.	FIGURES	DEPTH (m)	SAMPLES	LITHOLOGY	SEDIMENTARY STRUCTURES	MARL BEDS	MARL PERCENTAGE	SHORT DESCRIPTION	
Caradoc	Haljala Stage, Idavere Substage, Palukülä Formation, Upper Member	64		271.7	Ch		Irregularly thin-nodular or wavy thin-bedded	0.2-3 cm, D dark grey	90	Argillaceous **marl** with grey **limestone** nodules. Lower 5 cm sandy	follow up
				274.0	Ch G						
				274.5	Ch Ch E Ch Ch		Irregularly thin- to medium-bedded, dip 30°	< 0.2 cm, D dark grey	< 5	Light grey, sandy and silty, *very finely? crystalline* **limestone**	
		65									
				279.8	Ch Ch E Ch		Irregularly thin- to thick-bedded or massive	0.2-4 cm, > 10 cm, D grey to dark grey	95	Argillaceous and calcitic **marl**, in places silty. Argillaceous **limestone** nodules and interbeds occur. Core yield is 40%	
		66				Q F	Massive (horizontal bedded)			Light grey, medium-cemented **siltstone**. Grain size and proportion of cement increase downwards. Mostly monomineralic rock particles (quartz) are rounded to well-rounded and sorted. In places occur small quantities of feldspar, garnet, biotite, muscovite, magnetite, pyrite and glauconite	Turbidites
		67				Q F					
				296.0						Grey, *fine- to medium-grained*, weakly to medium-cemented **sandstone**. Monomineralic rock particles (quartz) are subrounded to well-rounded and grain size increases downwards. In places are found small quantities of feldspar, biotite, muscovite and pyrite	
		68	5			Q F	Thick-bedded; *PDFs occur*				
				300.0							
				301.2		Q F A Q F	Massive			Mottled, reddish-grey, medium- to weakly cemented unsorted **sandy-gravelly deposits** consisting of angular to subrounded quartz (50%), feldspar (30%), biotite, pyrite and amphibolite. Grain size increases downwards. In the lower part occur granite, clay and limestone angular clasts	

STANDARD UNITS	LOCAL STRATIGRAPHIC UNITS	CORE BOX NO.	FIGURES	DEPTH (m)	SAMPLES	LITHOLOGY	ROCK FABRIC	AGE & ABUNDANCE (%) OF MIXED CLASTS	SHORT DESCRIPTION	IMPACT-RELATED DEPOSITS
Caradoc	Haljala Stage Idavere Substage Kärdla Formation Upper Member	68 69	5	301.2			*Breccial*	PP, $€_1$, O_{2-3} 50-70	Mottled, reddish-grey **breccia** consisting mostly of granite and gneiss, less amphibolite, limestone, claystone, sandstone, argillite and siltstone fragments (diameter 1-10 cm) cemented with greenish-grey unsorted clayey-sandy-silty (mixtite-like) deposits	Resurge breccia
		70		313.0 317.2	X		Irregularly bedded, in places *breccial, dip 40°*	O_2	Light grey, *very finely crystalline* **limestone** (grains 10-25%, wackestone) block of the Lasnamägi Stage. Dark grey distinct marl beds (< 5%) are up to 0.2 cm thick. Characteristic are calcite-filled primary and secondary veins. Slightly impregnated discontinuity surfaces are pyritized	
		71			Ph XX Ph		*Breccial, deformed, breccial-conglomeratic*	PP, $€_1$, O_2	**Breccia** blocks consisting of granite, limestone, claystone, sandstone and migmatized gneiss fragments (diameter 0.2-10 (up to 30) cm) cemented sandy-clayey deposits.	
		72	6	326.0 329.0 332.7 334.0	Ph Ph	^?	Massive *Irregularly bedded, deformed* Irregularly bedded, *dip 90°*	$€_1$ 30-40 $€_1$, O_2 O_2	Block of light grey, *very fine-grained*, weakly to medium-cemented **sandstone** (Tiskre Formation) with strongly cemented sandstone globules (diam. up to 0.5 cm) Greenish-grey, in the lower part mottled, silty **claystone**, argillaceous **siltstone** and greenish-brown sandy **limestone** (Pakri Formation) blocks containing in places angular granite and limestone material (diameter 1-10 cm) Light brownish-grey, sandy, *finely crystalline* **limestone** block (Pakri Formation)	
		73		340.5 341.5			*Irregularly bedded, deformed* *Breccial*	$€_1$ PP; 90	Blocks of greenish-grey **claystone** containing interbeds of sandy-gravelly sediments of directional movement character (Lükati Formation). In the middle is silty claystone with light grey siltstone fragments (diameter 5 cm) Block containing reddish-brown angular **granite** fragments (diameter up to 15 cm) and veins of greenish-grey unsorted sandy-clayey material	Slumped breccia
		74 75			Ph X		*Breccial, deformed*	$€_1$	Blocks of greenish-grey silty **claystone** (60%), light greenish-grey, in places mottled argillaceous **siltstone** (10%) and light grey **siltstone** (20%) intercalated with greenish-grey unsorted clayey-gravelly sediments of directional movement character. Granitoid clasts are gravel- and pebble-sized. On the lower boundary occurs a reddish-brown fragment from the basement weathering crust (thickness 15 cm)	

STANDARD UNITS	LOCAL STRATIGRAPHIC UNITS	CORE BOX NO.	FIGURES	DEPTH (m)	SAMPLES	LITHOLOGY	ROCK FABRIC	AGE & ABUNDANCE (%) OF MIXED CLASTS	SHORT DESCRIPTION	IMPACT-RELATED DEPOSITS
Caradoc	Haljala Stage Idavere Substage Kärdla Formation Upper Member	75		360.5					☞ follow up	
		76	A B 7 C	378.5	PhK Ph T K TTT T Ph		*Breccial, deformed,* in places *clasts are fissured, PDFs occur*	PP, $€_1$ > 30	Crystalline rock-derived **breccia** containing **granite** blocks and fragments (diameter 0.2-5 and 5-30 (up to 100) cm, rock often altered). In places deformed claystone (Lükati Formation) pockets occur. Contacts with interbeds of light greyish-brown or pinkish-red, in places greenish-grey, strongly cemented, crushed to submicroscope scale rock are distinct or indistinct	Suevite-like breccia
		77		383.0 385.0	NF		Irregularly thin-bedded, *deformed*	$€_1$	Light greenish-grey, with red-brown spots argillaceous **siltstone** block with muscovite flakes (Voosi Formation)	Slumped breccia
							Deformed	$€_1$	Light grey *coarse-grained* **siltstone** block, containing > 90% quartz, a little pyrite and muscovite (Tiskre and Soela formations)	
							Irregularly bedded, deformed	$€_1$	Light greenish-grey, with red-brown spots, in places sandy, argillaceous **siltstone** block with rare sand- and siltstone interbeds (Voosi Formation)	
		78		397.2 408.0	Ph		Massive	$€_1$	Blocks of light grey *coarse-grained* **siltstone** (> 90% quartz), (Tiskre and Soela formations)	
							Deformed, breccial	$€_1$ (PP)	Light greenish-grey, with red-brown spots, argillaceous **siltstone** and silty **claystone** blocks. Interbeds of sandy gravelly sediments of directional movement character and granitic fragments occur (Voosi Formation)	

STANDARD UNITS	LOCAL STRATIGRAPHIC UNITS	CORE BOX NO.	FIGURES	DEPTH (m)	SAMPLES	LITHOLOGY	ROCK FABRIC	AGE & ABUNDANCE (%) OF MIXED CLASTS	SHORT DESCRIPTION	IMPACT-RELATED DEPOSITS
Caradoc	Haljala Stage, Idavere Substage, Kärdla Formation, Upper Member	78		424.5					☞ follow up	Slumped breccia
		79		438.6			*Fissured, deformed*	$€_1$	Blocks of light greenish-grey **sandstone** containing silt- to gravel-sized particles and argillaceous interbeds. In the lower part grain size increases and red-brown spots occur (Voosi Formation)	
						core is missing			Only red-bown sandy gravelly sediment fragments available (typical cover of the basement weathering crust). Gamma logging showed the presence of **sandstone**	
	Lower Member	80	D	471.0	S S S Ph Ph Ph S Ph T S S S S T S Ph Ph S Ph T N F S S Ph Ph T S		*Breccial*	PP 50-60	Reddish-brown **breccia** contains angular blocks and fragments of granite (amphibolite), diameter 0.2-5 cm, up to 10 cm, often edged. At 475.0-477.0 m breccia is greenish-grey. At 477.0-485.5 m occur mainly fragments of granitoids, less migmatized amphibolites, banded biotite gneisses and biotite-amphibolite gneisses (all > 0.5 cm in diameter). Breccia is pink to greenish-grey, strongly cemented and crushed to submicroscopic scale	Impact breccia
		81		485.5	S S S Ph S Ph S		*Breccial, cataclastic*	PP	Blocks of pinkish-grey or orange-pink **plagioclase-microcline granite** (60-70%) and crystalline rock-derived **breccia** (clasts diameter < 10 cm). Contacts are indistinct, some veins are distinct. In the lower part rock is reddish-brown	
		82	E	492.0 493.0	S XNF	V	*Breccial-conglomeratic*	PP, ($€_1$)	Mottled (yellowish- to greenish-grey, reddish-brown) quartz and feldspar clasts (diameter < 3 cm) containing weathered **breccio-conglomerate**. A 30 cm thick bed of *coarse- to fine-grained* **sandstone** occurs in the upper part	

STANDARD UNITS	LOCAL STRATIGRAPHIC UNITS	CORE BOX NO.	FIGURES	DEPTH (m)	SAMPLES	LITHOLOGY	ROCK FABRIC	AGE & ABUNDANCE (%) OF MIXED CLASTS	SHORT DESCRIPTION	IMPACT-RELATED DEPOSITS
Caradoc	Haljala Stage Idavere Substage Kärdla Formation Lower Member	82	F	493.0 496.6	Ph S TT TT S TT Ph Ph K T NF Ph X S S		*Breccial-conglomeratic, PDFs occur*	PP, ($Є_1$) < 40	Light pinkish-grey **suevitic breccio-conglomerate** (clasts diameter < 1, seldom up to 5 cm). In places green chloritized amphibolite and greenish-grey claystone fragments (diameter up to 1 cm) are found. At 495.6-496.6 m rock is reddish- to greyish-brown. At 495.8 m chloritized **amphibolite** (thickness 10 cm) occur	Impact breccia
		83 84 85	G		T S Ph S X S S T Ph Ph S S S S TT T T S T Ph Ph Ph NF S S S S X S S T NF S 516.0 T T T T S	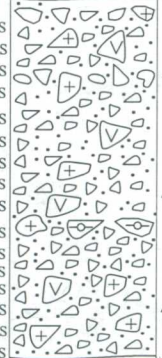	*Breccial, fissured, PDFs occur*	PP 40-60	Light pinkish-grey to greenish-grey or reddish-brown, in places light brownish-grey crystalline rock-derived **suevitic breccia**. Fragments mostly 1-2 cm, granitoid clasts 10-20 cm in diameter, amphibolite is chloritized. Cement (40-60%) consists of clastic material crushed to submicroscopic scale. Characteristic are calcite-filled secondary veins	
					Ph S S S S NF Ph S	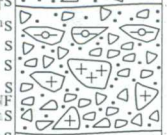	*Breccial, PDFs occur*	PP 60	Mottled (light brown to reddish-brown, dark grey) crystalline rock-derived **suevitic breccia** with granitoid clasts (diameter 1-20 cm). Cement contains clastic material crushed to submicroscopic scale	
		86 87 88	H I	522.8	Ph S S X S S S Ph T S S S Ph Ph NF S T X Ph S X K S S S T Ph S S S S S	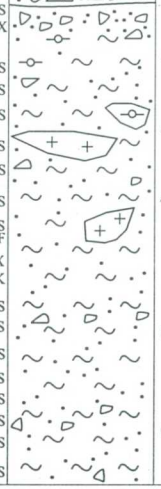	*Breccial*, folded; in upper part dip 20-40°; in lower part cataclastic	PP	Brownish-red, in the lower part pinkish-red, finely-folded **biotite-gneiss** and *medium- to coarse-grained* **migmatite granite**, in places slightly altered and crushed. In branch-like veins (thickness 1-20 cm) and lenses (both amount to 20-30%) occurs grey, unsorted clastic material of directional movement character, crushed to submicroscopic scale. Contacts of veins are distinct or indistinct. In the interval 543.0-553.0 m core yield is 20%	Strongly fractured basement (crater floor)

STANDARD UNITS	LOCAL STRATIGRAPHIC UNITS	CORE BOX NO.	FIGURES	DEPTH (m)	SAMPLES	LITHOLOGY	ROCK FABRIC	AGE & ABUNDANCE (%) OF MIXED CLASTS	SHORT DESCRIPTION	IMPACT-RELATED DEPOSITS
Caradoc	Haljala Stage Idavere Substage Kärdla Formation Lower Member								☞ follow up	Strongly fractured basement (crater floor)
		89		553.0			*Breccial, cataclastic*, folded, dip 30-50°; in lower part gneissic	PP	Brownish-red, folded, *fine- to coarse-grained* **migmatite granite** (70%) with crystalline rock-derived **breccia** interbeds. In indistinct lenses and distinct veins (thickness 10-20 cm) occurs grey rock, crushed to submicroscopic scale, in places weathered	
		90		567.5			*Breccial*	PP 40-50	Greyish-pink or red, in places greenish-grey crystalline rock-derived **breccia**. Granitic fragments are 1-10 cm in diameter. Contacts are mainly distinct. Rare amphibolite clasts are chloritized	
			J	570.6			*Breccial*	PP 40-50	Pinkish (orange) to reddish-brown crystalline rock-derived **breccia** with granitoid fragments (diameter 1-5 cm). Contacts are in places indistinct	
		91	K	573.6			*Breccial*, in places *cataclastic*	PP 40-70	Yellowish-, pinkish- (orange-), greenish- and brownish-grey **breccia**. In the interval 573.6-580.0 m (core yield 27%) occurs yellowish-grey sandy cement with quartzite pebbles (diameter 1-2 cm). At 580.0-581.0 m are dark pinkish-grey migmatite granite fragments. In the lower part clastic material (diameter up to 7 cm) contains quartzite, less granitoids and amphibolite. At 588.3 m chloritized amphibolite fragments (thickness 10 cm) occur	
		92	L	588.5				40-50		
Palaeoproterozoic	West Estonian block	93		596.5			*Breccial*, in places *fissured*, gneissic or pegmatoid		Pinkish-red, mainly *medium-grained* **migmatite granite**, in places with gneissic outlook. At 589.0-590.6 m (rarely lower) porous **breccia**, below 593.0 m single amphibolite veins (thickness 5-20 cm) occur	Fractured basement
		94		597.9			Dip 40-50°, massive		Greenish-black melanocratic *medium-grained* **amphibolite** with *coarse- to medium-grained* **granite** patches (10%). In the middle occur curved calcite-filled veins	
				601.6			*Breccial, cataclastic, fissured*		Intercalation of *medium-grained* **amphibolite** (30%) and *medium- to coarse-grained* **granitoid**. Veins are filled with thin-crushed breccia	

STANDARD UNITS	LOCAL STRATIGRAPHIC UNITS	CORE BOX NO.	FIGURES	DEPTH (m)	SAMPLES	LITHOLOGY	ROCK FABRIC	AGE & ABUNDANCE (%) OF MIXED CLASTS	SHORT DESCRIPTION	IMPACT-RELATED DEPOSITS
Palaeoproterozoic	West Estonian block	95		601.6 604.0	KKTTS PhNF S S		*Fissured*, dip 30-40°		Greenish-grey, melanocratic, *medium-grained* **amphibolite** with single pinkish-red **granitoid** veins. Some veins are calcite-filled	Fractured basement
		96		611.4	PhNFTS S S TS S TS PhNFS S PhS S NFS		*Cataclastic, fissured*		Pinkish-red, *fine- to coarse-grained* **migmatite granite** with interbeds (thickness up to 30 cm) and relicts of weathered **amphibolite** (10%, in the lower part up to 40%). Rock clasts in veins are chloritized	
		97		619.2	S TS S PhTS S		*Cataclastic, deformed,* massive		Pinkish-red or orange-red, mainly *medium-grained* **migmatite granite** (in places after metabasite) with relicts of slightly weathered **amphibolite** (<10%; in the lower part 50%). At 612.9-613.6 m occurs dark greenish-grey melanocratic **amphibolite**, whose lower boundary is marked by a mylonitic vein (thickness 1 cm)	
		98		625.8	S PhKTS S S PhXNFTS S S XS		*Cataclastic, deformed,* in places *breccial*		Reddish-pink, pinkish-red or greenish-pink, *fine- to coarse-grained* **migmatite granite** with interbeds and relicts of **amphibolite**. In places rock is penetrated by sets of fissures. The lower part contains **migmatite** interbeds and up to 1 cm thick breccial veins	
		99			S S S TS S S		*Breccial, cataclastic, deformed,* in places massive		Greyish- or reddish-pink to pinkish-red (orange), *fine- to coarse-grained*, in places *medium-grained* **migmatite granite** and *fine- to coarse-grained* **granite**. At 626.2-634.6 and 635.0-639.6 m rock is often crushed, penetrated by sets of impact-related fissures. In the interval of 635.1-636.6 m very *coarse-grained* **plagioclase-microcline granite-pegmatite** occurs. At 641.2 and 642.8 m are lenses (thickness up to 5 cm) of **amphibolite**	
		100	M	643.0 645.6	S S TS PhTS S S		*Deformed* *Breccial, cataclastic,* in places *porous,* in lower part bedded	PP (50)	Orange to red **granite-pegmatite**. Plagioclase is kaolineous and white. Slickensides dip is 45° Greyish-brown or red, *fine- to coarse-grained* **plagioclase-microcline migmatite granite** with **amphibolite** relicts. Rock is strongly influenced by the shock. **Breccia** intervals contain granitic fragments. In places rock is slightly weathered	
		101		650.8	S S S PhS		*Breccial, cataclastic porous,* in places massive		Reddish- to pinkish-grey, *fine- to coarse-grained*, mainly *medium-grained* **plagioclase-microcline granite**	
		102								

APPENDIX 1, SHEET 13

STANDARD UNITS	LOCAL STRATIGRAPHIC UNITS	CORE BOX NO.	FIGURES	DEPTH (m)	SAMPLES	LITHOLOGY	ROCK FABRIC	AGE & ABUNDANCE (%) OF MIXED CLASTS	SHORT DESCRIPTION	IMPACT-RELATED DEPOSITS
Palaeoproterozoic	West Estonian block	102		660.8	KKTTS S S TS S				☞ follow up	Fractured basement
		102–103		668.2	S S Ph Ph S TS S S		*Breccial, porous*		Brownish-red, greyish-pink or grey, *fine- to coarse-grained* **migmatite granite** with crystalline rock-derived **breccia** interbeds and veins. Rock is strongly influenced by the shock	
		103–106		699.7	NF S S S TS S S S S S T S Ph T S S S S S Ph KT S S S S Ph S S T S Ph S S		*Breccial, cataclastic,* in places massive		Pinkish-red, *fine- to coarse-grained* **plagioclase-microcline migmatite granite** with rare **amphibolite** relicts (diameter up to 1 cm). In places thin veins of secondary carbonate, crystalline rock-derived breccia lenses and impact related fissures occur	
		106		703.2	KS S XT S		*Breccial, cataclastic, porous*		Yellowish- or beigish-grey to dark grey or reddish-brown *fine- to coarse-grained* **granite**, strongly influenced by the shock	
		107			S Ph NF S S S Ph T S		*Breccial, cataclastic,* in places massive or *fissured*		Pinkish-grey, dark grey or reddish-brown, *medium- to coarse-grained* **plagioclase-microcline granite** with rare **amphibolite** relicts. Rock is penetrated by tight sets of impact-related fissures. Slickensides are chloritized. The lower boundary is marked by a brecciated vein (thickness 0.1 m) containing granite fragments (30%)	

STANDARD UNITS	LOCAL STRATIGRAPHIC UNITS	CORE BOX NO.	FIGURES	DEPTH (m)	SAMPLES	LITHOLOGY	ROCK FABRIC	AGE & ABUNDANCE (%) OF MIXED CLASTS	SHORT DESCRIPTION	IMPACT-RELATED DEPOSITS
Palaeoproterozoic	West Estonian block	107		712.5	S S			PP; 30	☞ follow up	Fractured basement
		108			S S Ph K T T S S S S T S		*Breccial, cataclastic,* gneissic, in places *fissured* and *porous*		Reddish-brown, pinkish-red or reddish-grey, mainly *medium-grained* **migmatite granite** (in places **granite gneiss**) with rare **amphibolite** (**amphibole gneiss**) relicts. In places penetrated by impact-related sets of fissures	
		109			Ph S S Ph T S S S					
		110			S T S Ph S S S S S Ph N F S T S S Ph S Ph S					
		111		745.9	S S S T S		*Cataclastic,* in places *breccial* and *porous*		Reddish-brown and dark grey, *coarse- to medium-grained* **migmatite granite** with indistinct **amphibolite** relicts (10-20%). In places rock is influenced by the shock. At 745.9 m a brownish-red haematized vein occurs, underlain by a white calcite-cemented brecciated impact-related veins (both are 3 cm thick)	
		112		751.2	S Ph S S T S S S Ph S S		*Breccial, cataclastic,* in places *porous*		Reddish-brown with dark grey spots, *fine- to medium-grained* **migmatite granite** with rare **amphibolite** relicts. In places rock is influenced by the shock. Chloritized veins occur	
				762.8						

STANDARD UNITS	LOCAL STRATIGRAPHIC UNITS	CORE BOX NO.	FIGURES	DEPTH (m)	SAMPLES	LITHOLOGY	ROCK FABRIC	AGE & ABUNDANCE (%) OF MIXED CLASTS	SHORT DESCRIPTION	IMPACT-RELATED DEPOSITS
Palaeoproterozoic	West Estonian block	113		762.8	Ph S, S, KTT S, S, S		*Breccial, cataclastic*		Intercalation of greenish-black, *fine- to medium-grained* migmatized **amphibolite** (< 70%) and reddish-brown *coarse-grained* **plagioclase-microcline granite**. In places rock is chloritized and weathered	Fractured basement
				769.0	TPhXS		*Breccial, porous, cataclastic*		Greyish-brown **migmatite granite** with rare **amphibolite** relicts. Reddish-brown veins are impregnated with iron oxides	
				771.3	S					
		114			S, PhTS, S, S, KTS, S		*Breccial, cataclastic,* in places massive		Greyish- to reddish-brown, *coarse- to fine-grained* **migmatite granite** and *coarse- to fine-grained* **granite** with greenish-black **amphibolite** interbeds (thickness up to 40 cm) and lenses. In places occur weathered veins with iron oxides	
				780.7	S					
		115			NFTS		Homogenous		Greenish-black, *medium-grained* **amphibolite**, in places migmatized	
				781.6	PhS, S		*Breccial, cataclastic*		Greyish-brown **migmatite granite** with greenish-black **amphibolite** relicts	
				783.8	PhTS		Homogenous		Greenish-black, *medium- to fine-grained* **amphibolite**, in places migmatized	
				784.9	S, S, TS, S, TS		*Breccial, cataclastic*		Mottled greyish-brown, *coarse- to fine grained* **migmatite granite** with greenish-black **amphibolite** relicts (20%). Rock is weathered in places	
		116		790.9	NFS, S, XS, PhS, TS		*Breccial, cataclastic*		Greyish-brown, *coarse- to fine-grained* **migmatite granite** with **amphibolite** relics, impregnated with iron oxides. Rock is strongly influenced by the shock	
				796.8	S		*Fractured*		Mottled black, reddish-brown, white and greenish-grey, *coarse- to fine-grained* **migmatite granite**, weathered, impregnated with iron oxides, influenced by shock	
				798.3	S		*Porous*			
				798.9	TS				Whitish-pink weathered **migmatite granite** vein, chloritized slickenside	
		117			S, XNF S, TS, PhKS		*Breccial, cataclastic, porous*; in lower part dip 30-50°, gneissic		Greyish-brown, *coarse- to fine-grained* **migmatite granite** (in the lower part **granite gneiss**), with greenish-black **amphibolite** relicts (thickness up to 25 cm). Rock is strongly influenced by the shock	
				805.0	S, TS, PhS		Homogenous, gneissic or *cataclastic*, in places *fractured*, dip 30-50°		Pinkish-red and greyish-brown, *fine- to medium-grained* **granite gneiss** with rare **amphibolite** relicts and brecciated veins	
		118			S, S, S, PhPhKTS					
				815.2+						

APPENDIX 2

Chemical composition of the Soovälja (K–1) core (wt %)

Sample No.	Sample depth (m)	Formation *Erathem*	Rock	SiO_2	TiO_2	Al_2O_3	Fe_2O_3	FeO	MnO	MgO	CaO	Na_2O	K_2O	P_2O_5	S t	LOI	Total	Fe_2O_3t	CO_2	$K_2O\backslash Na_2O$
13610	361.0–361.2	Kärdla	brec mat	71.69	0.28	11.63	1.04	2.30	0.03	1.26	0.33	0.19	8.50	0.10	<0.10	1.38	98.73	3.60		44.74
13720	372.0–372.2		gran clast	72.26	0.23	12.54	0.89	2.01	0.01	0.90	0.33	0.13	11.17	0.08	<0.10	0.86	101.41	3.12	0.27	85.92
3733830	383.0		brec mat	72.70	0.48	11.20			0.06	1.77	0.20	0.13	7.71	0.11		1.62	100.50	4.49		59.31
3734836	483.6		gran clast	65.20	0.74	14.10			0.05	2.76	0.10	0.14	9.06	0.07		1.65	99.50	5.67		64.71
3734925	492.5		brec mat	54.10	1.94	13.40			0.06	4.61	0.52	0.10	6.99	0.29		4.27	99.90	13.60		69.90
14950	495.0–495.2		brec mat	69.64	0.33	12.29	0.95	3.74	0.03	1.98	0.43	0.13	8.60	0.08	<0.10	1.82	100.02	5.11		66.15
3734952	495.2		brec mat	72.20	0.59	11.80			0.02	0.97	0.10	0.21	9.28	0.08		0.61	98.70	2.78		44.19
3735090a	509.0		brec mat	60.70	0.96	14.40			0.05	4.94	0.51	0.17	7.05	0.11		3.94	99.40	6.54		41.47
3735150	515.0		brec mat sandy	87.10	0.14	6.10			0.02	0.10	0.03	0.12	4.85	0.02		0.20	99.10	0.44		40.42
3735210	521.0		brec mat	67.30	0.47	10.80			0.02	1.11	0.07	0.13	8.46	0.05		8.47	99.80	2.91		65.08
3735347	534.7		gran brec	69.20	0.55	13.20			0.11	1.76	0.12	0.36	8.72	0.09		1.36	99.90	4.52		24.22
15570	557.0–557.2		brec mat	63.55	0.39	15.51	2.41	2.87	0.05	2.01	0.41	0.04	10.17	0.11	<0.10	2.33	99.85	5.60	0.27	254.25
3735710	571.0		brec mat	74.80	0.56	12.50			0.03	0.50	0.10	0.26	9.49	0.04		0.47	99.90	1.18		36.50
15720	572.0–572.2		brec mat gran clast	70.68	0.23	12.02	2.77	1.11	0.02	1.03	0.22	0.21	10.17	0.07	<0.10	1.08	99.61	4.00	0.19	48.43
15778	577.8–578.0		brec mat	82.78	0.09	7.38	0.32	1.15	0.01	0.52	0.22	0.09	5.80	0.03	<0.10	0.41	98.80	1.60	0.19	64.44
15820	582.0–582.2		brec vein fill	69.96	0.37	11.68	2.24	2.66	0.02	2.50	0.36	0.16	7.59	0.08	<0.10	1.93	99.55	5.19		47.44
3735870	587.0		brec mat	70.20	0.45	11.90			0.03	1.97	0.12	0.25	7.68	0.08		3.35	99.90	3.89		30.72
3735887	588.7	*Palaeoproterozoic*	brec	68.50	0.77	14.20			0.03	2.25	0.08	0.15	7.31	0.09		2.38	99.90	4.11		48.73
3735895	589.5		gran brec	70.90	0.65	12.30			0.03	1.38	0.06	0.22	9.39	0.06		0.85	99.40	3.61		42.68
3735920	592.0		gran brec	73.10	0.47	12.20			<0.01	0.60	0.09	0.34	9.77	0.07		0.69	99.50	2.20		28.74
15950	595.0–595.2		gran	69.64	0.33	12.29	0.95	3.74	0.03	1.98	0.43	0.13	8.60	0.08	<0.10	1.82	100.02	5.11		66.15
3735960	596.0		amph	49.30	0.98	15.50			0.20	6.32	12.13	0.27	2.87	0.13		2.40	99.20	9.12		10.63
3735970	597.0		amph	47.50	1.79	13.60			0.09	10.80	3.33	0.79	3.47	0.20		5.24	99.90	13.10		4.39
15985	598.5–598.7		amph mig	60.70	0.39	12.80	2.46	4.99	0.04	6.60	0.41	0.36	6.25	0.12	<0.10	3.91	99.03	8.00	0.19	17.36
3735990	599.0		amph-gran brec	62.10	0.67	12.80			0.05	6.25	0.47	0.27	6.11	0.06		4.39	99.80	6.64		22.63
16018	601.8–602.2		amph wk crushed	44.60	0.46	15.68	4.53	8.76	0.12	10.18	7.22	2.29	2.00	0.14	<0.10	3.38	99.36	14.26		0.87

Sample No.	Sample depth (m)	Formation *Erathem*	Rock	SiO_2	TiO_2	Al_2O_3	Fe_2O_3	FeO	MnO	MgO	CaO	Na_2O	K_2O	P_2O_5	S t	LOI	Total	Fe_2O_3t	CO_2	$K_2O\backslash Na_2O$
3736030	603.0	*Palaeoproterozoic*	amph	46.20	1.04	13.90			0.18	10.30	7.90	1.82	2.26	0.09		2.31	99.80	13.80		1.24
3736060	606.0		gran brec	77.20	0.19	10.60			<0.01	0.69	0.16	0.29	8.13	0.01		0.62	99.90	2.02		28.03
3736144	614.4		gran brec	75.70	0.19	10.20			<0.01	0.73	0.02	0.31	7.99	<0.01		0.70	98.80	3.01		25.77
3736180	618.0		amph fg	51.80	0.93	14.50			0.06	9.76	0.30	0.08	5.68	0.09		5.70	99.80	10.90		71.00
16280	628.0–628.2		gran fr	81.68	0.09	8.47	0.36	1.29	0.01	0.39	0.38	0.88	5.67	0.03	<0.10	0.43	99.68	1.79		6.44
3736320	632.0		gran brec	87.30	0.17	5.45			<0.01	0.28	0.04	0.20	4.14	0.02		0.60	99.90	1.75		20.70
16558	655.8–656.0		gran fr	80.80	0.24	8.36	0.45	1.37	0.01	0.39	0.48	0.42	6.72	0.03	<0.10	0.47	99.74	1.97		16.00
3736690	669.0		gran brec	85.30	0.21	6.60			<0.01	0.48	0.07	0.44	4.58	0.05		0.45	99.20	1.08		10.41
16890	689.0–689.2		gran fr	81.10	0.21	8.36	0.61	1.22	0.01	0.39	0.42	0.94	5.50	0.04	<0.10	0.47	99.27	1.97		5.85
17005	700.5–700.7		gran st crushed	84.77	0.09	6.35	0.64	0.65	0.01	0.54	0.33	0.07	5.60	0.05	<0.10	0.36	99.46	1.36	0.19	80.00
3737050	705.0		gran brec	84.30	0.33	7.11	1.16	0.05	<0.01	0.84	0.10	0.67	4.34	0.05		0.51	99.40	1.22		6.48
17170	717.0–717.2		gran wk crushed	72.66	0.36	12.53	1.19	1.51	0.02	0.78	0.36	0.98	9.22	0.06	<0.10	0.86	100.53	2.87		9.41
3737405	740.5		gran brec	74.00	0.45	12.00			<0.01	0.62	0.17	1.55	7.12	0.07		1.05	98.70	1.66		4.59
17660	766.0–766.4		amph wk crushed	45.40	0.49	15.48	4.34	7.71	0.15	9.31	9.17	3.55	1.61	0.06	<0.10	2.70	99.97	12.91		0.45
17780	778.0–778.2		gran wk crushed	69.58	0.25	13.88	0.72	2.26	0.02	1.72	0.54	1.27	8.50	0.06	<0.10	1.66	100.46	3.23		6.69
3737815	781.5		gran wk crushed	46.70	2.20	15.20			0.19	7.31	8.50	1.41	1.05	0.06		6.02	99.90	11.3		0.74
3737915	791.5		gran brec	68.10	0.35	14.80			<0.01	0.47	0.25	3.08	7.00	0.04		1.63	97.80	2.04		2.27
3738010	801.0		gran brec	81.50	0.26	6.67			<0.01	2.05	0.24	0.22	4.76	0.06		1.56	99.90	2.63		21.64
18045	804.5–804.7		gran st crushed	79.31	0.17	8.54	0.65	1.29	0.01	0.85	0.33	0.18	6.50	0.04	<0.10	0.83	98.97	2.08	0.27	36.11
18150	815.0–815.2		gran fr	72.52	0.38	12.56	1.15	1.47	0.01	0.60	0.19	1.11	9.00	0.03	<0.10	0.91	99.93	2.78	0.19	8.11

Notes: S t – total sulphur;
LOI – loss on ignition;
F_2O_3 t – total iron as Fe_2O_3 (Fe_2O_3 t=Fe_2O_3+1.111FeO);
"Total" includes Fe_2O_3t if Fe_2O_3 and FeO are not determined separately;
amph – amphibolite; brec – breccia, brecciated; carb – carbonate; fr – fractured; fg – fine-grained;
gran – migmatite-granite; mat – matrix; mig – migmatized; st – strongly; wk – weakly.

Samples collected by Kalle Suuroja, Mati Niin, Heino Koppelmaa, Jaan Kivisilla (all from the Geological Survey of Estonia) and Väino Puura (Institute of Geology, University of Tartu), analysed at the Laboratory of the Geological Survey of Estonia (samples 1...) and University of Vienna, Austria (samples 373...).

APPENDIX 3

XRF data of the Soovälja (K–1) core

Sample No.		3733830	3734836	3734925	3734952	3735090a	3735150	3735210	3735347	3735710	3735870	3735887	3735895	3735920	3735960	3735970	3735990	3736030	3736060	3736144	3736180	3736320	3736690	3737050	3737405	3737815	3737915	3738010
Sample depth (m)		383.0	483.6	492.5	495.2	509.0	515.0	521.0	534.7	571.0	587.0	588.7	589.5	592.0	596.0	597.0	599.0	603.0	606.0	614.4	618.0	632.0	669.0	705.0	740.5	781.5	791.5	801.0
		Kärdla Formation										Palaeoproterozoic Erathem																
Sampled material		brec mat	gran clast	brec mat	brec mat	brec mat	brec mat sandy	brec mat	gran brec	brec mat	brec mat	brec	gran brec	gran brec	amph	amph	amph-gran brec	amph	gran brec	gran brec	amph fg	gran brec	gran brec	gran brec	gran brec	amph carb	gran brec	gran brec
Sc	ppm	9.8	10.1	16.5	9.5	23.3	1.1	8.9	18.8	6.0	10.7	9.8	8.6	6.2	4.8	49.1	14.8	36.2	1.9	1.4	35.4	0.7	1.6	3.7	6.1	50.4	6.9	3.4
V	ppm	152.0	87.0	86.0	44.0	154.0	21.0	56.0	65.0	< 15.0	59.0	91.0	59.0	< 15.0	23.0	445.0	115.0	296.0	< 15.0	< 15.0	249.0	19.0	18.0	37.0	17.0	596.0	28.0	26.0
Cr	ppm	39.9	48.3	43.7	44.2	94.2	10.8	52.1	58.2	5.9	61.6	65.6	34.6	29.8	6.1	195.0	91.8	451.0	4.4	2.3	407.0	47.0	8.4	13.2	4.8	56.8	2.4	14.9
Co	ppm	9.9	12.6	28.9	6.6	13.7	1.7	8.5	11.7	3.0	14.3	12.0	10.4	3.6	8.0	46.1	16.0	42.7	3.7	2.0	21.4	2.7	2.1	2.7	2.4	42.9	5.0	3.3
Ni	ppm	17.0	28.0	53.0	15.0	37.0	7.0	14.0	26.0	7.0	31.0	26.0	18.0	12.0	18.0	43.0	53.0	129.0	9.0	< 9.0	68.0	14.0	< 9.0	< 9.0	8.0	37.0	< 9.0	6.0
Cu	ppm	< 2.0	< 2.0	< 2.0	< 2.0	< 2.0	< 2.0	< 2.0	< 2.0	< 2.0	< 2.0	9.0	< 2.0	< 2.0	2.0	< 2.0	< 2.0	< 2.0	< 2.0	< 2.0	< 2.0	< 2.0	< 2.0	< 2.0	7.0	89.0	< 2.0	< 2.0
Zn	ppm	61.5	59.8	166.5	34.0	59.3	8.4	38.0	45.8	30.2	42.0	78.0	41.0	30.0	14.0	88.9	39.8	92.5	61.0	27.0	91.6	13.0	12.0	14.0	23.0	83.6	36.0	15.0
As	ppm	0.2	< 1.0	1.0	< 0.5	0.1	0.6	< 0.6	< 0.8	0.6	0.3	< 0.4	0.1	0.1	< 0.5	1.3	0.1	< 2.0	< 0.5	< 0.5	< 1.0	< 0.5	< 0.3	< 0.1	0.3	< 2.0	< 1.0	< 1.0
Rb	ppm	137.7	157.7	191.3	155.0	131.0	90.0	146.0	175.0	227.3	160.0	166.0	213.0	242.0	54.9	33.7	100.6	38.3	242.0	214.0	99.7	101.0	127.0	140.0	249.0	60.2	128.0	129.0
Sr	ppm	66.0	78.0	48.0	61.0	61.0	67.0	50.0	126.0	36.0	80.0	93.0	84.0	45.0	53.0	79.0	66.0	115.0	17.0	15.0	37.0	65.0	72.0	66.0	75.0	147.0	148.0	74.0
Y	ppm	25.0	50.0	153.0	23.0	23.0	10.0	21.0	46.0	31.0	30.0	172.0	23.0	26.0	25.0	71.0	34.0	25.0	53.0	27.0	21.0	10.0	11.0	15.0	21.0	46.0	23.0	23.0
Zr	ppm	186.7	255.0	323.0	220.0	221.0	49.8	217.0	254.0	343.0	231.0	241.0	279.0	339.0	220.0	203.0	247.0	79.7	224.0	310.0	127.0	121.0	90.3	101.0	324.0	247.0	181.0	147.0
Nb	ppm	16.0	16.0	27.0	16.0	17.0	7.0	15.0	14.0	21.0	14.0	15.0	14.0	20.0	17.0	23.0	17.0	11.0	18.0	14.0	22.0	6.0	7.0	10.0	18.0	13.0	12.0	10.0
Sb	ppm	0.1	< 1.0	0.8	< 0.1	0.1	0.2	0.1	< 0.2	0.1	0.1	< 0.1	< 0.1	0.1	0.1	< 1.0	0.1	< 1.0	< 0.1	< 0.1	0.1	< 0.1	< 0.1	< 0.1	< 0.1	2.2	0.1	0.1
Cs	ppm	1.2	2.7	4.9	1.6	2.0	0.3	1.8	2.5	1.5	2.5	3.0	2.6	1.7	0.5	0.4	1.5	0.5	0.7	0.5	1.7	0.6	0.4	1.0	1.5	2.5	0.8	0.9
Ba	ppm	1340.0	682.0	435.3	715.0	573.0	580.0	542.0	1320.0	743.3	781.0	1090.0	1030.0	863.0	196.0	133.7	414.3	180.0	105.0	69.6	161.3	617.0	642.0	602.0	1080.0	187.0	946.0	561.0
La	ppm	59.5	56.5	67.7	25.3	38.3	18.5	31.0	51.6	26.7	59.4	47.4	16.7	62.0	38.8	18.3	77.1	12.5	207.0	116.0	36.2	31.8	12.0	28.9	45.5	17.5	64.5	15.5
Ce	ppm	117.0	114.0	155.0	56.2	73.3	39.8	59.3	98.9	53.4	117.0	97.1	34.3	110.0	81.1	49.6	173.0	27.2	423.0	205.0	66.6	58.5	22.8	54.1	88.0	38.3	125.0	32.0
Nd	ppm	43.8	45.4	71.4	24.9	32.2	13.6	26.1	46.3	20.2	50.2	47.9	12.4	43.1	37.3	26.3	75.0	15.0	198.0	86.9	25.8	26.1	11.9	27.0	36.2	22.2	56.3	12.5
Sm	ppm	8.0	9.2	14.6	5.7	5.5	2.5	4.3	8.6	4.5	9.7	9.7	3.0	6.9	5.8	7.5	14.0	3.6	32.7	14.1	4.5	4.4	2.0	5.0	5.2	5.6	8.2	2.2

Sample depth (m)		383.0	483.6	492.5	495.2	509.0	515.0	521.0	534.7	571.0	587.0	588.7	589.5	592.0	596.0	597.0	599.0	603.0	606.0	614.4	618.0	632.0	669.0	705.0	740.5	781.5	791.5	801.0
		Kärdla Formation										Palaeoproterozoic Erathem																
Sampled material		brec mat	gran clast	brec mat	brec mat	brec mat	brec mat sandy	brec mat	gran brec	brec mat	brec mat	brec	gran brec	gran brec	amph	amph	amph-gran brec	amph	gran brec	gran brec	amph fg	gran brec	gran brec	gran brec	gran brec	amph carb	gran brec	gran brec
Eu	ppm	1.2	1.8	2.2	0.9	1.3	0.9	0.8	1.5	1.1	1.6	2.0	0.8	1.2	0.6	1.7	1.8	1.4	1.3	0.9	0.6	0.6	0.5	0.6	0.8	1.5	1.4	0.6
Gd	ppm	6.1	7.9	16.2	5.3	4.7	2.2	3.6	8.0	4.9	6.9	15.2	3.4	6.4	5.1	9.4	10.5	4.9	23.8	10.6	3.8	2.8	1.8	5.4	5.0	6.7	7.3	2.7
Tb	ppm	0.9	1.3	3.1	0.8	0.8	0.4	0.6	1.3	0.9	1.1	3.1	0.6	0.8	0.8	1.8	1.6	0.9	3.3	1.3	0.7	0.4	0.3	0.7	0.7	1.3	0.9	0.5
Tm	ppm	0.4	0.6	1.5	0.4	0.4	0.2	0.3	0.9	0.5	0.5	1.5	0.4	0.4	0.5	1.5	0.7	0.5	0.9	0.5	0.4	0.1	0.2	0.3	0.4	1.0	0.3	0.3
Yb	ppm	2.6	3.7	9.8	2.6	2.9	0.9	2.3	6.2	3.6	3.1	9.2	2.5	2.8	3.3	10.8	4.4	3.4	5.3	2.6	2.7	0.8	1.0	2.1	2.5	7.0	2.1	2.1
Lu	ppm	0.4	0.5	1.3	0.4	0.4	0.1	0.3	1.0	0.5	0.5	1.3	0.4	0.4	0.5	1.6	0.6	0.5	0.6	0.4	0.4	0.1	0.1	0.3	0.4	1.1	0.3	0.3
Hf	ppm	5.5	6.9	4.8	5.6	4.8	1.6	6.8	7.6	10.1	6.3	7.4	9.4	10.8	6.5	4.4	6.7	2.0	10.6	11.0	3.3	4.0	2.2	2.8	10.2	4.9	5.5	4.2
Ta	ppm	0.8	0.7	1.4	1.0	0.9	0.1	0.8	0.7	1.4	0.8	0.6	0.7	1.1	0.6	1.8	0.8	1.0	0.4	0.2	1.4	0.1	0.1	0.7	1.0	1.5	0.3	0.4
Th	ppm	14.0	13.2	17.9	14.2	14.1	7.7	15.1	18.2	19.5	14.3	17.3	17.1	20.3	14.2	1.9	13.5	0.8	26.2	17.5	6.7	35.5	4.7	13.1	12.7	4.1	13.1	5.4
U	ppm	2.0	1.9	3.6	2.3	3.6	0.7	2.3	3.7	3.0	2.6	3.4	3.0	2.7	2.0	2.9	2.3	1.1	5.7	2.9	3.0	1.4	0.7	2.1	2.5	3.8	1.0	1.0
Ir	ppb	89±18	< 2.0	< 1.0	< 3.0	< 2.0	< 1.0	< 1.0	< 1.0	< 1.0	< 2.0	0.9	< 1.0	0.1	0.2	< 2.0	< 2.0	< 3.0	< 0.8	< 0.6	2.0	0.2	< 0.6	0.5	< 1.0	< 1.0	< 1.0	< 1.0
Au	ppb	5.0	< 9.0	< 9.0	6.8	< 2.0	2.0	< 11.0	< 18.0	2.0	7.3	1.7	7.6	3.6	< 11.0	< 14.0	1.0	6.0	3.2	3.6	< 10.0	7.7	< 9.0	1.5	7.5	4.0	< 24	< 12
Th / U		6.9	7.0	4.9	6.3	3.9	11.8	6.5	4.9	6.5	5.5	5.0	5.7	7.6	7.1	0.7	5.8	0.8	4.6	6.0	2.3	26.3	7.1	6.1	5.2	1.1	13.8	5.4
La / Th		4.3	4.3	3.8	1.8	2.7	2.4	2.1	2.8	1.4	4.2	2.7	1.0	3.1	2.7	9.6	5.7	15.1	7.9	6.6	5.4	0.9	2.5	2.2	3.6	4.2	4.9	2.9
Zr / Hf		33.9	36.8	67.4	39.1	45.9	30.9	31.8	33.2	34.0	36.8	32.6	29.8	31.4	33.7	45.7	36.6	39.5	21.1	28.2	39.0	30.1	41.6	36.6	31.8	50.2	33.1	35.0
Hf / Ta		7.3	10.3	3.3	5.6	5.2	11.5	8.2	10.8	7.3	8.0	11.9	13.6	10.2	10.7	2.5	8.2	2.1	28.6	55.0	2.4	33.5	15.5	3.8	10.7	3.4	21.9	12.0
La / Yb		15.5	10.3	4.7	6.6	9.0	13.3	9.3	5.6	5.1	12.8	3.5	4.5	15.2	8.1	1.1	11.7	2.5	26.5	30.3	9.2	28.7	8.3	9.4	12.2	1.7	20.6	4.9
Eu/ Eu*		0.5	0.6	0.4	0.5	0.8	1.1	0.6	0.5		0.6	0.5	0.8	0.5	0.3	0.6	0.5	1.0	0.1	0.2	0.4	0.5	0.9	0.4	0.5	0.7	0.5	0.8
K / U		31650	40160	16047	34068	16229	62179	30388	19430	26538	24427	17760	25997	30493	11958	9971	21759	17438	11803	22881	16045	25556	56965	16900	24119	2309	61404	39667

* Eu normalized value obtained by interpolating between the normalized values of Sm and Gd.
Notes: amph – amphibolite; brec – breccia, brecciated; carb – carbonate; fg – fine-grained; gran – migmatite-granite; mat – matrix.

Samples collected by Kalle Suuroja, Mati Niin, Heino Koppelmaa, Jaan Kivisilla (all from the Geological Survey of Estonia) and Väino Puura (Institute of Geology, University of Tartu).
Analysed at the University of Vienna, Austria.

APPENDIX 4

List of samples for semiquantitative emission spectral analyses of major and trace elements of the Soovälja (K–1) core

Sample numbers								
14710	15074	15454	15844	16204	16580	16984	17392	17793
14725	15086	15466	15858	16215	16594	16997	17406	17799
14740	15098	15478	15872	16227	16608	17009	17418	17807
14754	15110	15490	15886	16245	16620	17021	17432	17816
14768	15120	15504	15890	16258	16632	17033	17446	17827
14787	15132	15518	15902	16268	16644	17046	17459	17838
14790	15144	15531	15914	16279	16656	17060	17472	17849
14805	15156	15544	15926	16290	16670	17073	17485	17860
14820	15168	15556	15938	16300	16682	17086	17498	17872
14832	15180	15568	15952	16314	16696	17100	17512	17884
14838	15192	15581	15965	16328	16710	17113	17525	17896
14848	15204	15596	15979	16342	16724	17126	17538	17909
14858	15216	15610	15992	16351	16738	17140	17550	17920
14870	15228	15624	16004	16366	16752	17154	17563	17932
14882	15242	15638	16016	16379	16766	17168	17576	17944
14894	15256	15650	16028	16392	16780	17182	17590	17956
14905	15270	15662	16040	16405	16794	17196	17602	17968
14919	15284	15675	16054	16418	16808	17210	17614	17980
14930	15298	15690	16067	16430	16822	17224	17628	17992
14944	15312	15704	16080	16443	16836	17238	17642	18004
14959	15326	15718	16093	16456	16850	17252	17657	18016
14965	15340	15732	16104	16470	16864	17266	17668	18030
14978	15354	15746	16114	16485	16878	17280	17682	18044
14990	15368	15760	16129	16496	16892	17294	17696	18058
15002	15382	15771	16136	16508	16906	17308	17710	18072
15014	15394	15782	16147	16520	16920	17322	17724	18086
15026	15406	15792	16158	16532	16934	17336	17738	18100
15038	15418	15805	16169	16544	16948	17350	17753	18114
15050	15430	15818	16180	16556	16960	17364	17768	18128
15062	15442	15830	16192	16568	16972	17378	17780	18140

The first digit in the sample number denotes the number of the drill hole, other digits show the sample depth in decimetres.

Samples collected by Jaan Kivisilla and Mati Niin, analysed by Kiira Orlova in 1991 (all from the Geological Survey of Estonia).

APPENDIX 5

Thin sections from Palaeoproterozoic rocks of the Soovälja (K–1) core

Thin section*	Rock name	Mineralogical composition (%) / plagioclase No. (An%)	Texture	Structure	Notes
14760	Breccia-cataclasite				Brown groundmass contains some angular fine (quartz, feldspar) and coarse grains (quartz, feldspar, granite)
14816	Fine- to medium-grained plagioclase-microcline granite	Q 35–40; Mi 35–40; Pl 20–25; Bt 1–2; Op 0.5; Ap, Zrc	Granitic	Massive	
14835	Fine-grained biotite-gneiss (banded migmatite)	Q 25–30; Mi 20–25; Pl 30–35; Bt 10–15; Op	Lepidogranoblastic	Gneissic, banded	
14850	Breccia-cataclasite		Cataclastic		Similar to thin section 14760
14950	Breccia-cataclasite		Cataclastic		Brown groundmass contains some angular fine to coarse grains and fragments (quartz, feldspar, granite)
14980	Breccia-cataclasite		Cataclastic		Similar to thin section 14950, groundmass is darker
15080	Breccia-cataclasite		Cataclastic		Similar to thin sections 14950 and 14980
15150	Microbreccia		Cataclastic		Quartz-feldspar groundmass containing angular fine quartz grains, seldom K-feldspar and granite (Q 80%; diameter 1 cm)
15300	Fine-grained migmatized biotite-gneiss	Q 35–40; Mi 20–25; Pl 25–30; Bt 10–15; Op, Zrc	Lepidograno-blastic, cataclastic	Gneissic	
15360	Medium-grained plagioclase-microcline granite	Q 30–35; Mi 35–40; Pl 20–25; Bt 3–5; Hbl, Op, Zrc, Ru, Chl	Granoblastic, cataclastic	Massive	
15500	Fine-grained plagioclase-microcline granite	Q 50–55; Mi 30–35; Pl 10–15; Bt 1–2; Op < 0.5; Zrc	Granitic, cataclastic	Massive	
15630	Medium-grained plagioclase-microcline granite	Q 35–40; Mi 35–40; Pl 20–25; Bt 2–3; Op, Zrc	Granitic, cataclastic	Massive	
15680	Microbreccia		Cataclastic		Fine-grained groundmass with angular quartz and rare feldspar grains
15750	Microbreccia	Q, Mi, Pl, Bt, Op	Cataclastic		Brecciated granite
15820	Breccia after granite		Cataclastic		Fine-grained crushed groundmass with angular quartz and feldspar grains
15880	Metabasite				Light green isotropic serpentine with brown xenomorphic grains (mica, kaolinite), ore minerals, biotite and apatite
15930	Fine-grained plagioclase-microcline granite	Q 35–40; Mi 35–40; Pl 20–25; Bt 3–5; Op 1–2; Ap, Zrc	Granitic	Massive	

Appendix 5 continued

Thin section*	Rock name	Mineralogical composition (%) / plagioclase No. (An%)	Texture	Structure	Notes
15970	Fine- to medium-grained amphibolite	Pl 40–45; Hbl 45–50; Bt 5–10; Op, Ap / An% 40	Granonemato-blastic	Massive	
16018a	Fine-grained amphibolite	Pl 42.2; Hbl 46.0; Bt 7.4; Q 2.3; Mi 0.5; Op 1.6; Ap / An% 33	Nemato-granoblastic	Massive	Quartz grains are rounded
16018b	Fine-grained amphibolite	Pl 33.8; Hbl 61.1; Bt 3.9; Op 0.9; Mi 0.3; Ap	Nemato-granoblastic	Massive	
16060	Fine- to medium-grained plagioclase-microcline granite	Q 35–40; Mi 40–45; Pl 15–20; Bt, Op, Ap	Granitic, cataclastic	Massive	With veins
16100	Medium- to coarse-grained plagiogranite	Q 40–45; Pl 55–60; Bt < 0.5; Ap, Op, Zrc, Carb	Granitic, cataclastic	Massive	
16130	Fine- to medium-grained metabasite		Cataclastic		Brecciated; contains serpentine, mica, plagioclase grains and biotite flakes
16200	Fine- to medium-grained plagioclase-microcline granite	Q 30–35; Mi 45–50; Pl 10–15; Bt < 1; Gr, Op, Ap, Zrc	Cataclastic	Massive	
16226	Microbreccia after metabasite		Cataclastic		Green isotropic groundmass with angular grains and fragments of carbonate, plagioclase, quartz
16280	Fine- to medium-grained plagioclase-microcline granite	Q 45.5; Mi 43.4; Pl 7.8; Bt 3–5; Op 0.4; Ap, Zrc / An% 25	Granitic	Massive	Quartz grains are rounded
16320a	Medium-grained plagioclase-microcline granite	Q 45–50; Mi 30–35; Pl 15; Bt 1–2; Op, Zrc	Granitic, cataclastic	Massive	
16320b	Medium-grained plagioclase-microcline granite	Q 50–55; Mi 30–35; Pl 10–15; Bt 1–2; Hbl?, Op, Zrc	Granitic, cataclastic	Massive	
16400	Medium- to coarse-grained plagioclase-microcline granite	Q 35–40; Mi 40–45; Pl 15–20; Bt 1–2; Op, Zrc	Granitic	Massive	
16470	Fine- to medium-grained plagioclase-microcline granite	Q 45–50; Mi 35–40; Pl 10–15; Bt 0.5; Op, Zrc, Carb	Cataclastic	Massive	
16558a	Fine-grained plagioclase-microcline granite	Q 59.1; Mi 20.9; Pl 17.2; Bt 1.9; Op 0.9 / An% 27	Granitic	Massive	Quartz grains are rounded, microcline grains are xenomorphic
16558b	Fine-grained plagioclase-microcline granite	Q 48.2; Mi 33.1; Pl 14.5; Bt 3.6; Op 0.6, Ap	Granitic	Massive	Quartz grains are rounded and xenomorphic
16660	Fine-grained plagioclase-microcline granite	Q; Mi; Pl; Bt; Op	Cataclastic		With net-like veins
16720	Medium-grained plagioclase-microcline granite	Q 30–35; Mi 40–45; Pl 20; Bt 2–3; Op 1, Ap, Zrc	Granitic	Massive	

Appendix 5 continued

Thin section*	Rock name	Mineralogical composition (%) / plagioclase No. (An%)	Texture	Structure	Notes
16780	Fine-grained plagioclase-microcline granite	Q 25–30; Mi 45–50; Pl 20–25; Bt 3–5; Op 0.5, Ap, Zrc	Granitic	Massive	
16835	Fine-grained plagioclase-microcline granite	Q 30–35; Mi 35–40; Pl 25–30; Bt 3–5; Op 1–2, Ap, Zrc	Granitic	Massive	
16890	Fine-grained plagioclase-microcline granite	Q 35–40; Mi 35–40; Pl 20–25; Bt 2–3; Op 0.2–0.3, Ap, Zrc	Granitic	Massive	
16960	Fine- to medium-grained plagioclase-microcline granite	Q 30–35; Mi 35–40; Pl 20–25; Bt 5; Op 0.5, Amph?, Ap, Zrc	Granitic	Massive	
17020	Breccia after quartz-rich granitoid	Q 70–75; Pl, Mi, Bt	Cataclastic		
17090	Medium-grained plagioclase-microcline granite	Q 50–55; Mi 30–35; Pl 10–15; Bt 1; Op, Ap	Granitic	Massive	
17170a	Medium-grained plagioclase-microcline granite	Q 37.1; Mi 40.6; Pl 16.5; Bt 4.7; Op 1.1, Ap	Granitic, cataclastic	Massive	Quartz grains are rounded and fissured
17170b	Medium-grained plagioclase-microcline granite	Q 35.8; Mi 37.1; Pl 21.4; Bt 4.5; Op 1.2	Granitic	Massive	Different-size quartz grains are xenomorphic
17230	Medium-grained plagioclase-microcline granite	Q 25–30; Mi 35–40; Pl 25–30; Bt 3–5; Op 1–2; Ap, Zrc	Granitic	Massive	
17270	Plagioclase-microcline granite	Q, Mi, Pl, Bt, Op	Cataclastic		Brecciated
17320	Breccia after granite	Q, Mi, Pl			
17425	Fine- to medium-grained plagioclase-microcline granite	Q 30–35; Mi 35–40; Pl 25–30; Bt 5; Op 1–2, Ap	Granitic	Massive	
17506	Fine- to medium-grained migmatized biotite-gneiss	Q 40–45; Mi 1–2; Pl 40–45; Bt 10–15; Op <0.5, Ap, Zrc / An% 15	Lepidogranoblastic, cataclastic	Banded	
17560	Fine- to medium-grained plagioclase-microcline granite	Q 30–35; Mi 45–50; Pl 15–20; Bt 1; Op 0.5, Ap	Granitic, cataclastic	Massive	
17660a	Fine- to medium-grained amphibolite	Pl 38.5; Hbl 51.9; Bt 5.4; Op 1.9; Carb 1.9; Mi 0.4 / An% 42	Granoblastic, blastogabbroic, cataclastic	Massive	
17660b	Fine- to medium-grained amphibolite	Pl 39.1; Hbl 54.5; Bt 5.9; Op 0.5 / An% 41	Blastogabbroic	Massive	
17700	Fine- to medium-grained plagioclase-microcline granite	Q 35–40; Mi 30–35; Pl 25–30; Bt, Op, Ap	Cataclastic	Massive	
17734	Fine- to medium-grained amphibolite	Pl 45–50; Hbl 45–50; Bt 1–2; Op 1, Ap, Sec / An% 39	Blastogabbroic, nematogranoblastic	Slightly banded	
17780	Medium-grained plagioclase-microcline granite	Q 30–35; Mi 45–50; Pl 20; Bt 1–2; Op, Ap, Zrc / An% 2	Granitic	Massive	Different-size quartz grains

Appendix 5 continued

Thin section*	Rock name	Mineralogical composition (%) / plagioclase No. (An%)	Texture	Structure	Notes
17810	Fine- to medium-grained amphibolite	Pl 45–50; Hbl 45–50; Q 3–5; Mi 1–2; Op 1, Ap 0.5 / An% 37	Nemato-granoblastic	Massive	
17840	Fine-grained amphibolite	Pl 40–45; Amph+sec 45–50; Bt + Op 5–10	Blastogabbroic	Massive	
17880	Fine-grained plagioclase-microcline granite	Q 30–35; Mi 40–45; Pl 20–25; Op 1–2 / An% 3	Granitic	Massive	
17900	Breccia after granite	Q, Mi, Pl, Bt, Op	Cataclastic		
17960	Fine- to medium-grained plagioclase-microcline granite	Q 30–35; Mi 30–35; Pl 30–35; Bt 2–3; Py? 1; Op 0.5; Ap, Zrc	Granitic	Massive	
17990	Breccia after granite		Cataclastic		Containing about 80% quartz
18150	Quartz-feldspar gneiss	Q 38.0; Pl 13.0; Mi 43.0; Bt 4.5; Op 1.5; Ap / An% 25	Granoblastic	Weakly gneissic	

* The first digit in the sample number denotes the number of the drill hole, other digits show the sampling depth in decimetres.
Abbreviations: Amph – amphibole; Ap – apatite; Bt – biotite; Carb – carbonates; Chl – chlorite; Op – opaque; Gr – garnet; Hbl – hornblende; Mi – microcline; Pl – plagioclase; Py – pyroxenes; Q – quartz; Ru – rutile; Zrc – zircon; sec – secondary minerals.
Collected and described by Mati Niin (Geological Survey of Estonia).

APPENDIX 6

Data of semiquantitative analyses of the mineral composition of the Soovälja (K–1) core

Sample No.	Sample depth (m)	Formation *Erathem*	Quartz	Kaolinite	Hydromica, illite–smectite	Montmorillonite-chlorite	Montmorillonite-hydromica, illite–smectite	Chlorite	Haematite	Orthoclase	Albite	Amphibole	Biotite
			%										
14925	492.5	Kärdla	17	0	0	0	31	27	9	16	0	0	0
14962	496.2		5	0	0	0	5	85	0	5	0	0	0
15000	500.0		22	0	0	0	14	49	0	14	0	0	1
15130	513.0		68	0	10	0	0	4	0	18	0	0	0
15240	524.0		38	8	7	0	3	3	0	37	0	0	4
15360	536.0		44	9	0	0	12	3	0	26	0	0	6
15630	563.0		52	17	0	0	7	3	0	15	0	0	7
15774	577.4		8	36	29	0	0	15	4	9	0	0	0
15870	587.0		46	5	0	0	6	12	0	27	0	0	5
15880	588.0		4	0	5	0	0	86	0	3	0	0	3
15970	597.0	*Palaeoproterozoic*	4	0	0	63	0	0	0	12	10	11	0
16320	632.0		67	4	4	0	0	3	0	23	0	0	0
16354	635.4		9	3	14	0	0	10	0	64	0	0	0
17020	702.0		57	1	6	0	0	6	0	29	0	0	0
17700	770.0		36	3	4	0	0	9	0	49	0	0	0
17934	793.0		21	5	12	0	0	19	7	19	17	0	0
18010	801.0		58	0	5	0	0	6	0	30	0	0	1

Samples collected by Kalle Suuroja, analysed at the Institute of Geology, University of Tartu.

APPENDIX 7

Thin sections of the Soovälja (K–1) core with planar deformation features (PDFs)

Thin section	Sample depth (m)	Number of PDFs systems	Thin section	Sample depth (m)	Number of PDFs systems
K13660B	366.0	1–2	K15073-1	507.3	1–2
K13735-1	373.5	1–2–3	K15073-2	507.3	1–2
K13735-2	373.5	1–2	K15075-1	507.5	1–2
K13737-1	373.7	1–2	K15075-2	507.5	1–2
K13750A	375.0	1–2	K15159-1	515.9	1–2
K14945-1	494.5	1–2	K15159-2	515.9	1
K14945-2	494.5	1–2	K15162-1	516.2	1–2
K14947-1	494.7	1–2	K15162-2	516.2	1–2
K14947-2	494.7	1	K15425	542.5	Not found
K15032A	503.2	1–2	K15887	588.7	Not found

Investigated by Juho Kirs, Ulla Preeden and Väino Puura
(all from the Institute of Geology, University of Tartu).

APPENDIX 8

Grain-size distribution of insoluble residue in the Soovälja (K–1) core

Sample No.	Sample depth (m)	Formation	Insoluble residue (%)	>10	10–7	7–5	5–3	3–2	2–1	1–0.5	0.5–0.25	0.25–0.1	0.1–0.05	<0.05
				mm										
10684	68.4	Kõrgessaare	20.94							0.01	0.04	0.12	0.41	99.42
10932	93.2	Paekna	37.49							0.02	0.10	0.22	0.16	99.50
10985	98.5	Paekna	16.81						0.09	0.23	0.64	1.00	0.63	97.41
11344	134.4	Hirmuse	24.30						0.04	0.17	0.20	0.58	0.36	98.65
11405	140.5	Kahula	55.28						<0.01	<0.01	0.02	0.07	0.07	99.84
11406	140.6	Kahula	21.70						0.03	<0.01	0.03	0.08	0.05	99.81
11460	146.0	Kahula	8.33				0.16	0.11	<0.01	<0.01	0.05	0.48	2.22	96.98
11517	151.7	Kahula	5.08					0.14	0.14	0.07	0.07	0.29	0.21	99.08
11724	172.4	Kahula	48.35				0.26	0.01	0.12	0.21	0.26	0.23	0.07	98.84
11764	176.4	Kahula	20.59			0.12	0.12	0.29	1.20	1.89	1.96	4.44	2.98	87.00
11822	182.2	Paluküla	57.12	33.8	15.21	6.41	5.00	2.65	1.70	0.74	0.75	1.34	1.42	30.99
11920	192.0	Paluküla	35.13						0.03	0.08	0.19	1.31	2.92	95.47
11930	193.0	Paluküla	18.39				0.16	0.04	0.16	0.18	0.33	2.29	4.34	92.50
12211	221.1	Paluküla	19.05					0.02	0.07	0.11	0.20	1.68	3.33	94.59
12212	221.2	Paluküla	52.52						0.01	0.01	0.07	2.24	3.75	93.92
12517	251.7	Paluküla	51.45						<0.01	0.02	0.04	1.20	1.93	96.81
12548	254.8	Paluküla	61.21							<0.01	0.01	0.79	1.61	97.59
12561	256.1	Paluküla	51.21					<0.01	<0.01	0.01	0.05	1.15	2.49	96.30
12602	260.2	Paluküla	30.50				0.72	0.93	1.47	2.65	11.00	14.84	3.41	64.98
12615	261.5	Paluküla	59.45							<0.01	0.01	1.01	5.15	93.83
12640	264.0	Paluküla	9.19						<0.01	0.05	1.34	15.88	9.95	72.78
12667	266.7	Paluküla	28.09						0.02	0.02	0.06	10.14	25.14	64.62
12686	268.6	Paluküla	47.54				0.04		0.01	0.04	0.32	7.79	16.29	75.51
12690	269.0	Paluküla	65.70	18.3	15.2	8.67	3.48	0.79	0.18	0.26	1.13	1.63	21.45	28.94
12714	271.4	Paluküla	85.48							<0.01	0.01	1.08	11.35	87.56
12742	274.2	Paluküla	70.50						<0.01	0.02	0.66	5.13	30.39	63.80

Samples collected by Kalle Suuroja (Geological Survey of Estonia), analysed at the Laboratory of the Geological Survey of Estonia.

APPENDIX 9

CaO, MgO, CO_2 and insoluble residue in the Ordovician rocks of the Soovälja (K–1) core

Sample No.	Sample depth (m)	Regional stage	CaO	MgO	CO_2	Insoluble residue	Rock name
			%				
12526	252.6	Haljala	34.95	0.97	28.67	28.52	Calcitic marl
12550	255.0		15.31	0.98	14.32	62.18	Argillaceous marl
12602	260.2		35.19	0.33	27.87	33.94	Calcitic marl, slightly silty and sandy
12620	262.0		19.05	1.34	16.83	53.42	Argillaceous marl, slightly silty and sandy
12641	264.1		49.45	0.33	38.94	8.88	Limestone
12682	268.2		25.83	0.78	21.27	45.28	Calcitic marl
12758	275.8		6.67	0.74	7.94	78.28	Siltstone
12807	280.7		7.72	0.43	7.48	81.64	Siltstone

Samples collected by Anne Põldvere, analysed at the Laboratory of the Geological Survey of Estonia.

APPENDIX 10

List of chitinozoan samples from the Soovälja (K–1) core

Sample No.	Sampled interval (m)	Sample No.	Sampled interval (m)
M-14106	255.70–255.80	M-14093	268.10–268.20
M-14105	256.20–256.27	M-14092	269.60–269.67
M-14104	257.30–257.40	M-14091	270.30–270.35
M-14103	258.70–258.75	M-14090	271.10–271.15
M-14102	259.80–259.90	M-14089	271.40–271.47
M-14101	261.00–261.10	M-14088	272.30–272.40
M-14100	262.00–262.10	M-14087	273.90–274.00
M-14099	263.00–263.10	M-14086	274.50–274.55
M-14098	264.30–264.35	M-14085	275.20–275.25
M-14097	265.10–265.20	M-14084	275.90–275.97
M-14096	266.00–266.05	M-14083	276.90–276.97
M-14095	266.70–266.80	M-14082	279.30–279.35
M-14094	267.30–267.40	M-14081	280.10–280.17
		M-14080	280.80–280.90

Samples collected by Anne Põldvere (Geological Survey of Estonia), analysed by Jaak Nõlvak (Institute of Geology at Tallinn Technical University).

XRF data of the K-bentonite beds of the Soovälja (K–1) core

Sample No.	Sample depth (m)	No. on core box	U	Y	Pb	Sr	Rb	Th	As	Br	Bi	Zn	Ni	Mn	Ba	Nb	Zr	Ga	CaO	K_2O	TiO_2	Fe_2O_3t
			ppm																%			
K–1–1	173.10		5.7	26.0	< 4.0	84.0	142.4	11.7	1.6	3.8	1.3	8.9	4.9	46.3	131.2	12.3	139.4	19.6	0.69	6.35	0.20	2.70
K–1–2	177.22	1	2.0	18.8	15.5	136.3	101.9	13.7	8.4	5.9	1.3	19.6	14.5	116.2	138.1	12.7	125.7	14.8	10.14	7.02	0.33	2.51
K–1–3	177.35	2	6.0	18.5	19.3	95.6	128.3	12.9	9.2	5.6	0.5	20.0	17.7	59.7	145.5	18.7	137.5	25.7	2.06	6.26	0.33	3.34
K–1–4	177.45	2	4.5	10.1	5.0	92.7	137.0	12.1	0.2	4.4	0.0	13.8	8.3	20.0	99.4	16.7	137.9	26.3	0.77	5.94	0.25	2.74
K–1–5	177.62	3	4.3	38.0	5.8	84.1	114.8	25.1	5.7	5.4	0.0	6.3	12.8	22.2	19.3	31.4	352.6	25.2	0.85	5.90	0.32	2.79
K–1–6	177.90	4	3.4	38.0	29.9	88.3	128.3	20.3	14.9	2.7	0.2	20.8	23.5	73.7	89.3	25.6	300.9	23.7	1.60	6.04	0.46	4.42
K–1–7	178.00	4	6.1	37.9	14.3	87.4	125.7	26.9	10.2	2.6	0.6	7.0	12.9	10.4	22.9	35.8	392.9	25.8	0.61	5.83	0.26	2.90
K–1–8	178.83	5	2.7	25.3	30.8	174.9	85.3	14.8	30.0	4.6	2.4	21.9	20.5	178.6	189.0	12.4	196.2	14.3	12.27	4.96	0.42	4.27
K–1–9	178.90	6	6.7	53.1	15.6	87.6	118.7	21.3	9.2	3.8	1.8	10.1	11.7	30.2	49.6	25.7	458.7	20.4	2.18	6.76	0.60	3.40
K–1–10	179.05	7	4.0	24.3	21.9	95.3	132.1	18.3	13.3	3.0	0.0	29.3	19.3	82.5	114.4	13.9	171.9	19.3	2.19	6.04	0.43	4.44
K–1–11	179.10	7	6.9	23.7	10.1	98.6	126.8	22.8	3.6	2.8	0.0	10.5	7.1	43.4	18.5	16.4	223.0	21.1	2.18	5.82	0.33	2.70
K–1–12	180.32	8	6.7	40.9	19.8	91.9	126.8	20.4	4.8	3.3	0.0	6.6	16.5	14.7	14.2	29.6	403.1	20.9	0.87	6.17	0.72	2.85
K–1–13	180.90	9	2.9	15.9	25.6	148.2	93.9	10.2	20.1	2.7	1.3	25.3	25.3	185.0	122.1	10.3	129.3	15.2	9.33	4.80	0.51	4.23
K–1–14	181.02	10	< 0.2	14.4	38.7	100.0	103.0	6.8	35.8	3.4	2.1	21.9	39.4	108.5	127.2	13.3	154.7	16.4	4.00	6.62	0.97	4.79
K–1–15	181.40	11	6.9	26.7	11.7	105.2	126.9	23.5	13.3	3.7	0.0	12.4	16.3	8.8	20.2	26.7	339.7	22.3	1.25	5.55	0.89	3.10
K–1–16	181.70	12	3.2	21.6	20.6	99.0	84.0	11.6	29.4	4.6	3.1	42.7	20.4	122.4	125.6	14.9	196.2	12.8	5.69	8.08	1.31	2.51
K–1–17	181.90	13	2.1	16.8	26.1	108.4	113.3	14.0	37.3	4.8	0.0	34.8	30.7	127.4	120.3	16.5	151.9	12.8	4.16	6.47	0.90	3.87
K–1–18	182.60	14	5.0	24.7	15.5	89.2	135.3	11.7	16.2	6.2	1.0	38.3	28.8	80.3	173.8	17.4	237.7	20.5	0.89	6.30	0.97	4.78
K–1–19	185.32	15	3.3	17.9	41.5	56.9	107.9	15.4	14.2	5.5	3.7	7.6	50.4	36.1	88.1	24.5	319.0	20.3	0.42	7.76	1.68	3.57
K–1–20	186.40	16	1.2	13.7	34.7	48.3	86.1	8.5	20.6	7.7	5.1	9.2	64.1	49.7	132.1	14.9	172.8	8.3	2.20	10.33	1.38	4.14
K–1–21	197.21	17	1.3	14.5	42.8	250.4	88.3	6.7	11.0	9.1	2.9	28.9	44.0	264.6	178.9	8.0	141.6	11.7	12.22	6.00	0.71	4.97
K–1–22	198.15	18	4.8	22.5	33.7	129.0	142.3	14.6	13.7	4.8	0.7	50.9	44.0	163.7	216.9	21.2	239.6	18.0	4.39	6.16	0.67	5.82
K–1–23	198.25	18	5.1	53.0	21.3	81.8	137.2	20.6	2.0	5.1	0.5	17.4	21.6	45.9	190.0	37.7	590.8	17.6	0.64	5.83	0.69	5.64
K–1–24	203.03	19	3.8	16.3	24.2	77.4	122.9	34.2	2.2	4.3	3.3	22.0	26.7	94.5	252.0	20.9	230.7	18.7	0.78	6.41	0.49	4.45
K–1–25	255.98	20	5.1	32.9	438.2	74.4	72.9	13.9	19.2	4.7	4.5	9.6	87.9	139.9	47.5	24.4	406.6	17.1	1.55	4.98	1.38	7.62

Fe_2O_3t – total iron as Fe_2O_3 ($Fe_2O_3t = Fe_2O_3 + 1.111$ FeO).
Samples collected by Kalle Suuroja and Tarmo Kiipli (both from the Geological Survey of Estonia), analysed in the Laboratory of the Geological Survey of Estonia.

APPENDIX 12

Results of physical measurements from the Soovälja (K–1) core

Sample depth (m)	Series / Erathem	Rock type	Grain density (kg m^{-3})	Wet density (kg m^{-3})	Porosity (%)	P-wave velocity (m s^{-1})	Electric resistivity (Ω m)	Thermal conductivity (W m^{-1} K^{-1})	Magnetic susceptibility (x 10^{-6} SI)	Intensity of the natural remanent magnetization (mA m^{-1})	Koenigsberger ratio (–)	Measurements performed by...
69.3	O_3	Sedimentary rock	2 704	2 602	6.01	4 670	126		30	40	31.3	JP
118.6	O_3		2 737	2 636	5.85	4 090	190		60	30	11.7	JP
163.3	O_3		2 707	2 472	13.76	3 310	57		80	10	2.9	JP
211.2	O_3		2 665	2 405	15.60	3 210	36		60	130	50.9	JP
256.5	O_3		2 648	2 416	14.06	3 420	86		40	50	29.4	JP
321.2	O_3	Crystalline- and sedimentary-rock-derived allochthonous breccia	2 718	2 610	6.28	4 200			38			AS
324.5	O_3		2 887	2 704	9.69				436			AS
328.5	O_3		2 552	2 209	22.14				17			AS
333.5	O_3		2 907	2 822	4.45	4 800			380			AS
348.0	O_3		2 519	2 145	24.64				14			AS
361.0	O_3		2 624	2 451	10.66				851			AS
362.0	O_3		2 526	2 318	13.62			2.41	270	140	12.2	AJ
375.0	O_3		2 515	2 382	8.78			3.15	1 015	90	2.2	AJ
400.5	O_3		2 557	2 470	5.56			2.79	3 160	130	1.0	AJ
475.0	O_3		2 669	2 535	8.06	3 740	266		160	120	17.6	JP
475.0	O_3		2 648	2 600	2.92	4 600			8 686			AS
475.3	O_3		2 632	2 557	4.58			3.05	450	60	3.0	AJ
476.5	O_3		2 635	2 634	0.13	5 880	118 950		8 420	400	1.1	JP
482.6	O_3		2 534	2 405	8.45	4 100			12 010			AS
482.8	O_3		2 650	2 535	6.94	3 810	581		9 190	460	1.2	JP
483.6	O_3		2 646	2 501	8.83			2.36	7 480	300	1.0	AJ
484.8	O_3		2 528	2 310	14.26	3 320	229		550	90	3.8	JP
485.0	O_3		2 561	2 316	15.65				247			AS
489.1	O_3		2 520	2 436	5.41	5 050	1 603		6 970	350	1.2	JP
490.4	O_3		2 541	2 459	5.31	4 580	1 620		1 760	120	1.6	JP
493.8	O_3		2 585	2 344	15.21				160			AS
495.0	O_3		2 596	2 341	15.99	3 200			700			AS
495.2	O_3		2 492	2 295	13.15			2.36	770	50	1.6	AJ
496.2	O_3		2 444	2 270	11.95	3 500	346		720	40	1.3	JP
499.1	O_3		2 479	2 321	10.67	4 170	308		1 670	120	1.7	JP
503.2	O_3		2 517	2 392	8.29	4 300	316		1 690	80	1.1	JP
503.3	O_3		2 538	2 440	6.38			2.79	660	60	2.1	AJ
508.5	O_3		2 598	2 319	17.42	3 380	179		910	80	2.1	JP
508.5	O_3		2 626	2 362	16.29				745			AS
509.0	O_3		2 740	2 315	24.37			2.79	860	20	0.7	AJ
516.8	O_3		2 594	2 417	11.08	3 520	171		3 120	150	1.1	JP
521.9	O_3		2 488	2 333	10.38	3 190	1 100		3 850	160	1.0	JP
523.0	O_3	Strongly brecciated basement	2 635	2 516	7.29				6 300	210	0.8	AJ
529.9	O_3		2 607	2 415	11.93	2 520	260		2 380	140	1.4	JP
534.5	O_3		2 599	2 505	5.89			3.16	3 370	300	2.2	AJ
534.7	O_3		2 552	2 442	7.18	4 300	393		2 460	140	1.3	JP
536.8	O_3		2 546	2 349	12.74	3 160	179		760	20	0.6	JP
542.0	O_3		2 545	2 363	11.79			2.35	4 090	150	0.9	AJ
553.5	O_3		2 662	2 495	10.02	3 120	275		4 600	110	0.6	JP
556.0	O_3		2 684	2 477	12.30			2.85	2 660	120	1.1	AJ
557.0	O_3		2 641	2 378	16.06				886			AS
564.5	O_3		2 636	2 432	12.43	2 570	184		380	20	1.2	JP

Appendix 12 continued

Sample depth (m)	Series / Erathem	Rock type	Grain density (kg m^{-3})	Wet density (kg m^{-3})	Porosity (%)	P-wave velocity (m s^{-1})	Electric resistivity (Ω m)	Thermal conductivity (W m^{-1} K^{-1})	Magnetic susceptibility (x 10^{-6} SI)	Intensity of the natural remanent magnetization (mA m^{-1})	Koenigsberger ratio (–)	Measurements performed by...
568.5	O_3	Strongly brecciated basement	2 517	2 347	11.16			2.77	370	10	0.4	AJ
571.1	O_3		2 474	2 345	8.84	4 150	797		660	50	1.8	JP
574.0	O_3		2 536	2 387	9.68			2.56	2 610	70	0.6	AJ
577.5	O_3		2 578	2 356	14.08				630			AS
577.7	O_3		2 500	2 359	9.51	3 140	631		740	40	1.3	JP
584.5	O_3		2 648	2 362	17.35			2.71	420	170	9.8	AJ
589.4	*PP*	Fractured basement	2 517	2 463	3.56	4 860	3 070		3 810	30	0.2	JP
591.5	*PP*		2 454	2 318	9.37	3 440	1 980		3 920	120	0.7	JP
595.0	*PP*							2.61	4 440	50	0.3	AJ
603.0	*PP*		2 939	2 886	2.69			1.86	1 510	580	9.4	AJ
606.4	*PP*		2 513	2 449	4.11	4 970	2 514		12 450	1 640	3.1	JP
614.0	*PP*		2 570	2 509	3.89			3.34	3 425	320	3.4	AJ
616.3	*PP*		2 482	2 372	7.58	4 550	868		5 810	600	2.4	JP
623.0	*PP*		2 504	2 389	7.66			2.51	8 470	710	2.1	AJ
628.0	*PP*		2 614	2 595	1.13	5 570	8 236		8 590	1 280	3.5	JP
632.5	*PP*		2 592	2 554	2.35			4.71	5 120	740	3.5	AJ
647.7	*PP*		2 516	2 398	7.62	4 600	495		1 110	150	3.2	JP
654.0	*PP*		2 577	2 535	2.66			3.27	1 540	90	1.4	AJ
664.3	*PP*		2 606	2 569	2.26			3.18	9 890	890	2.2	AJ
664.7	*PP*		2 543	2 497	3.06	5 120	3911		6 140	780	3.0	JP
684.0	*PP*		2 525	2 416	7.12			2.67	2 290	90	1.0	AJ
688.8	*PP*		2 583	2 541	2.70	5 170	2 330		7 960	540	1.6	JP
694.0	*PP*		2 612	2 540	4.43			2.86	2 560	190	1.8	AJ
697.8	*PP*		2 501	2 423	5.21	4 740	514		2 130	220	2.4	JP
704.2	*PP*		2 558	2 462	6.18			3.92	1 590	210	3.3	AJ
708.6	*PP*		2 529	2 420	7.05	3 690	517		480	40	2.0	JP
716.8	*PP*		2 594	2 556	2.33	5 300	1 493		2 990	120	0.9	JP
724.0	*PP*		2 557	2 485	4.59			2.73	4 510	530	2.9	AJ
726.5	*PP*		2 507	2 427	5.32	4 730	516		710	40	1.3	JP
734.0	*PP*		2 516	2 414	6.75			3.07	2 020	250	3.0	AJ
740.8	*PP*		2 561	2 510	3.22	5 260	958		240	40	3.9	JP
744.2	*PP*		2 609	2 567	2.55			2.65	2 310	510	2.4	AJ
745.3	*PP*		2 628	2 622	0.43	5 760	26 118		10 700	1 170	2.6	JP
753.5	*PP*		2 534	2 429	6.88			3.32	1 850	100	1.3	AJ
760.3	*PP*		2 528	2 423	6.78	4 810	314		6 590	360	1.3	JP
763.5	*PP*		2 700	2 655	2.63			3.07	490	80	4.1	AJ
769.9	*PP*				3.78	5 580	1 150		19 550	810	1.0	JP
774.0	*PP*		2 567	2 501	4.21			3.08	1 270	220	4.3	AJ
782.4	*PP*		2 600	2 551	3.02	5 310	440		240	40	3.9	JP
784.0	*PP*		2 894	2 802	4.83			1.72	600	70	2.8	AJ
794.0	*PP*		2 589	2 526	3.97				170	100	14.8	AJ
803.7	*PP*		2 561	2 501	3.87			3.79	1 550	170	2.7	AJ
808.7	*PP*		2 603	2 574	1.94	5 210	2 068		2 940	270	2.2	JP
813.5	*PP*				2.28	5 340	928		2 230	110	1.2	JP
814.0	*PP*		2 582	2 527	3.47			3.43	1 460	240	4.0	AJ

Notes: O_3 – Upper Ordovician, *PP* – Palaeoproterozoic.
Samples collected by Kalle Suuroja (Geological Survey of Estonia).
Measurements performed by Jüri Plado (JP) and Argo Jõeleht (AJ), both from the Institute of Geology, University of Tartu, and Alla Shogenova (AS) from the Institute of Geology at Tallinn Technical University.

Other issues in the series

Estonian Geological Sections:

Tartu (453) drill core (Bulletin 1; 1998)
Taga-Roostoja (25A) drill core (Bulletin 2; 1999)
Valga (10) drill core (Bulletin 3; 2001)

Forthcoming issue:

Ruhnu (500) drill core